TECH LIBRARY KAFB, NM
0099447

NASA CONTRACTOR REPORT

NASA CR-575

NASA CR-575

EVALUATION OF HIGH-TEMPERATURE GAS TRANSPORT PROPERTIES

Prepared by
AVCO CORPORATION
Wilmington, Mass.
for

NATIONAL AERONAUTICS AND SPACE ADMINISTRATION • WASHINGTON, D. C. • SEPTEMBER 1966

TECH LIBRARY KAFB, NM
0099447

NASA CR-575

EVALUATION OF HIGH-TEMPERATURE GAS TRANSPORT PROPERTIES

Distribution of this report is provided in the interest of information exchange. Responsibility for the contents resides in the author or organization that prepared it.

Prepared under Contract No. NASw-1188 by
AVCO CORPORATION
Wilmington, Mass.

for

NATIONAL AERONAUTICS AND SPACE ADMINISTRATION

For sale by the Clearinghouse for Federal Scientific and Technical Information
Springfield, Virginia 22151 – Price $3.00

CONTENTS

I. INTRODUCTION AND SUMMARY..... 1

A. Introduction..... 1
B. Summary..... 1

II. THE CALCULATION OF THERMAL CONDUCTIVITY FROM CONSTRICTED ARC DATA..... 6

III. EXPERIMENTAL APPARATUS AND MEASUREMENT TECHNIQUES..... 14

A. Experimental Apparatus..... 14

1. Nitrogen Arc..... 14
2. Hydrogen Arc..... 16
3. Power Supply..... 17
4. Optical System..... 18

B. Temperature Measurements..... 21
C. Voltage Gradient Measurements..... 30
D. Electrical Conductivity Data Analysis..... 36

1. Linear Approximation for σ..... 36
2. Energy Approximation for σ..... 38
3. Collisional Cross Section Approximation for σ.... 39

IV. DISCUSSION OF RESULTS..... 42

A. Nitrogen..... 42
B. Sensitivity of the Analysis..... 54

1. Input Power..... 54
2. Errors in the Temperature Profile..... 62
3. Visible Radiation..... 62
4. Vacuum Ultraviolet Continuum..... 65
5. Vacuum Ultraviolet Lines..... 67
6. Local Thermal Equilibrium..... 70

a. Influence of Column Voltage on LTE..... 71
b. Influence of Radial Temperature Gradients.... 73

C. Hydrogen..... 78

V. REFERENCES..... 85

APPENDICES

I. TREATMENT OF RADIATIVE TRANSPORT IN THE ARC COLUMN..... 87

II. RADIATION CALCULATIONS.....117

ILLUSTRATIONS

Figure 1: Cross Section of a Cylindrically Symmetric Arc Column..... 8

Figure 2: Diagram of the Constricted Arc Unit..... 15

Figure 3: Photograph of the Argon Arc at 60 Amperes and Atmospheric Pressure..... 19

Figure 4: Diagram of Optical System..... 20

Figure 5: Radial Temperature Distribution for 50- and 80-Ampere Nitrogen Arcs at a Pressure of 0.5 Atmosphere..... 22

Figure 6: Radial Temperature Distribution For 60- and 100-Ampere Nitrogen Arcs at a Pressure of 0.5 Atmosphere..... 23

Figure 7: Radial Temperature Distribution for 40-, 60-, and 100-Ampere Nitrogen Arcs at a Pressure of 1 Atmosphere..... 24

Figure 8: Radial Temperature Distributions for 50-, 80-, and 150-Ampere Nitrogen Arcs at a Pressure of 1 Atmosphere..... 25

Figure 9: Radial Temperature Distributions For 42-, 55-, and 72-Ampere Nitrogen Arcs at a Pressure of 2 Atmospheres..... 26

Figure 10: Radial Temperature Distributions of 1 Atmosphere Hydrogen Arc At Various Currents..... 27

Figure 11: Theoretical Hydrogen Continuum Intensity at 5500Å at a Pressure of One Atmosphere and and Intensity Curve Use in Error Analysis of The Measurement of Thermal Conductivity..... 28

Figure 12: Comparison of Our Data and That of Wiese for the Radial Temperature Distribution of a 40-Ampere Hydrogen Arc at One Atmosphere Showing the Effect of Bulging on the Temperature Profile..... 29

Figure 13: Circuit for Measuring Voltage Gradients in an Arc Column..... 32

ILLUSTRATIONS (Cont'd)

Figure 14: Voltage Gradients as Determined by Various Methods of a One Atmosphere Hydrogen Arc..... 33

Figure 15: Voltage Gradients of a Nitrogen Arc as Determined by the Balanced Current Method..... 34

Figure 16: Linear Approximation to the Electrical Conductivity as Obtained by Using Various Cur-Off Temperatures from the Temperature Profiles of One Atmosphere Hydrogen Arcs Run at 20-, 30-, 40-, 50-, and 70-Amperes..... 36

Figure 17: Parabolic Approximation to the Electrical Conductivity Using Yos' Theoretical Value for Thermal Conductivity and Data Obtained from 30-, 40-, 50-, and 70-Ampere Hydrogen Arc Runs at One Atmosphere. Also Included Are the Curve Fitted Results Obtained by Determining the Necessary Electron-Neutral and Electron-Ion Collisional Cross-Sections... 40

Figure 18: Thermal Conductivity of Nitrogen at 0.5 Atmosphere from the Calculated-Current Method Without the Inclusion of Radiative Losses..... 43

Figure 19: Thermal Conductivity of Nitrogen at 1 Atmosphere from the Calculated-Current Method Without the Inclusion of Radiative Losses..... 44

Figure 20: Thermal Conductivity of Nitrogen at 2 Atmospheres from the Calculated-Current Method Without the Inclusion of Radiative Losses..... 45

Figure 21: Thermal Conductivity of Nitrogen at 1 Atmosphere Obtained Utilizing the Arc Column Radiative Transfer Calculations For $\lambda > 0.0$Å..... 46

ILLUSTRATIONS (Cont'd)

Figure 22: Power/Unit Length vs. r for the Various Power Transport Mechanisms in a 100-Ampere Nitrogen Arc at One Atmosphere.... 50

Figure 23: Power/Unit Length vs. r for the Various Power Transport Mechanisms in a 100-Ampere Nitrogen Arc at One Atmosphere.... 51

Figure 24: Power/Unit Length vs. r for the Various Power Transport Mechanisms in a 50-Ampere Nitrogen Arc at One Atmosphere..... 52

Figure 25: Power/Unit Length vs. r for the Various Power Transport Mechanisms in a 50-Ampere Nitrogen Arc At One Atmosphere..... 53

Figure 26: Effect of Variation of Input Power on Calculated Thermal Conductivity..... 55

Figure 27: Electrical Conductivity Deduced from Arc Column Temperature Profiles of Nitrogen at One Atmosphere..... 58

Figure 28: Power/Unit Length vs. r for the Various Power Transport Mechanisms in a 100-Ampere Nitrogen Arc at One Atmosphere.... 59

Figure 29: Power/Unit Length vs. r for the Various Power Transport Mechanisms in a 50-Ampere Nitrogen Arc at One Atmosphere..... 60

Figure 30: Radial Temperature Distribution of 50-Ampere Hydrogen Arc at One Atmosphere Used in Determining Effect of Error in Temperature Profile on Calculated Thermal Conductivity... 63

Figure 31: Illustration of the Effect of Using Different Temperature Profiles in the Calculation of Thermal Conductivity..... 64

ILLUSTRATIONS (Cont'd)

Figure 32: Vacuum Ultraviolet Continuum Compared with Burgess and Seaton at 12,000°K, One Atmosphere..... 66

Figure 33: Radiative Loss Averaged over the Spectral Range 0.1 to 0.2μ at 12,000°K with $\varepsilon = 1.0$..... 68

Figure 34: Degree of Inequilibrium of Hydrogen and Nitrogen Arcs at Various Currents and One Atmosphere Pressure as Determined Using the Arc Column Voltage Gradient..... 72

Figure 35: Calculated Equilibrium Distances in One Atmosphere Nitrogen and Hydrogen Arcs as a Function of Arc Central Core Temperatures..... 75

Figure 36: Degree of Inequilibrium of Hydrogen and Nitrogen Arcs at Various Currents and One Atmosphere Pressure as Determined Using the Average Equilibrating Distance..... 76

Figure 37: Degree of Inequilibrium of Hydrogen and Nitrogen Arcs at Various Currents and One Atmosphere Pressure as Determined by the Average Equilibrating Distance Relaxed by a Factor of Ten..... 77

Figure 38: Power/Unit Length vs. r for Various Power Transport Mechanisms in a 50-Ampere Hydrogen Arc at One Atmosphere..... 79

Figure 39: Power/Unit Length vs. r for Various Power Transport Mechanisms in a 70-Ampere Hydrogen Arc at One Atmosphere..... 80

Figure 40: Experimental Thermal Conductivity of Hydrogen as Calculated Using the Data of One Atmosphere Hydrogen Arc Runs of 40-, 50-, and 70-Amperes..... 83

ILLUSTRATIONS APPENDIX I

Figure I-1: Kernel for Radiative Transport Calculation.... 94

Figure I-2: Illustration of Straight Line Dependence of Temperature vs. r^2 Using As An Example the 20-, 30-, and 40-Ampere Hydrogen Arc Runs at One Atmosphere..... 98

Figure I-3: Evaluation of the Lorentzian Profile Integral as a Function of the Optical Depth Parameter.....104

Figure I-4: Evaluation of the Doppler Profile Integral as a Function of the Optical Depth Parameter.....106

Figure I-5: Error in Frequency Integration vs. Parameter Values for Continuum Radiation ($m = 0, \gamma = 8$, Two Terms in Gaussinan Quadrature; $n = 0$, $\gamma = .5$, Three Terms in Gaussian Quadrature).....109

Figure I-6: Error in Frequency Integration vs. Parameter Values for Continuum Radiation ($n = 0$, $\gamma = .8$, Two Terms in Gaussian Quadrature; $n = 0$, $\gamma = 0$, Three Terms in Gaussian Quadrature).....110

Figure I-7: Error in Frequency Integration vs. Parameter Values for Continuum Radiation ($n = 3$, $\gamma = .8$, Two Terms in Gaussian Quadrature).....111

Figure I-8: Error in Requency Integration vs. Parameter Values for Continuum Radiation ($n = 3$, $\gamma = .5$, Three Terms in Gaussian Quadrature)...112

Figure I-9: Error in Frequency Integration vs. Parameter Values for Continuum Radiation ($n = 3$, $\gamma = 0$, Three Terms in Gaussian Quadrature).....113

Figure I-10: Error in Frequency Integration vs. Parameter Values for Continuum Radiation ($n = 3$, $\gamma = 0$, Four Terms in Gaussian Quadrature).....114

ILLUSTRATIONS APPENDIX II

Figure II-1: Emission Coefficient of One Atmosphere Nitrogen for λ>2000Å Used in Calculation of Thermal Conductivity of Nitrogen.....122

Figure II-2: Emission Coefficient of One Atmosphere Nitrogen for λ>2000Å Used in Calculation of Thermal Conductivity of Hydrogen.....123

TABLES

Table I: Analysis of 50- and 100-Ampere Nitrogen Arc Runs...47

I. INTRODUCTION AND SUMMARY

A. Introduction

This is the final summary report submitted under contract NASw-1188, Evaluation of High Temperature Gas Transport Properties. The objectives of this program have been to determine the reason for the discrepancy between the theoretically calculated values of the thermal conductivity of high temperature nitrogen and the values for this quantity determined from measurements in the wall stabilized constricted arc; and, if and when the discrepancy is resolved, to use the wall stabilized constricted arc for experimental measurement of the transport properties of high temperature air. This program is sponsored by the Office of Advanced Research and Technology of NASA, and is a part of the Physics of Fluids program, of which Mr. Alfred Gessow is Chief.

The work reported here has been performed by personnel of the Research and Technology Laboratory of the Avco Space Systems Division. In particular, participants in the program have been Messrs. J. C. Morris, R. Rudis, and R. Liebermann, and Drs. J. Yos and C. F. Knopp. Dr. Stewart Bennett has been Program Director.

B. Summary

At the conclusion of a preceding program (contract NASw-916) in this technical area, several key facts had been established. First, fairly refined analytical estimates of the thermal conductivity of nitrogen had been made, and the effect of this substantial

improvement in the accuracy of the calculations was to adjust the previously estimated thermal conductivity by amounts of the order only of 35% (varying somewhat with the temperature at which the calculations are made). Second, experimental measurements had been made of the thermal conductivity of argon and nitrogen using the wall stabilized constricted arc at a pressure of one atmosphere, and these values agreed well with the results of previous investigators employing similar techniques, but poorly with the theoretical values; the disagreement with theory in nitrogen was much greater than the disagreement in argon, being of the order of a factor of 10 at temperatures of about 15,000°K. Third, a possible source of this discrepancy had been noted, namely, energy transfer by ultraviolet radiation (which is important at high temperatures in nitrogen), which would escape from the central region of the arc discharge, but which would not be detected outside of the apparatus. Thus, ultraviolet radiation comprises a mode of energy transfer which would not be noted in the experiments of other investigators and at this laboratory; and, if the energy transfer actually due to ultraviolet radiation was ascribed instead to thermal conductivity, this would result in measured thermal conductivity values much higher than the actual value.

The effort under the present program has been directed toward establishing whether, indeed, ultraviolet radiation by itself can account for the discrepancy between the measured and calculated values of thermal conductivity of nitrogen. To this end several paths of investigation have been followed.

Initially, efforts were made to operate the arc at pressures above and below one atmosphere, to discern if the discrepancy between theory and experiment varied as a function of pressure. The reasoning behind this approach is that radiation intensity is, in general, a strong function of pressure for a gas while the thermal conductivity is much more slowly varying in the pressure range being investigated. Thus, at low pressures the radiation should be much reduced and at high pressures much enhanced, while the thermal conduction should change little; consequently, it would be anticipated that the discrepancy should be smaller at low pressures and larger at high pressures. In practice, this has turned out not to be a useful method of evaluating the importance of radiation. For, at very low pressures the arc column departs significantly from local thermal equilibrium, and very high pressures result in strong self-absorption of radiation. Thus, the accessible pressure range is not large and physical phenomena other than the one of interest vary significantly. This makes it extremely difficult to draw unambiguous conclusions, and this technique was not pursued further.

Subsequently, in a parallel program,[14] rather precise measurements have been made of the continuum radiation intensity from nitrogen in the spectral range of interest ($\lambda < .2\mu$). The mathematical techniques by which the data obtained under the present program are processed to obtain thermal conductivity values have been adjusted to account for self-absorption of ultraviolet radiation. The continuum radiation intensity obtained under the present program, and the agreement between theory and experimental

values of thermal conductivity of nitrogen has been significantly improved. However, a sizeable discrepancy still exists.

We have examined two possible sources of the remaining discrepancy; these are line radiation (which is currently not included in consideration of the ultraviolet portion of the spectrum), and uncertainties in the estimates of electrical conductivity which are used in analysis of the data. Estimates have been made of the total line bandwidth which would be required to account for the discrepancy, and are detailed in the text of this report. The electrical conductivities have been evaluated from the present data and agree reasonably well with the theoretical estimates which have been used in the analysis for thermal conductivities. Further, an alternate set of theoretical electrical conductivities, calculated by Ahtye of the NASA/Ames Research Center, have been used in the analysis for thermal conductivity. It does not appear from these analyses that any appreciable portion of the remaining discrepancy can be associated with the electrical conductivity.

Finally, experimental measurements using the same apparatus and techniques have been made of the thermal conductivity of hydrogen. Hydrogen was selected because all pertinent properties can be calculated with much more confidence than for other gases. Thus, if the discrepancy is due to a cause such as improper evaluation of the radiative energy transport, it should be greatly reduced in hydrogen, while if it is due to a basic experimental inadequacy, such as lack of equilibrium, convective energy transport, etc., then

the discrepancy would probably not be much reduced in hydrogen. The results reported here indicate that the agreement with theory is much better in hydrogen than in nitrogen, thus lending further support to the notion that ultraviolet radiation including lines is indeed the cause of the discrepancy.

II. THE CALCULATION OF THERMAL CONDUCTIVITY FROM CONSTRICTED ARC DATA

The Thermal conductivities of high temperature, highly ionized gases maybe obtained from measurements of voltage and temperature gradients of a cylindrically symmetric constricted arc.

In the absence of convection, the energy balance for an arc column may be written in the form

$$\int_0^r \sigma E^2 \, 2\pi r \, dr = 2\pi r (q_K + q_{rad}) \tag{1}$$

where $\int_0^r \sigma E^2 \, 2\pi r \, dr$ is the electrical energy input per unit length to the gas inside a cylinder of radius r, and

$$q_K = -K \frac{dT}{dr} \tag{2}$$

and q_{rad} are the energy fluxes per unit area across the boundary of the cylinder due to conduction and radiation, respectively. If the arc column is optically thin to the emitted radiation, the radiated flux q_{rad} may be written simply as an integral over the radiated power per unit volume inside the cylinder,

$$2\pi r \, q_{rad} = \int_0^r P_{rad} \, 2\pi r \, dr \tag{3}$$

and one obtains the ordinary, "optically thin" Elenbaas-Heller equation

$$\sigma E^2 = -\frac{1}{r}\frac{d}{dr}\left(r K \frac{dT}{dr}\right) + P_{rad} \tag{4}$$

which has been used to evaluate K from measured values of E and T(r)[1]. As indicated in reference 1, however, the approximation of optical thinness is not adequate for the treatment of the high-temperature nitrogen arc, since for this (and many other) gases there is a sizeable contribution to the total energy balance due to far ultraviolet radiation, for which the absorption length is comparable to or smaller than the arc dimensions. It was therefore necessary to modify the previous analysis of the arc data to take account of the effects of the absorption of radiation within the arc volume itself.

For the purposes of clarifying the discussions given in later sections of this report, a descriptive account is given below of the process of energy transfer within the arc column. Referring to figure 1, which is a cross section of a cylindrically symmetric arc column, consider the cylindrical shell of thickness dr which is shaded. Since we have assumed that there is no flow, and since the temperature in the shell is constant in time, the energy transfer by non-convective processes from the shell must exactly balance the rate at which energy is released within the shell, equation 1. Of the non-convective energy transfer processes which may occur, we include thermal conduction and emission and absorption of radiation, while energy release is considered to originate exclusively with joule heating.

Since the arc column temperature profiles T(r) are invariably monotonic, (see figure 7, for example) decreasing from a peak

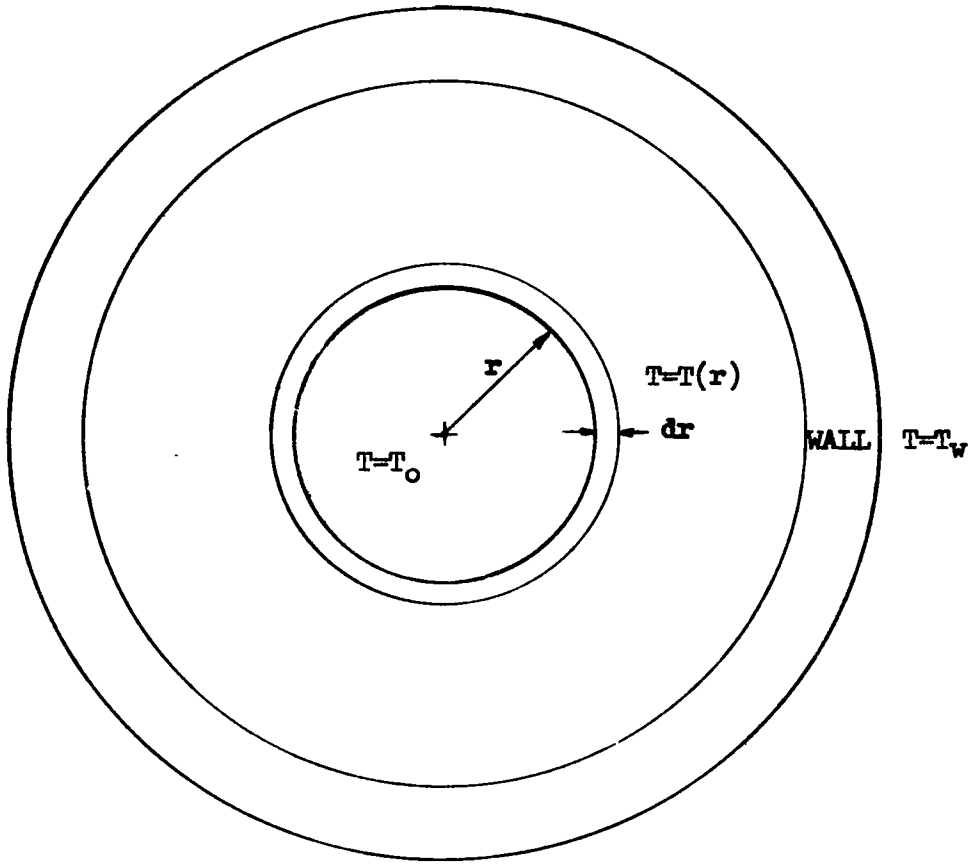

FIG. 1 . CROSS SECTION OF A CYLINDRICALLY SYMMETRIC ARC COLUMN

value T_o at the column centerline to the value of the wall temperature T_w at the wall boundary, the effect of thermal conduction is always to transfer heat out of the shell toward the wall. Similarly, the effect of radiation emission is always to transfer heat out of the shell, but this transfer is not necessarily toward the wall. The effect of radiation absorption within the shell is quite similar to the energy release by joule heating; that is, the energy absorbed must be transferred out of the shell in the steady state. Joule heating is given by the left hand of equation (1).

The energy released within a shell given by the right hand of equation 1 is determined by the integral of $\vec{j}\cdot\vec{E}$; assuming that the scalar form of Ohm's law is applicable, this is equivalent to σE^2, since $\vec{j} = \sigma\vec{E}$. The electrical conductivity σ is an input to the calculation, and the electric field strength E is a measured quantity in the experiment.

We can now consider a sample set of calculations for the thermal conductivity based upon a measured temperature profile, a measured voltage gradient E, and a set of values of the electrical conductivity as a function of temperature.

At first, one can assume that there is no radiation. In this case the energy balance equation has the simplest form, equation (4) and for each cylindrical shell the thermal conductivity must be such that the energy released in the entire arc discharge at smaller radii than the shell outer radius is conducted through the shell.

There is in fact no other way for this energy to leave the arc. Since the temperature gradients are measured everywhere, the thermal conductivity is then determined, and it must have values large enough to account for the complete transfer of energy from the arc to the wall.

Now assume that there is radiation, but no absorption. The energy release in each volume element of the arc is unchanged from the first case, because the temperatures and E are unchanged; there is now an energy transfer mechanism which operates in addition to thermal conduction. Since less energy must be transferred by thermal conduction than in the first case, and since the temperature gradients are unchanged from the first case, the thermal conductivities calculated in the second case will of necessity be smaller than in the first case.

Finally, one can assume both radiation and absorption. For each cylindrical shell there will be an amount of energy transferred in by thermal conduction from the portion of the arc lying at smaller radii, an amount transferred out by thermal conduction to portions of the arc lying at larger radii, an amount generated by joule heating within the shell, an amount lost by radiation from the shell, and an amount absorbed owing to radiation passing through the shell from other parts of the arc. The radiation and absorption are coupled for a given shell, since the same transition integrals in the oscillator strengths or transition probabilities are involved in emission and absorption of radiation.

The initial calculations of thermal conductivity performed under this program assumed radiation but no absorption. However, since only radiation in the wavelength range 0.25 to 6 microns was used, and since, for nitrogen at the arc conditions employed, there is relatively little radiation in this wavelength range (compared to the energy input per unit volume) there is little difference between calculations performed in this way and those performed neglecting radiation entirely. The thermal conductivities calculated in this way were quite high compared with theory, as was the case also with data reported by Maecker[2], a previous investigator.

At that time, a fairly careful investigation was made of possible sources of error in the experiment. Considerable attention was given to measuring the voltage gradient, to measuring the arc temperature profile in a number of ways to ensure local thermal equilibrium, to performing an error analysis of the calculational technique, to assuring that the arc had cylindrical symmetry, and to the theoretical values of the thermal conductivity themselves. No source of error was found of sufficient magnitude to account for the observed discrepancy in thermal conductivity.

From the nature of the calculation, which involves equating the energy input to a cylindrical shell in the arc to the energy output from the shell, it is clear that overly large values of the thermal conductivity can be obtained either if the energy input is overestimated or if there is a mechanism for energy transport from the arc column which has been neglected. In the

former case, unless the electric field strength has been measured incorrectly, the only possible source of error is in the assumed electrical conductivity of the plasma. We shall examine this point in more detail later in this report, but here we may say that an error in electrical conductivity large enough to account for the observed discrepancy is unlikely. Therefore, attention has been directed to energy transfer mechanisms other than those considered.

A particularly attractive mechanism is radiation in the ultraviolet portion of the spectrum, at wavelengths shorter than those measured up until recently at this laboratory. Earlier theoretical estimates[3,4] of the amount of this radiation indicate that it can be quite large at temperatures of the order of 12,000°K, typical of the region of interest to the present experiment.

The first treatment of the effect of this ultraviolet radiation was performed with the assumption of no absorption. The cross sections of Burgess and Seaton[3] were used to predict the continuum radiation, and a slight modification of the theory of Stewart and Pyatt[4] was used to predict the line radiation. With these values for vacuum ultraviolet radiation inserted into the analysis, the agreement between the new calculated values of thermal conductivity and the latest theoretical values was quite good. However, this treatment of the data is unsatisfactory on two counts. First, the estimates of vacuum ultraviolet radiation were not supported by experimental measurements. Second, it is expected that there would be some absorption of the radiation within the arc column so that the calculation was to this extent unrealistic even if the radiation values were correct.

After this initial calculation with vacuum ultraviolet radiation included we continued to refine the calculational procedure. Toward this end, we devise a computer program (see Appendix I) so that it treats continuum radiation correctly; that is, radiative transfer including emission and absorption processes. A detailed account of this new analysis and the computation procedure used to evaluate K from the experimental measurements of voltage gradients and temperature profiles in the arc column is given in Appendix I. The results of the new computations are discussed in Sections IV following a description of the apparatus and the measurements techniques.

III. EXPERIMENTAL APPARATUS AND MEASUREMENT TECHNIQUES

A. Experimental Apparatus

Although a description of the apparatus appears in references 5 and 6, it is repeated here for the sake of clarity and continuity; in addition, the modifications that were necessary in order to run hydrogen are included.

1. Nitrogen Arc

The wall-stabilized arc facility used in this program is shown schematically in figure 2. This arc is capable of sustaining an axis temperature of 14,000°K in nitrogen or oxygen with an arc diameter of 4.8 mm and a current of 150 amperes. The arc column is confined within a series of water-cooled, copper constrictors electrically insulated from one another by molded silicone rubber gaskets. The gaskets are pierced for observation windows so that the arc column may be observed between any two constrictors or between the electrodes and a constrictor. The width of each constrictor is 8 mm. The distance between adjacent constrictors is 1.25 mm, except in the case of the two constrictors between which the spectroscopic measurements are normally made. These have a separation of 0.25mm. The observation window for spectroscopic measurements is made of schlieren quality sapphire, while the other observation windows are fused silica.

The constrictors, electrode housings, and windows of the wall-stabilized arc are made gas-tight with the insulating gaskets. The various gas inlets and exits are metered with flow gauges and regulating valves which are used to control the pressure and flow

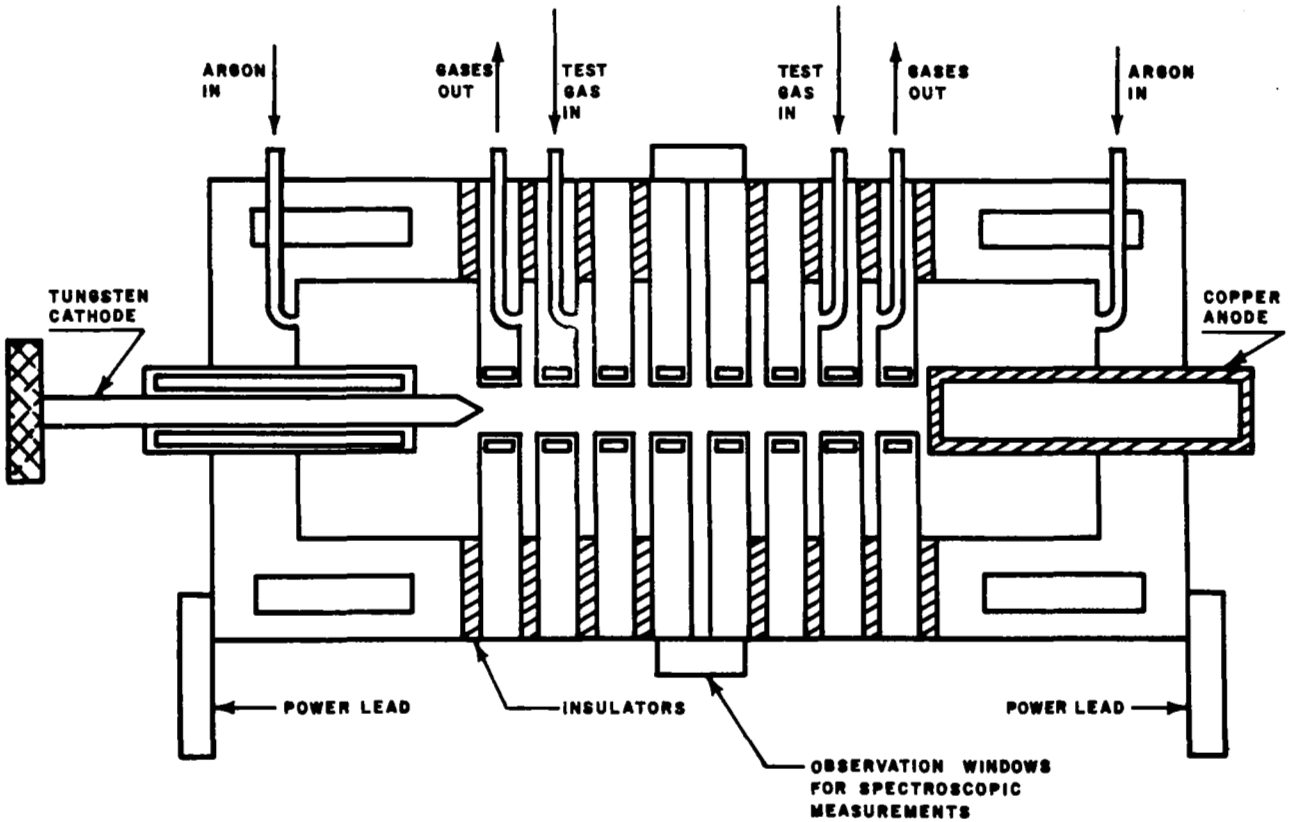

NOTE: SHADED AREAS INDICATE WATER COOLING PASSAGES

64-3213

Figure 2 DIAGRAM OF THE CONSTRICTED ARC UNIT

rates within the arc column. This arrangement allows the option of choosing any flow rate, ranging from stagnation to full flow through the observation chamber.

The correct pressure in the arc column is maintained with a needle valve located upstream of a mechanical vacuum pump in the case of 0.5-atmosphere runs, and by a needle valve exhausting to atmosphere for the 2-atmosphere tests. The pressure is monitored on a differential manometer which can be read to 1 mm Hg. This gives an accuracy of approximately $\pm$ 3 percent for the 0.5 atmosphere case and $\pm$ 1.5 percent for the 2-atmosphere case. In all cases, ambient atmospheric pressure was very close to the nominal value. No fluctuations in the pressure were discernible during any of the runs at either pressure. At each pressure, the cathode and anode of the arc are blanketed in argon to prevent the electrode erosion characteristic of high-current nitrogen arcs. Prior to each set of measurements, the flow rates of argon and nitrogen are adjusted such that there is no argon observed spectroscopically in the portion of the arc column used for the measurements.

2. Hydrogen Arc

Several modifications were necessary on the arc described above in order to run hydrogen. The bore diameter of the arc, which for nitrogen was 4.8 mm, was reduced to 3 mm. This was done since the hydrogen arc column runs in a more constricted manner than nitrogen for the same current. In addition, the gap between constrictors between which spectroscopic measurements were made, was increased to 1.25 mm. Little or no bulging was evident in spite of the increased distance between constrictors.

Due to the large voltage gradients in hydrogen a considerable power input was required. For example, at 20 amperes 1.87 Kw/cm was needed to sustain this hydrogen arc. As in the case for nitrogen the cathode and anode of the arc were blanketed with argon. Prior to each set of measurements, the flow rates of argon and hydrogen were adjusted such that there was no argon observed spectroscopically in the portion of the arc column used for the measurements.

3. Power Supply

Power for the arc is supplied by 84 truck batteries arranged in 4 banks of 21 batteries. These banks may be used in series or parallel combinations to obtain open circuit voltages of 252, 504, or 1008 volts. The line batteries are charged by a three-phase rectifier on the 220-volt ac service line.

Gross adjustments to the arc current are made with two variable, air-cooled ballast resistors, each capable of carrying 200 amperes. Fine adjustment and regulation of the arc current is accomplished by a water-cooled stainless steel tube with a sliding contact. Regulation is provided by a potentiometric reading of the difference in voltage across a precision shunt in the arc power lead and a pre-set reference voltage. The voltage difference is displayed upon a rotating beam galvanometer. As the beam swings to pre-set limits, photoconductive cells actuate the sliding contact on the stainless steel tubing. Using this system, it is possible to maintain constant arc current to within $\pm$ 0.001 ampere.

4. Optical System

A photograph of the arc operating in argon at atmospheric pressure and a current of 60 amperes is shown in figure 3

A 0.75-meter, f/10 grating monochrometer employing a Czerny-Turner mounting is used to obtain the spectroscopic measurements necessary for the determination of radial temperature distributions within the arc column. This instrument, which was constructed in our laboratory, has a reciprocal linear dispersion of 10.8 A/mm in the first order at 4000A. The radiation detector is an RCA type 1P21 or EMI type 6255B photomultiplier. The photomultiplier power supply has 0.01-percent regulation and ripple suppression. The photomultiplier signal is measured and amplified by a pico-ammeter having a linearity of 2 percent. The output signal of the amplifier is digitized and, along with the gain of the amplification system, punched onto computer cards in a semi-automatic manner.

Figure 4 depicts the optical system used to obtain the integrated intensity distribution of a spectral line or continuum band. The image of the arc column is focused upon the entrance slit of the monochrometer by the imaging lens. This lens is apertured to alleviate distortion and to provide a large depth of of field sufficient to ensure that both the front and back of the arc column are in focus when the lens is focused on the axis of the arc column.

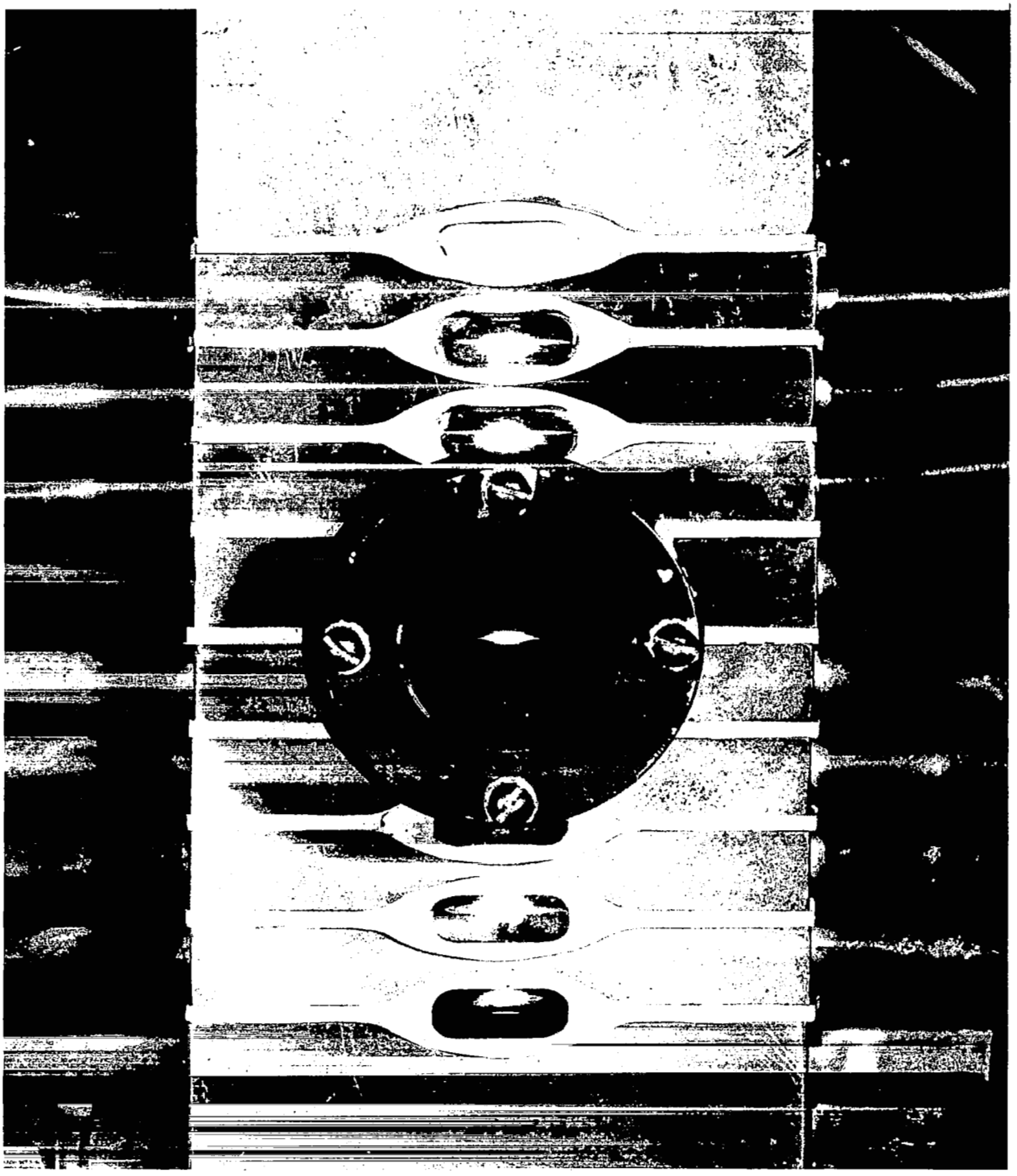

Figure 3 PHOTOGRAPH OF THE ARGON ARC AT 60 AMPERES, ATMOSPHERIC PRESSURE

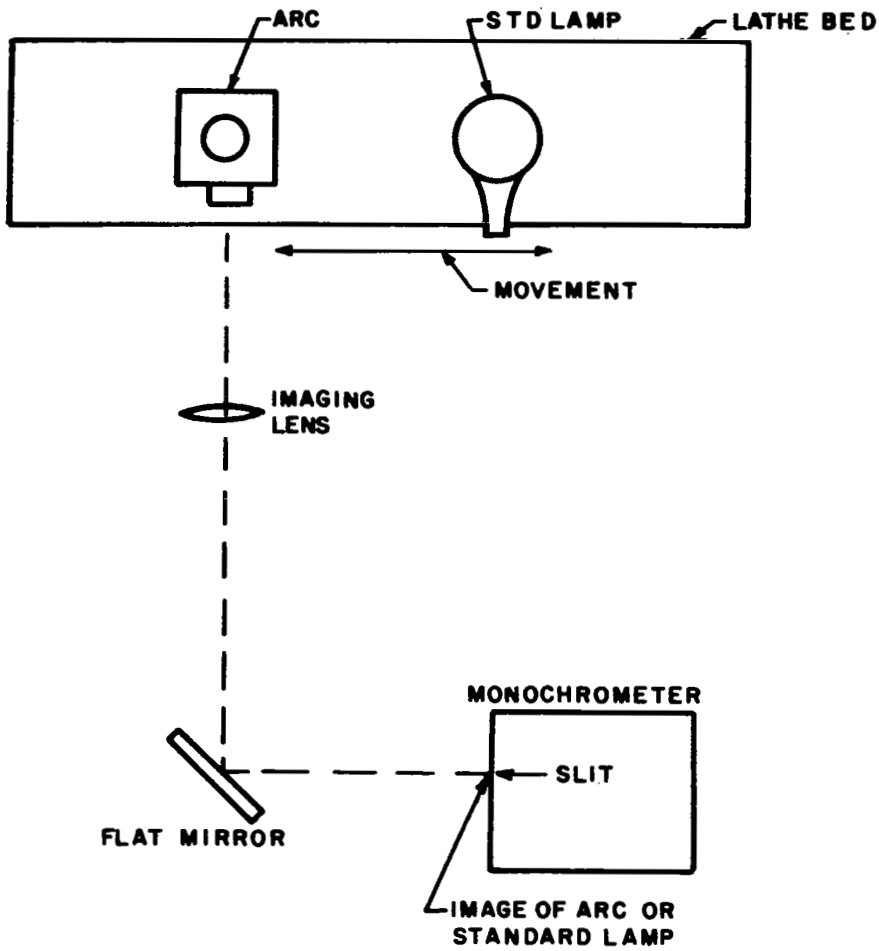

Figure 4 DIAGRAM OF OPTICAL SYSTEM

The arc column is imaged upon the entrance slit of the monochrometer in such a way that the axis of the arc is parallel to the entrance slit. Spatial resolution is accomplished by the use of a 25 micron entrance slit combined with a 0.65 mm slit placed in the same plane and perpendicular to the entrance slit. Based upon the effective slit widths and the magnification of the optical system, this arrangement provides an effective spatial resolution of approximately 0.2 mm along the axis of the column and approximately 0.05 mm perpendicular to the axis.

Calibration of the electronic and optical systems is provided by an NBS tungsten standard lamp located at the same position as that normally occupied by the arc facility.

B. Temperature Measurements

The temperature profiles shown in figures 5 through 9 for nitrogen and figure 10 for hydrogen were obtained from measurements of the continuum intensities (figure 11) which had been calibrated from the absolute intensities of atomic lines. The hydrogen continuum at 5500Å was calibrated against the H_β line intensity and the nitrogen 4955 continuum against the 4935Å line intensity.

Figure 12 comparison of our data with that of Wiese for the radial temperature distribution of a 40-ampere arc at one atmosphere and also shows the effect of bulging on the temperature profile.

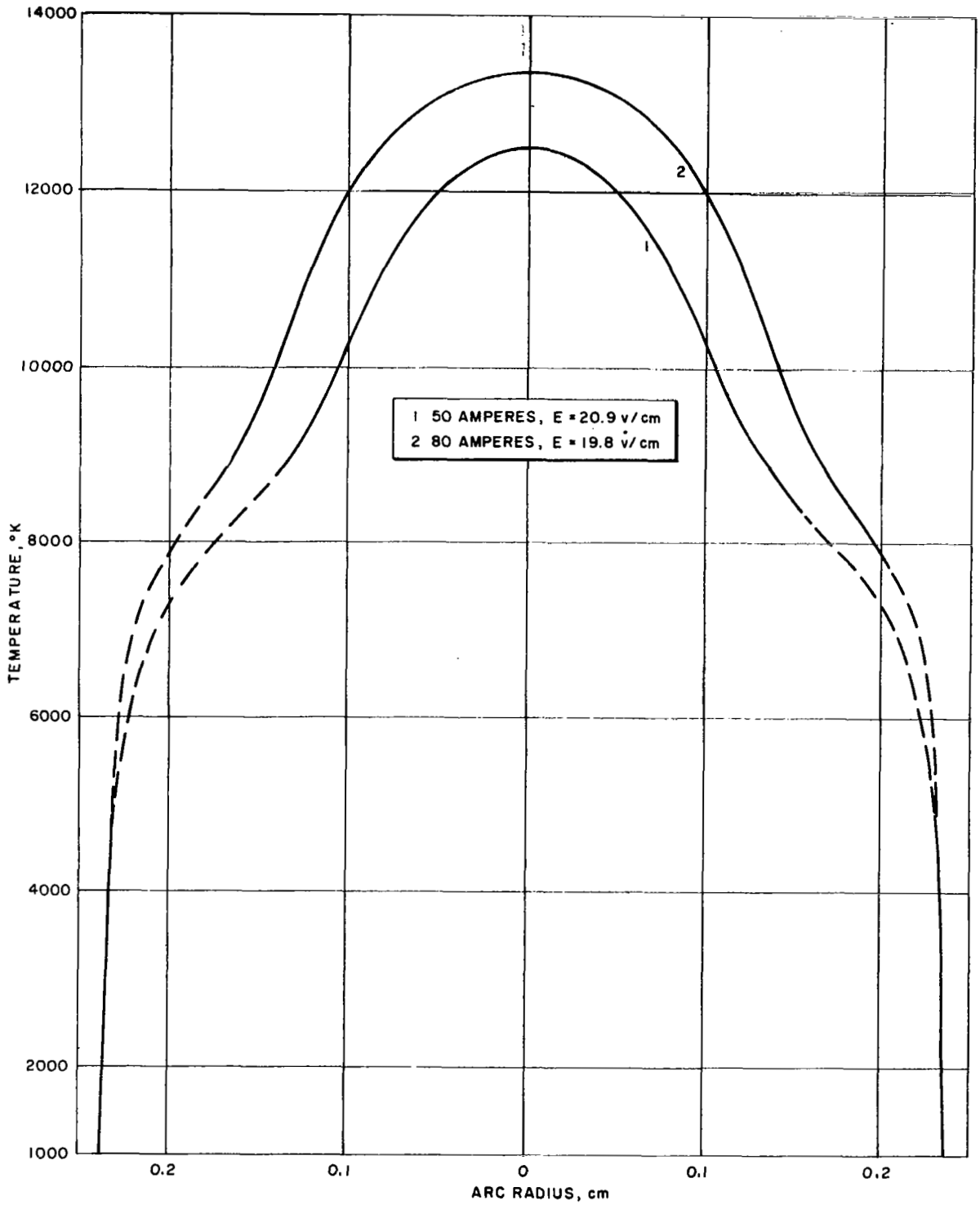

65-11610

Figure 5 RADIAL TEMPERATURE DISTRIBUTIONS FOR 50- AND 80- AMPERE NITROGEN ARCS AT A PRESSURE OF 0.5 ATMOSPHERE

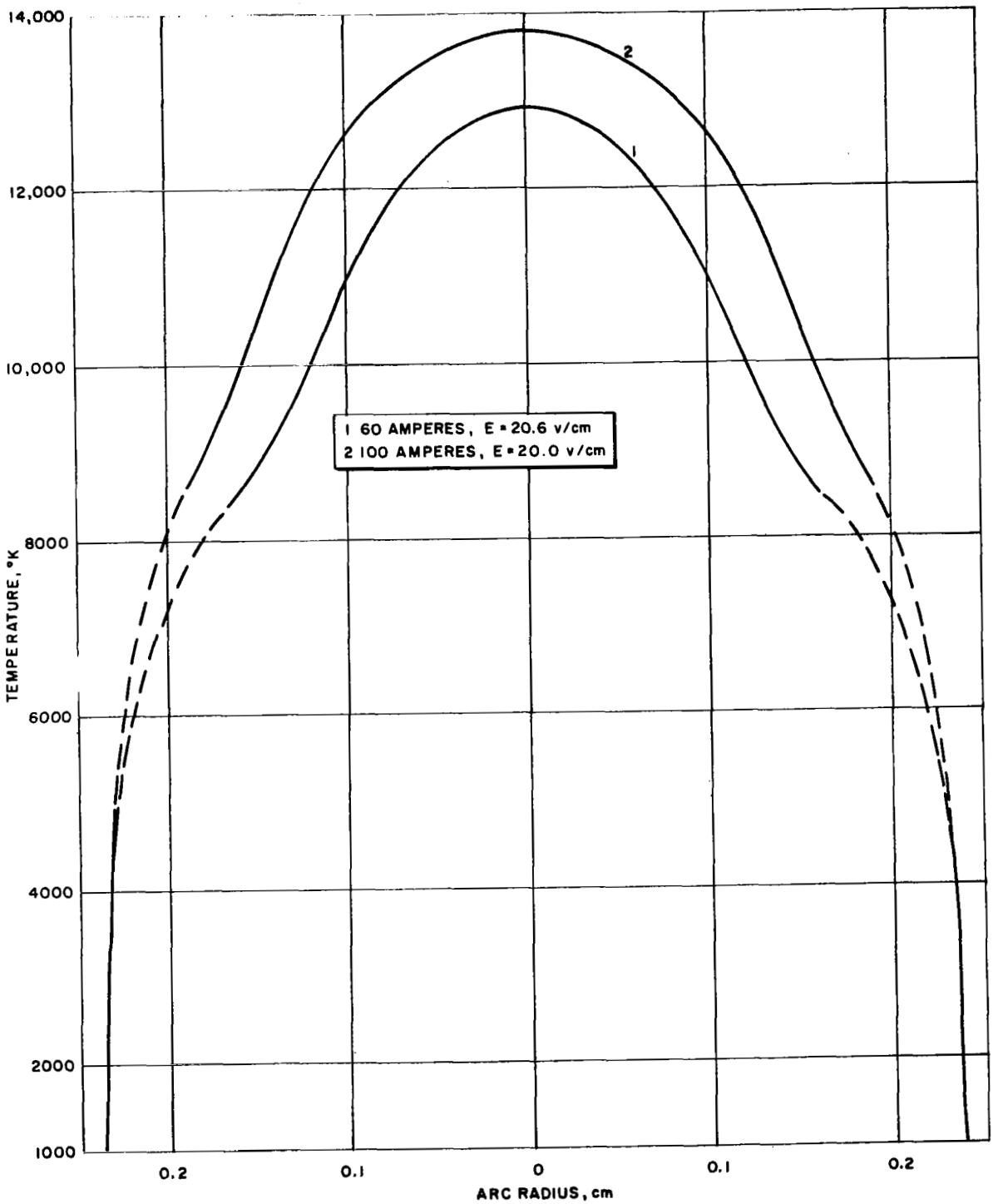

65-11611

Figure 6 RADIAL TEMPERATURE DISTRIBUTIONS FOR 60- and 100- AMPERE NITROGEN ARCS AT A PRESSURE OF 0.5 ATMOSPHERE

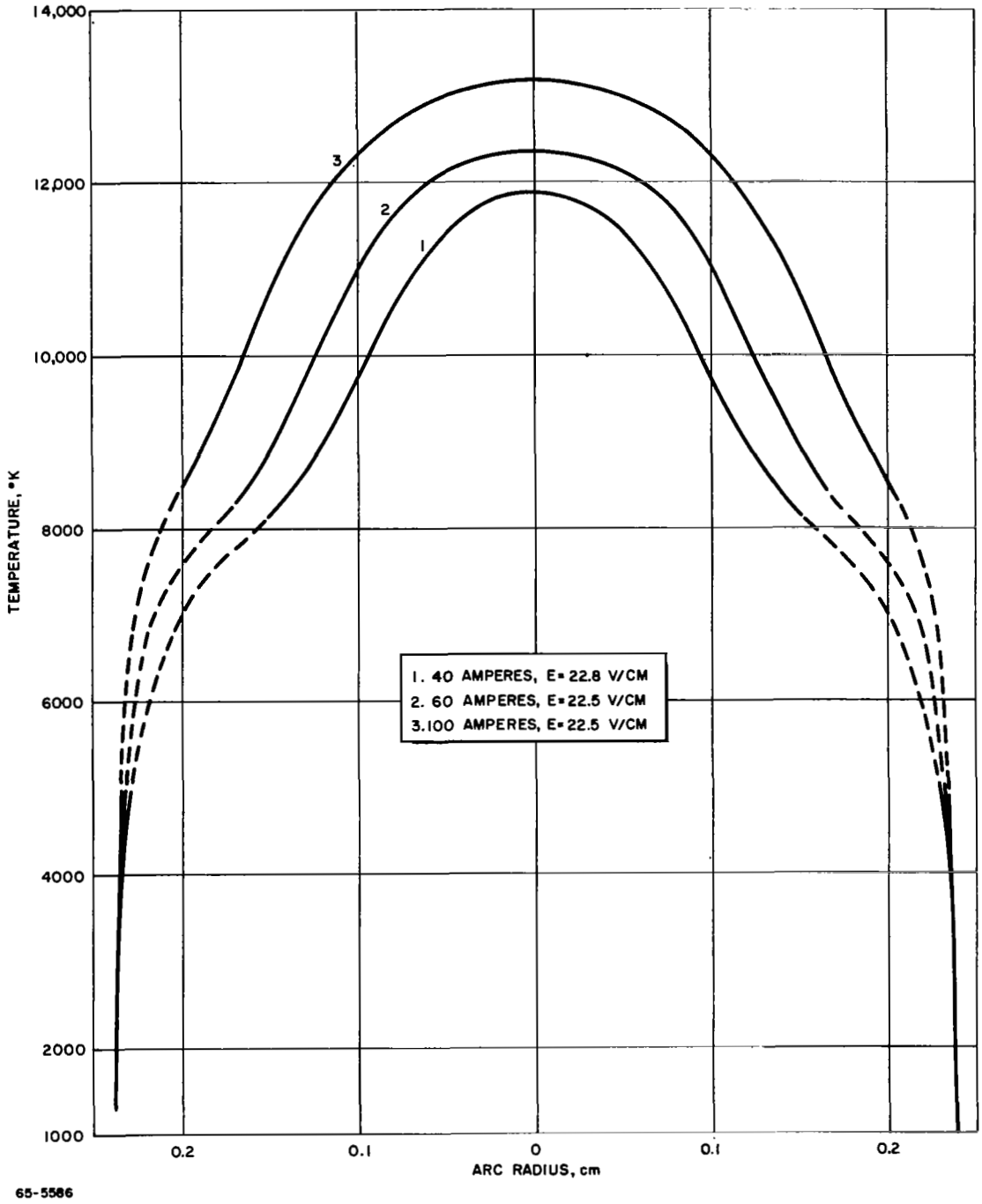

Figure 7 RADIAL TEMPERATURE DISTRIBUTIONS FOR 40-, 60-, AND 100-AMPERE NITROGEN ARCS AT A PRESSURE OF 1 ATMOSPHERE

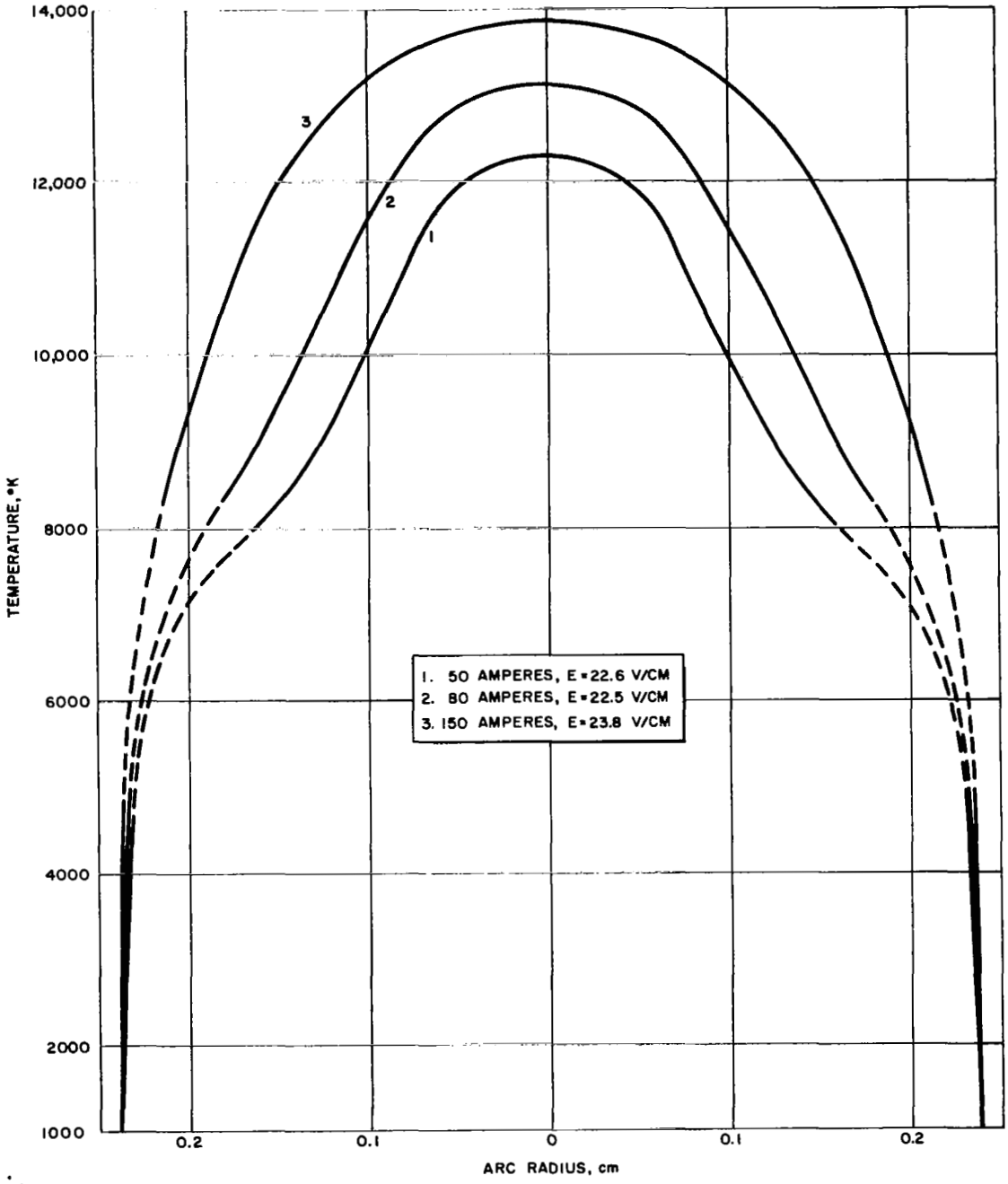

65-5587

Figure 8 RADIAL TEMPERATURE DISTRIBUTIONS FOR 50-, 80-, AND 150-AMPERE NITROGEN ARCS AT A PRESSURE OF 1 ATMOSPHERE

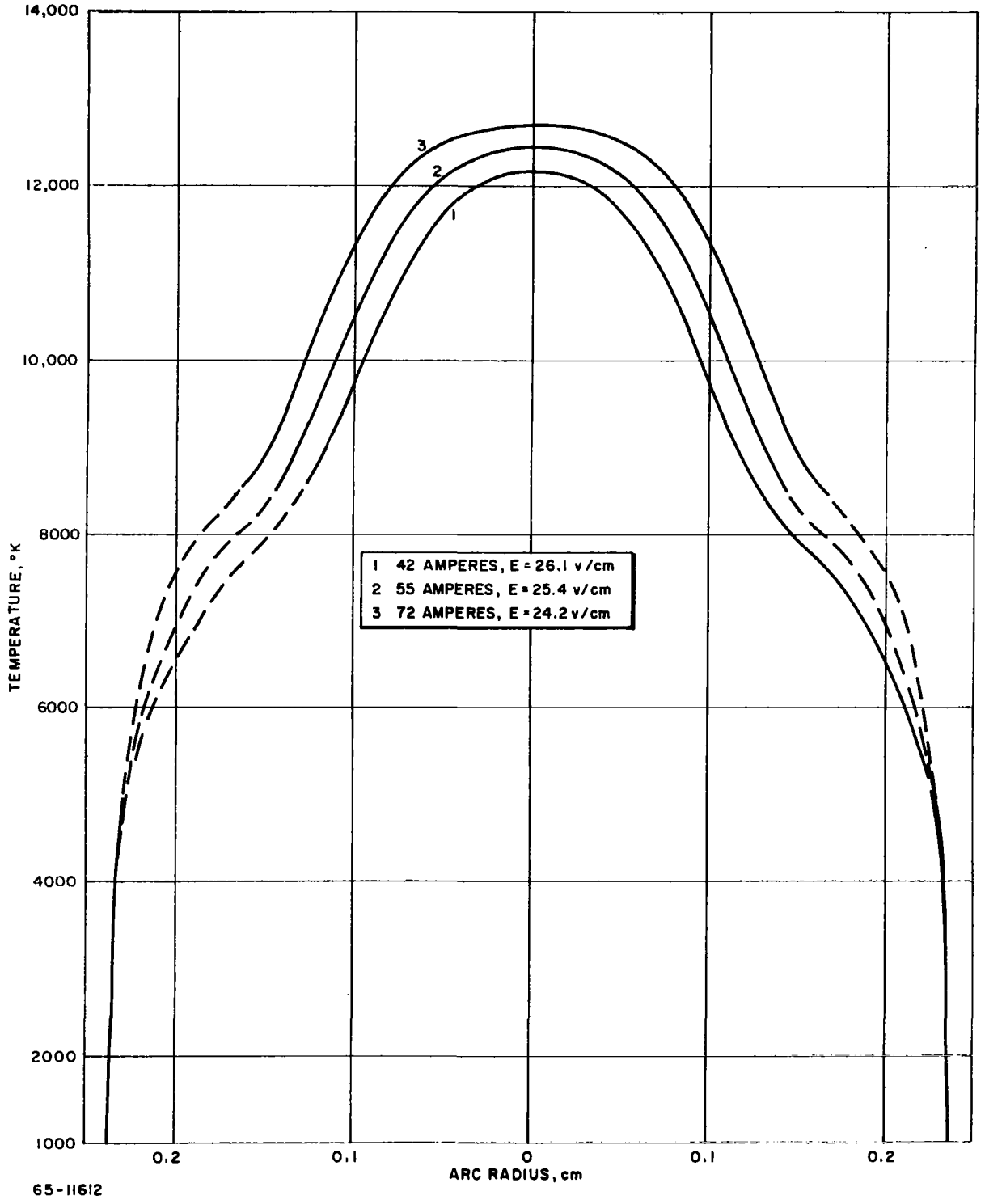

Figure 9 RADIAL TEMPERATURE DISTRIBUTIONS FOR 42-, 55-, AND 72-AMPERE NITROGEN ARCS AT A PRESSURE OF 2 ATMOSPHERES

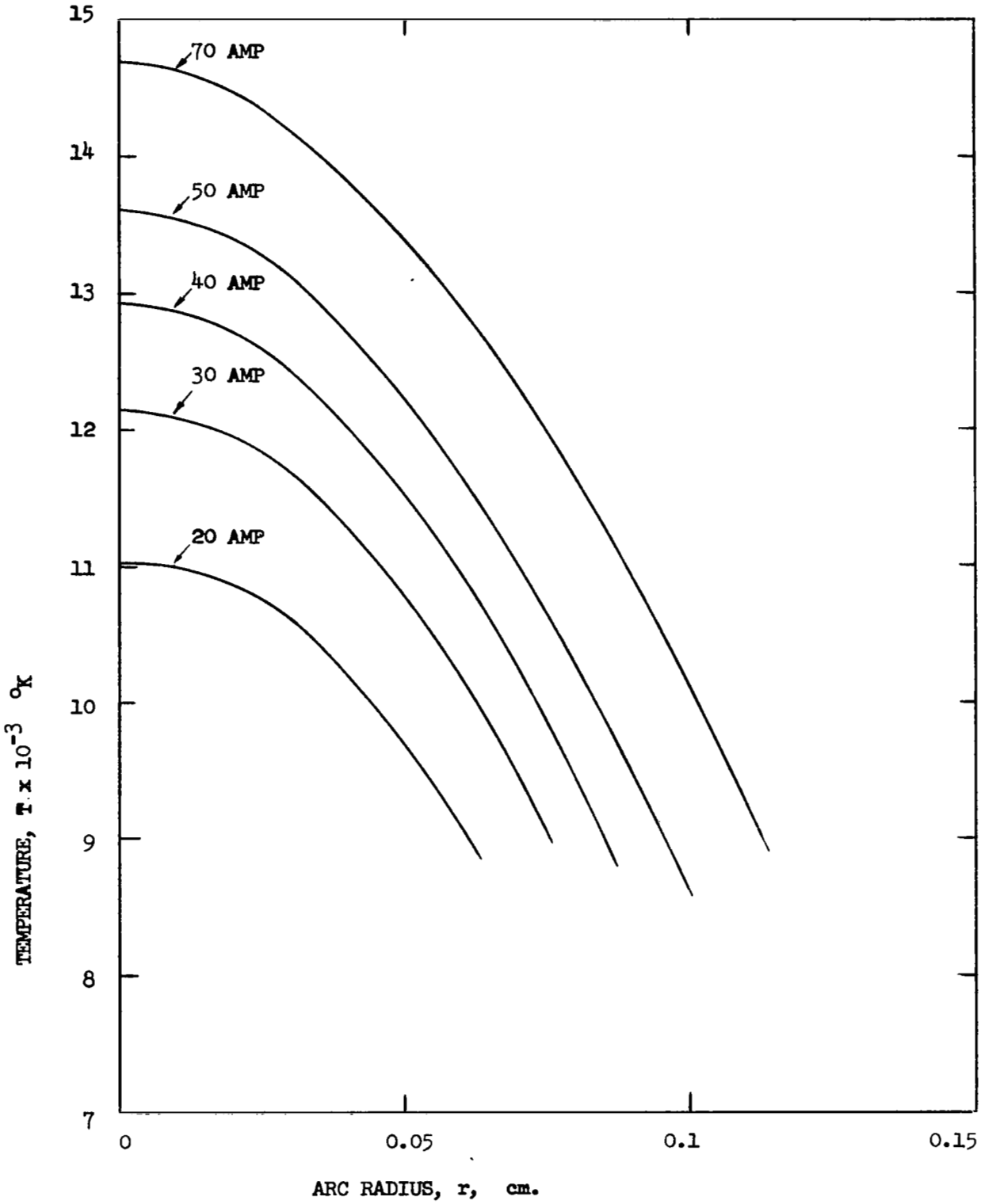

FIG. 10. RADIAL TEMPERATURE DISTRIBUTIONS OF 1 ATMOSPHERE HYDROGEN ARCS AT VARIOUS CURRENTS.

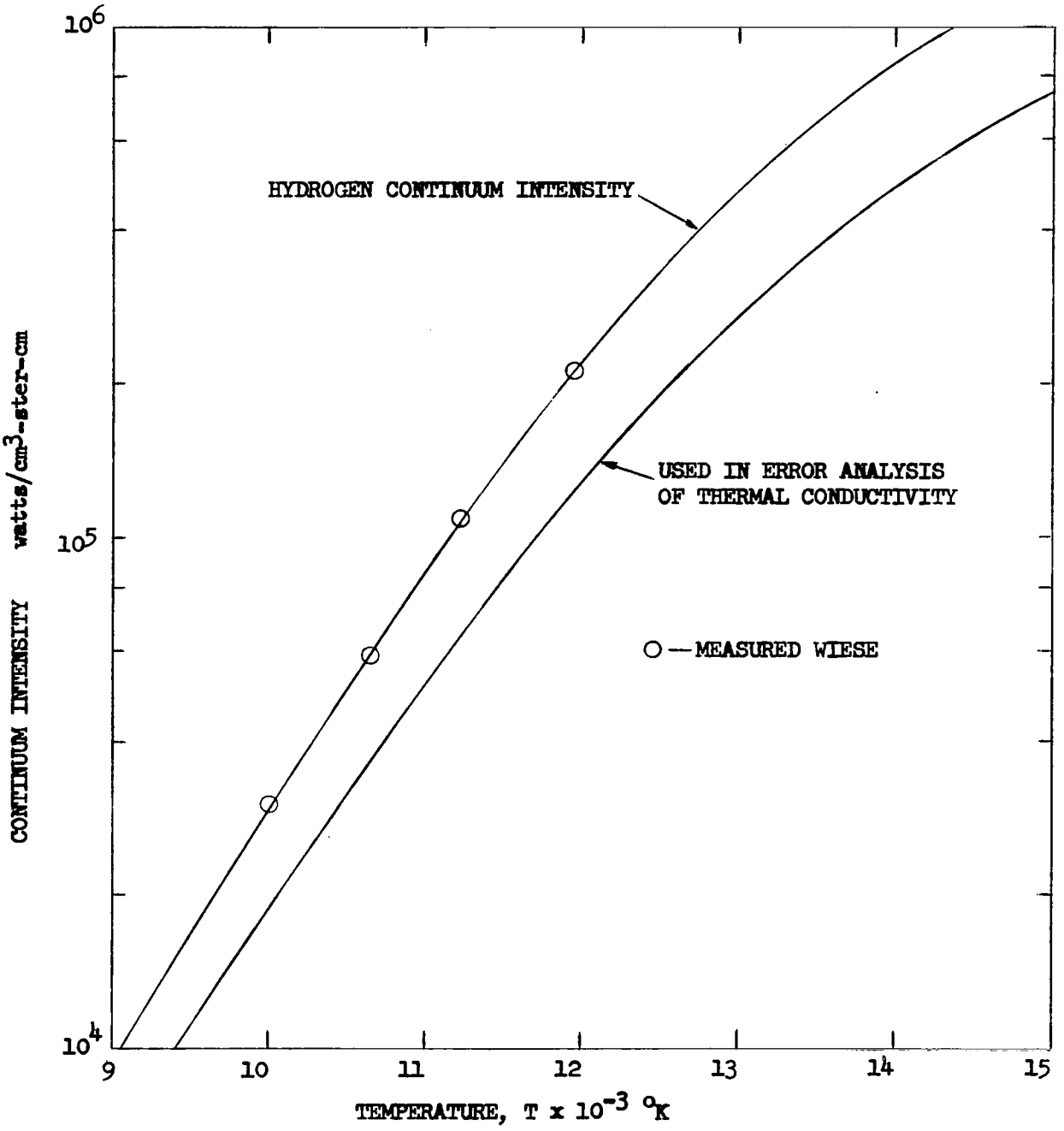

FIG. 11. THEORETICAL HYDROGEN CONTINUUM INTENSITY AT 5500 Å AT A PRESSURE OF ONE ATMOSPHERE AND THE INTENSITY CURVE USED IN THE ERROR ANALYSIS OF THE MEASUREMENT OF THERMAL CONDUCTIVITY.

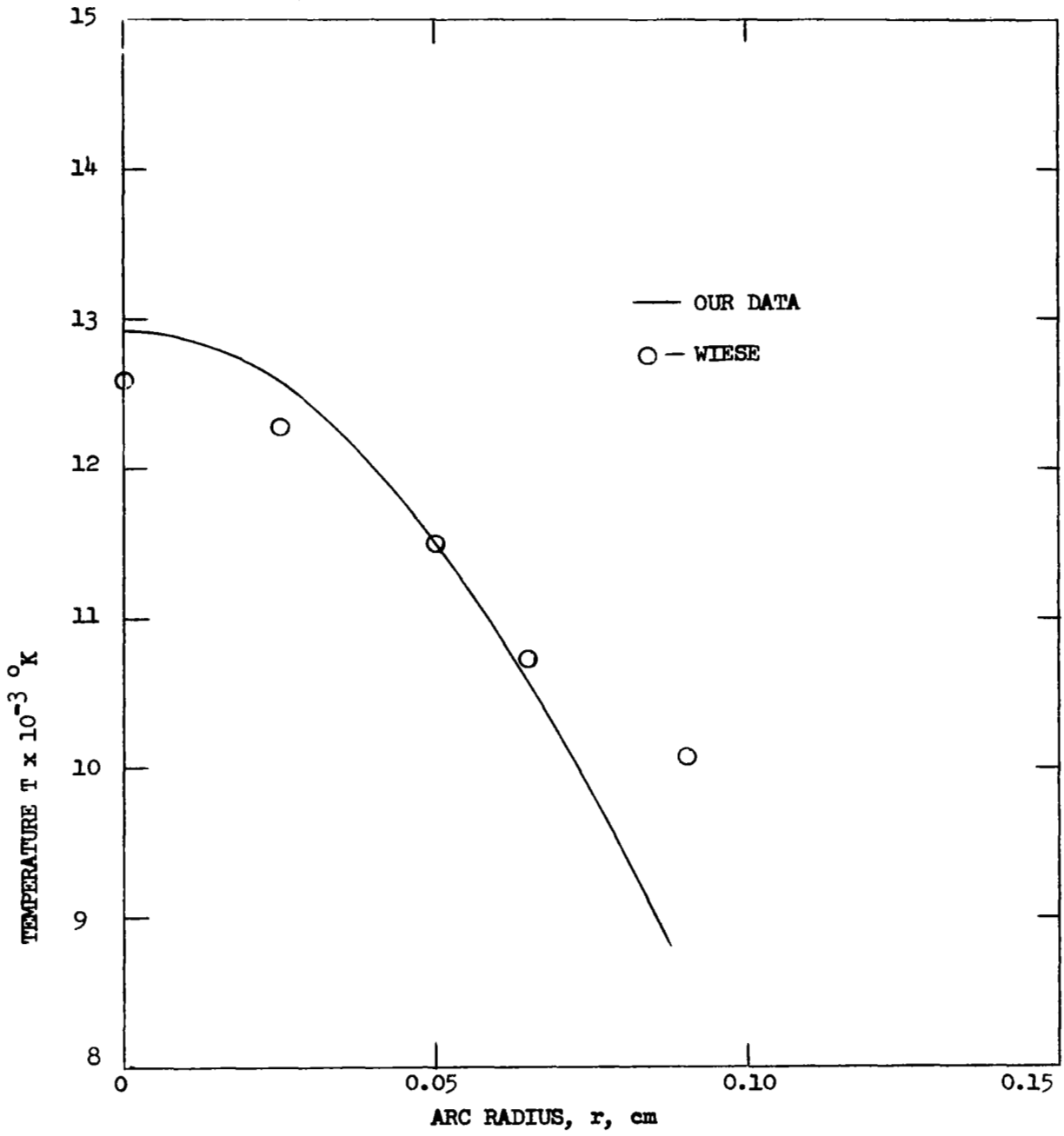

FIG. 12. COMPARISON OF OUR DATA AND THAT OF WIESE FOR THE RADIAL TEMPERATURE DISTRIBUTION OF A 40 AMPERE HYDROGEN ARC AT ONE ATMOSPHERE SHOWING THE EFFECT OF BULGING ON THE TEMPERATURE PROFILE

The standard relationship for the temperature dependence of an optically thin line is:

$$I = \int_0^\infty \frac{hc}{4\pi\lambda} Ag \frac{N(T)}{U(T)} e^{\frac{E}{KT}} L(\lambda) d\lambda \frac{\text{watts}}{\text{cm}^3\text{-ster}} \qquad (5)$$

where

h = Planck's constant

c = velocity of light

λ = wavelength

g = statistical weight of the upper level

E = energy of upper level

K = Boltzmann's constant

N(T) = specie number density

U(T) = specie partition function

A = transition probability

$L(\lambda)$ = the line shape parameter

The transition probabilities for the lines used were 1.93×10^6 sec^{-1} for 4935Å NI and 8.37×10^6 sec^{-1} for H_β 4861Å. The composition calculations used were those of Drellishak[7] and Burnhorn and Wienecke[8] respectively.

C. Voltage Gradient Measurement

The voltage gradients in the hydrogen and nitrogen arcs were measured using the balanced current method. This method which employs the circuit shown in figure 13, utilizes the constrictors at each end of the column of test gas as probes. A

small amount of current is supplied to the arc at these constrictors and is balanced so that the effect of the contact resistance of the probes, even if it is extremely high, is negligible; consequently the voltmeter reads the true voltage difference across the constrictors. This method of obtaining the voltage gradient was compared with two other techniques using hydrogen as the plasma source. The second method used a voltmeter with a resistance of 5×10^6 ohms to measure the voltage between constrictors of the arc. While this method gave results which agreed well with results obtained by other means, errors could have been introduced from high contact resistance between the constrictors and the arc column. The third method employed a calorimetric technique which served as an independent test of the measurements obtained from the two electric methods. Two center arc sections were isolated and used as a calorimeter. The temperature of the input and output flow of cooling water through these sections was monitored as well as the flow rate. The power input to these sections was converted to power per unit length which was divided by the current to obtain the voltage gradient. The results obtained are shown in figure 14 and are in reasonable agreement with the direct electric measurements. The voltage gradients of nitrogen arcs at various pressures as measured by the balanced current method are shown in figure 15.

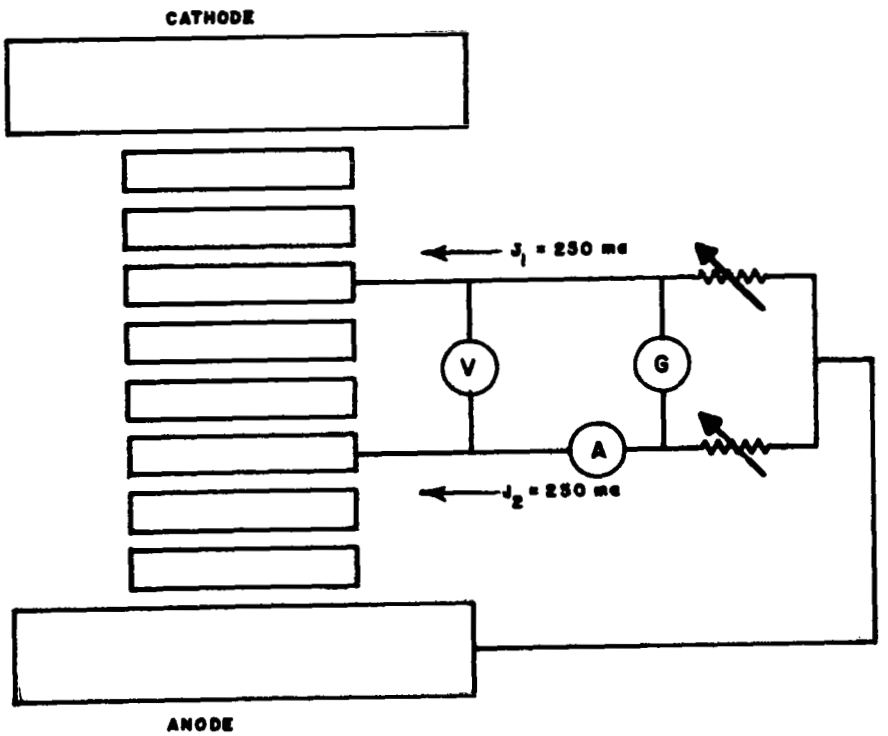

65-5588

Figure 13 CIRCUIT FOR MEASURING VOLTAGE GRADIENTS IN THE NITROGEN ARC COLUMN

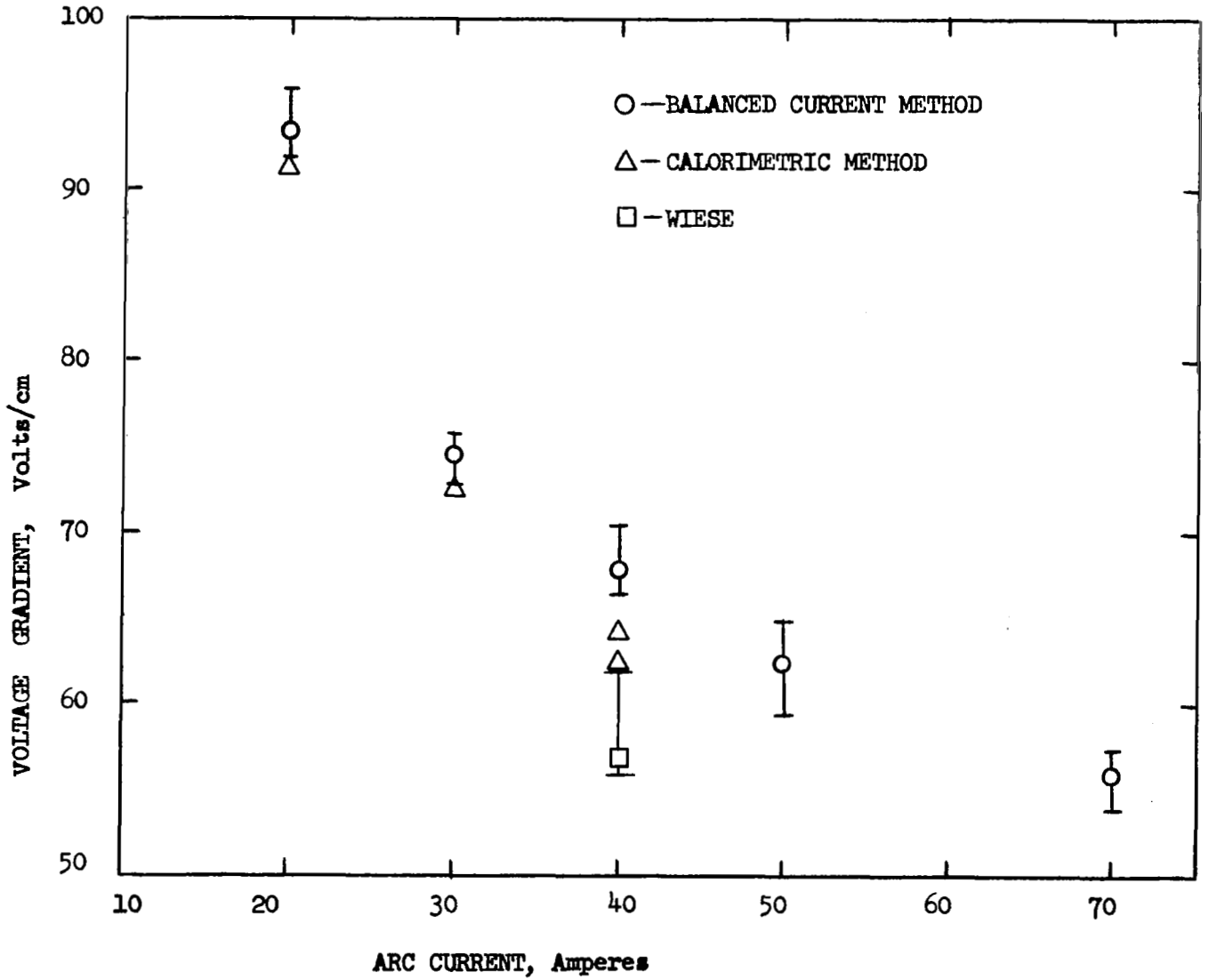

FIG. 14. VOLTAGE GRADIENTS AS DETERMINED BY VARIOUS METHODS OF A ONE ATMOSPHERE HYDROGEN ARC.

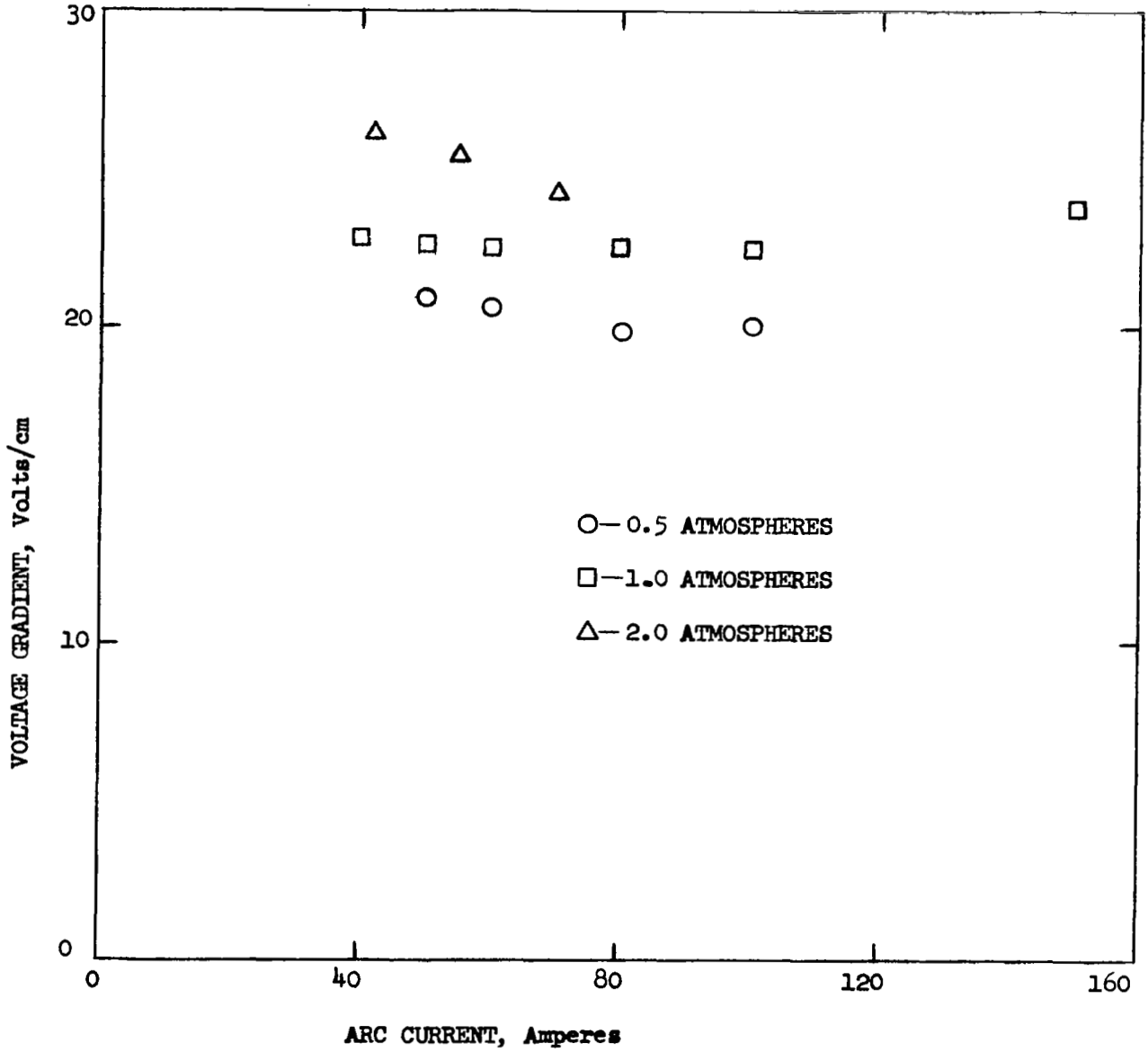

FIG. 15 . VOLTAGE GRADIENTS OF A NITROGEN ARC AT VARIOUS PRESSURES AS DETERMINED BY THE BALANCED CURRENT METHOD.

D. Electrical Conductivity - Data Analysis

The basic equation used in the determination of the electrical conductivity is the integrated Ohm's law for the arc column:

$$I = 2\pi E \int_{o}^{r_c} \sigma(r)\ r\ dr \qquad (6)$$

The general procedure is to measure the values of E and I and the radial temperature distribution T(r) for several different arc currents, and then attempt to find a single electrical conductivity function $\sigma(r)$ which, when substituted into (6), will reproduce the results of the experimental measurements for all currents. The above procedure has the advantage that it is not necessary to make any assumptions about the way in which energy is transported out of the arc column.

1. Linear Approximation for σ

The measurements of the arc current, I, and voltage gradient, E, correspond essentially to a measurement of the average conductivity for the column,

$$\bar{\sigma} = \frac{2\pi}{\pi r^2} \int_{o}^{R} \sigma(r) r\ dr = \frac{I}{\pi r^2 E} \qquad (7)$$

For a first approximation to $\bar{\sigma}(r)$ we assume a form for $\bar{\sigma}(T)$ which is linear in T above some critical temperature T_c and zero

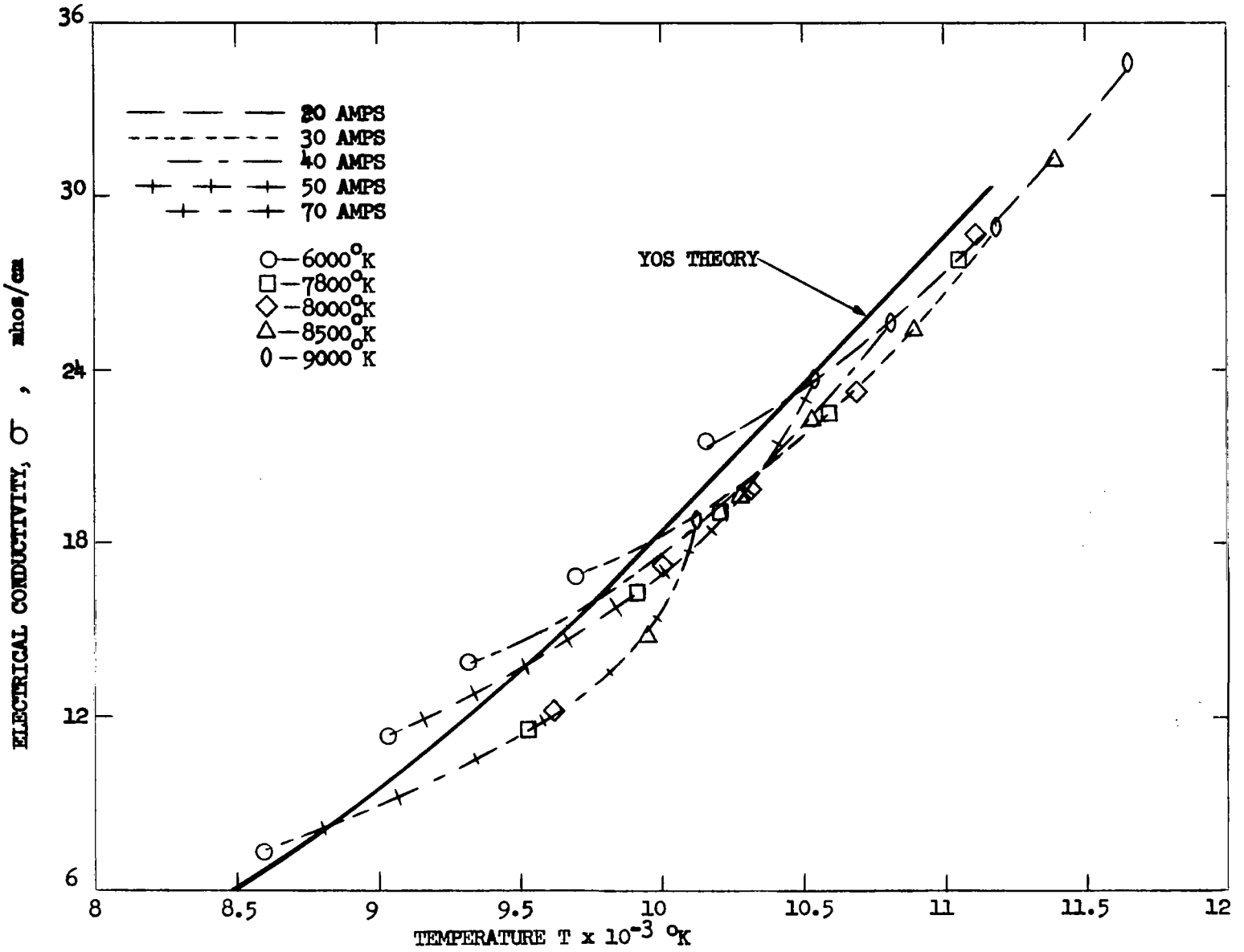

FIG. 16. LINEAR APPROXIMATION TO THE ELECTRICAL CONDUCTIVITY OF HYDROGEN AS OBTAINED BY USING VARIOUS CUT-OFF TEMPERATURES, T_C, FROM THE TEMPERATURE PROFILES OF ONE ATMOSPHERE HYDROGEN ARC RUNS AT 20-, 30-, 40-, 50-, AND 70-AMPERES.

below T_c, i.e.,

$$\bar{\sigma} = a\bar{T}-b; \qquad T \geq T_c$$
$$\bar{\sigma} = 0; \qquad T < T_c \tag{8}$$

To obtain $\bar{T}$ we use

$$\bar{T} = \frac{2}{r_c^2} \int_0^{r_c} T\, rdr \tag{9}$$

where $r_c = R$ is the radius at which $T = T_c$, and $\bar{T}$ is the average temperature. Choice of T_c is arbitrary, but if iteratively chosen for each temperature profile the extrapolated value T at $\sigma = 0$ becomes equivalent, i.e., an unique value of T_c is obtained. Figure 16 demonstrates the above technique for hydrogen arc data runs of 20, 30, 40, 50, and 70 amperes. As a first choice T_c was set equal to $6000^{\circ}K$. Then for each arc current run the corresponding r_c's at $T_c = 6000^{\circ}K$ was found from the temperature profiles T(r) and $\bar{\sigma}$ was computed by use of equation (7). By numerical integration, equation (9) yielded the $\bar{T}$. However when plotted the extrapolated value of T at $\sigma = 0$ yielded $T_c = 7800^{\circ}K \neq 6000^{\circ}K$. T_c was then chosen to be $7800^{\circ}K$ with new r_c values being found from the T(r) and by employing equations (6) and (8), the new extrapolated value of T at $\sigma = 0$ yielded $T_c = 8400^{\circ}K \neq 7800^{\circ}K$. This process was repeated for $T_c = 8000$, 8500, and $9000^{\circ}K$. As seen in figure 16 the correct value of T_c is approximately $8350^{\circ}K$ for all arc currents with the exception of the 20 ampere data which is of some question in terms of LTE. Disregarding the

20 ampere data this data analysis procedure yields hydrogen electrical conductivities of

$$\sigma \simeq 1.01 \times 10^{-2} \ (T - 8350) \tag{10}$$

For comparison purposes the theoretical values of Yos was included in figure 16. As noticed the data, represented by equation (10), is lower in value.

2. Energy Approximation for σ

If the arc column has radial symmetry and the transfer of energy, generated by Ohmic heating, is only due to thermal and radiative mechanisms then the input-output energy balance of a cylindrical shell volume is

$$\Delta EI = 2\pi E^2 \int_r^{r+\Delta r} \sigma(r)\, r dr = \Delta\left[-2\pi r' K(r') \frac{dT}{dr} + W(r')\right] \tag{11}$$

where $W(T')$ is the outward radiant transfer energy per unit arc length and $K(r')$ is the thermal conductivity at radius $r+\Delta r \geq r' \geq r$ having a temperature gradient $\frac{dT}{dr}$. Assuming $\sigma(T)$ to have a temperature dependence of the form shown in equation (10), and $T(r)$ to be linear in r^2 over the Δr increment, then we may rewrite equation (11) as

$$\Delta EI = \pi E^2 \left[\frac{\sigma(r+\Delta r) + \sigma(r)}{2}\right] \cdot \left[(r+\Delta r)^2 - r^2\right] \tag{12}$$

and interpret the resulting electrical conductivity terms as the average value of the cylindrical shell

$$\frac{\sigma(r+\Delta r) + \sigma(r)}{2} \equiv \sigma(r') \tag{13}$$

Hence, by use of equations (11), (12), and (13):

$$\sigma(r') = \sigma(T') \stackrel{\Delta}{=} \frac{W(r') - 2\pi r' K(r')\frac{dT}{dr}}{\pi E^2\left[(r+\Delta r)^2 - r^2\right]} \tag{14}$$

Equation (14) has been solved for each arc current data run of hydrogen using the theoretical values of Yos for K and results of the previously mentioned arc column net radiative energy transfer computer program (see Appendix I) for $W(r') = P_{vis}(r') + P_{vuv}(r')$. Figure 17 shows these solutions as a function of T, and compares them to the theoretical values of Yos. As noticed these experimental values of σ are considerably lower than those determined by equation (10). However solution of equation (14) were dependent upon theoretical values of K, where as the results of equation (10) were not.

3. Collisional Cross Section Approximation for σ

Also included in figure 17 is an estimate of electrical conductivities for hydrogen based on the data and the results of equation (14), i.e., we have curve fitted the results of (14) by determining their necessary electron-neutral and electron-ion collisional cross sections. This was performed by solving simultaneously the expression

$$\sigma \simeq n_e T^{-1/2} \left[nQX + n_+Q_+Y\right] \tag{15}$$

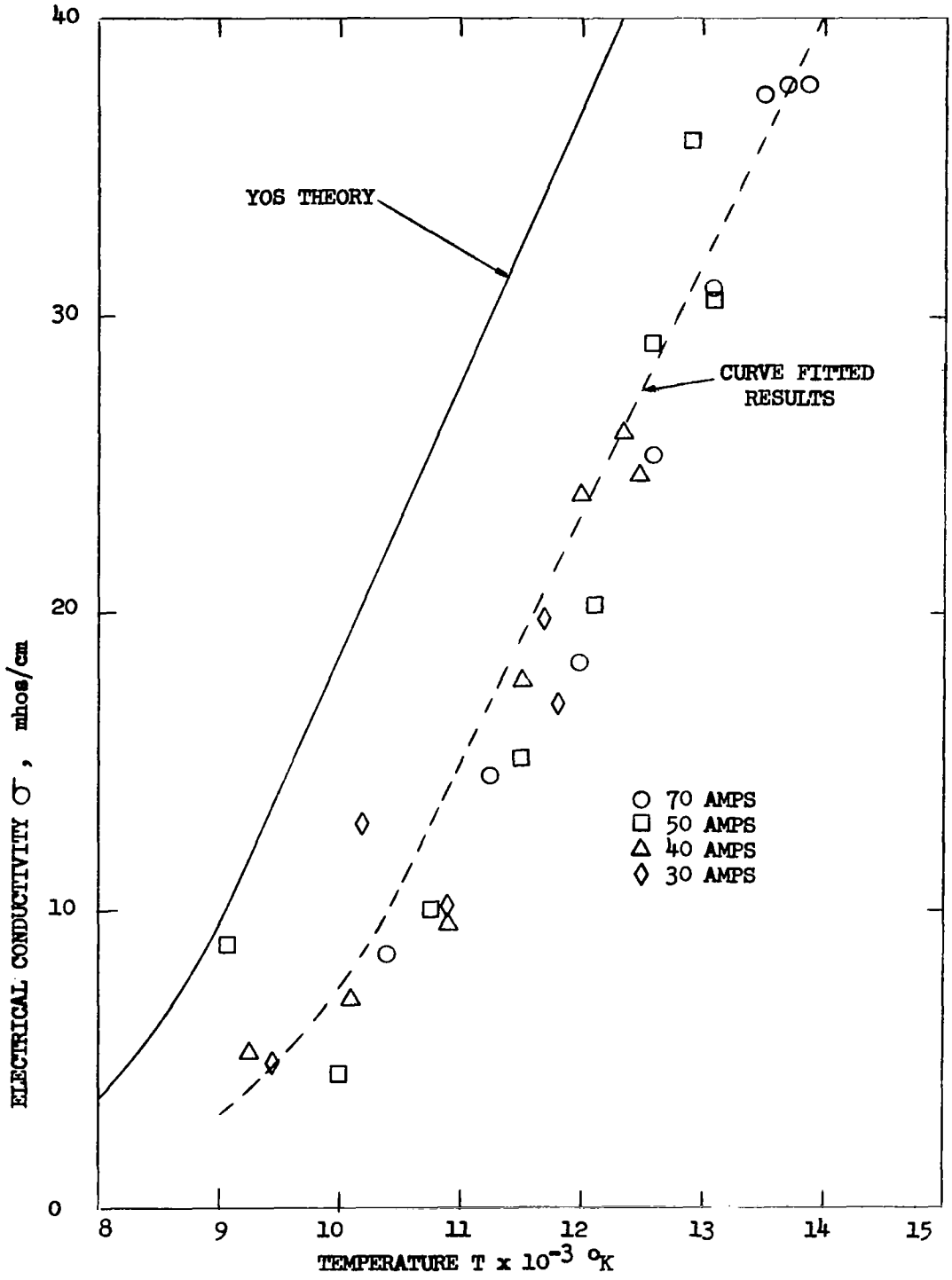

FIG. 17 . PARABOLIC APPROXIMATION TO THE ELECTRICAL CONDUCTIVITY USING YOS' THEORETICAL VALUE FOR THERMAL CONDUCTIVITY AND DATA OBTAINED FROM 30, 40, 50, AND 70-AMPERE HYDROGEN ARC RUNS AT ONE ATMOSPHERE. ALSO INCLUDED ARE THE CURVE FITTED RESULTS OBTAINED BY DETERMINING THE NECESSARY ELECTRON-NEUTRAL AND ELECTRON-ION COLLISIONAL CROSS-SECTIONS.

for the electron-neutral collisional cross section Q and the electron-ion collisional cross section Q_+ at $T = 10{,}000^{\circ}K$ and $T = 14{,}000^{\circ}K$ based on the results of (14) where n_e is the electron number density, n is the neutral number density, n_+ is the ion number density, and where X and Y represent the normalized temperature dependence functions of their associated collision cross section with respect to a gas temperature of $T = 10{,}000^{\circ}K$, i.e., at $T = 10{,}000^{\circ}K$, $X = Y = 1.0$, and at $T = 14{,}000^{\circ}K$: $Q = Q\ (T = 10{,}000^{\circ}K)\ X(T)$, and $Q_+ = Q_+\ (T = 10{,}000^{\circ}K)\ Y(T)$. The normalized temperature dependence functions were obtained from the Gvosdover[13] relation

$$Q_+ \sim \frac{1}{T^2} \ln \left(\frac{kT}{e^2 n_+^{1/3}}\right) \tag{16}$$

and the temperature fit

$$Q \sim \left\{1 + \frac{T}{3300}\right\}^{-1/2} \tag{17}$$

It was found by the above procedure that at $T = 10{,}000^{\circ}K$, $Q_+ = 1.73 \times 10^{-13}$ and $Q = 1.04 \times 10^{-14} cm^2$. Hence the values obtained from equation (14) appear somewhat unrealistic in that these Q values when used to recalculate K would yield lower values of K then initially used in equation (14) to determine σ.

IV. DISCUSSION OF RESULTS

A. Nitrogen

Figures 18 through 20 gives the thermal conductivity of nitrogen for three pressures 0.5, 1.0, and 2.0 atmospheres calculated assuming no radiative loss. Figure 21 gives K for 50 and 100 amps at 1 atmosphere, which includes radiative losses for $\lambda > 0.0$Å, utilizing the arc column radiative energy transfer computer program described in Appendix I.

It is useful to examine in detail the analysis of particular arc runs in nitrogen, in order to assess the sensitivity of the results to variations of the assumed electrical conductivity and radiation. We have chosen the arc runs in nitrogen at currents of 50 and 100 amperes at atmospheric pressure as being typical. The temperature profiles (obtained from the Abel[15] transform of the measured lateral intensity distribution, and the previously measured dependence of continuum intensity on temperature) for these conditions are given in figures 7 and 8.

These temperature profiles, temperature gradients calculated from the profiles, a table of electrical conductivity as a function of temperature, a table of radiation per unit volume in the spectral range 0.2 to 6μ as a function of temperature, and spectral absorption coefficients describing the six most important vacuum ultraviolet continuum absorption edges and (computed from the absorption cross sections of Burgess and Seaton[3]) are supplied as input to the IBM 7094 computer. The computer output for these runs is given in Table 1.

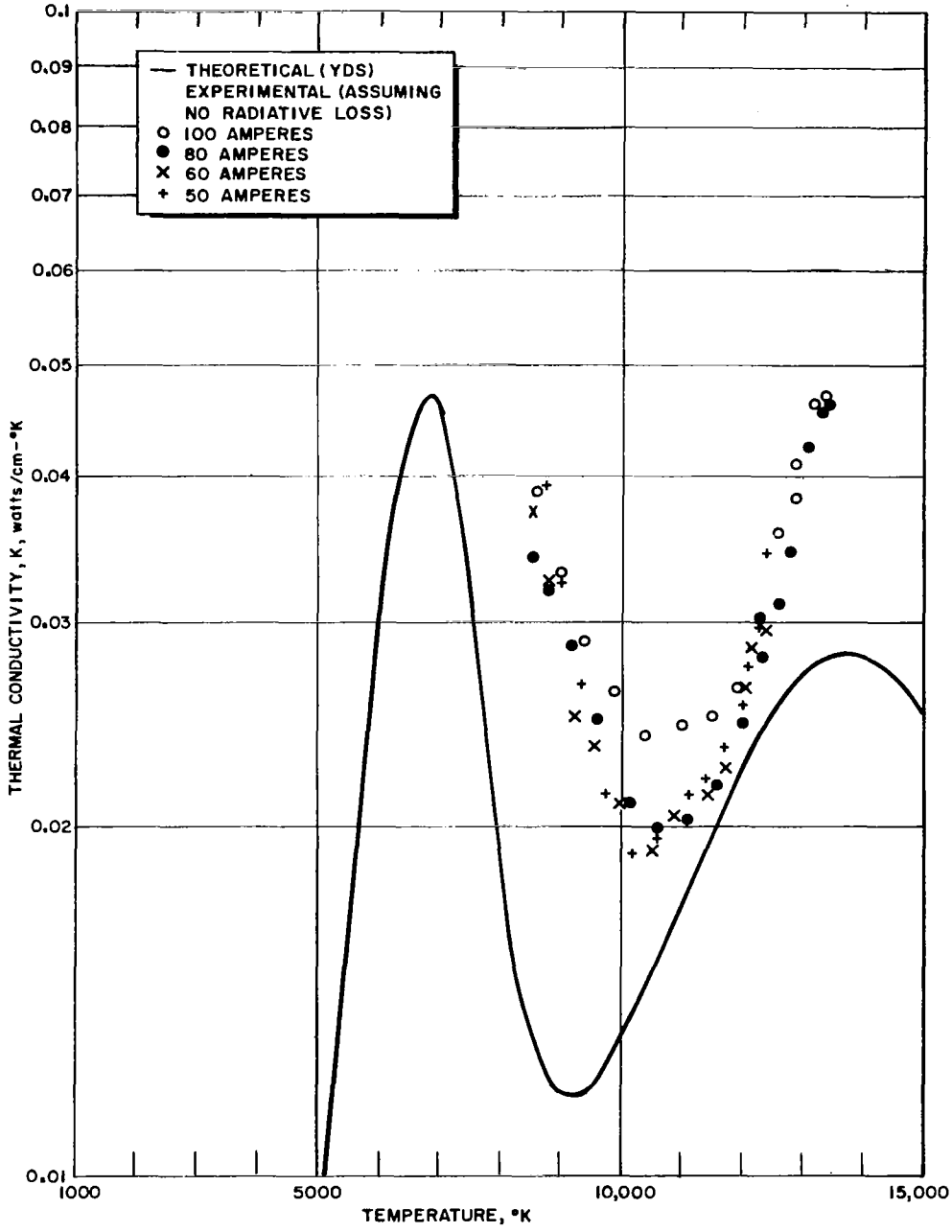

65-11614

Figure 18 THERMAL CONDUCTIVITY OF NITROGEN AT 0.5 ATMOSPHERE FROM THE CALCULATED-CURRENT METHOD WITHOUT THE INCLUSION OF RADIATIVE LOSSES

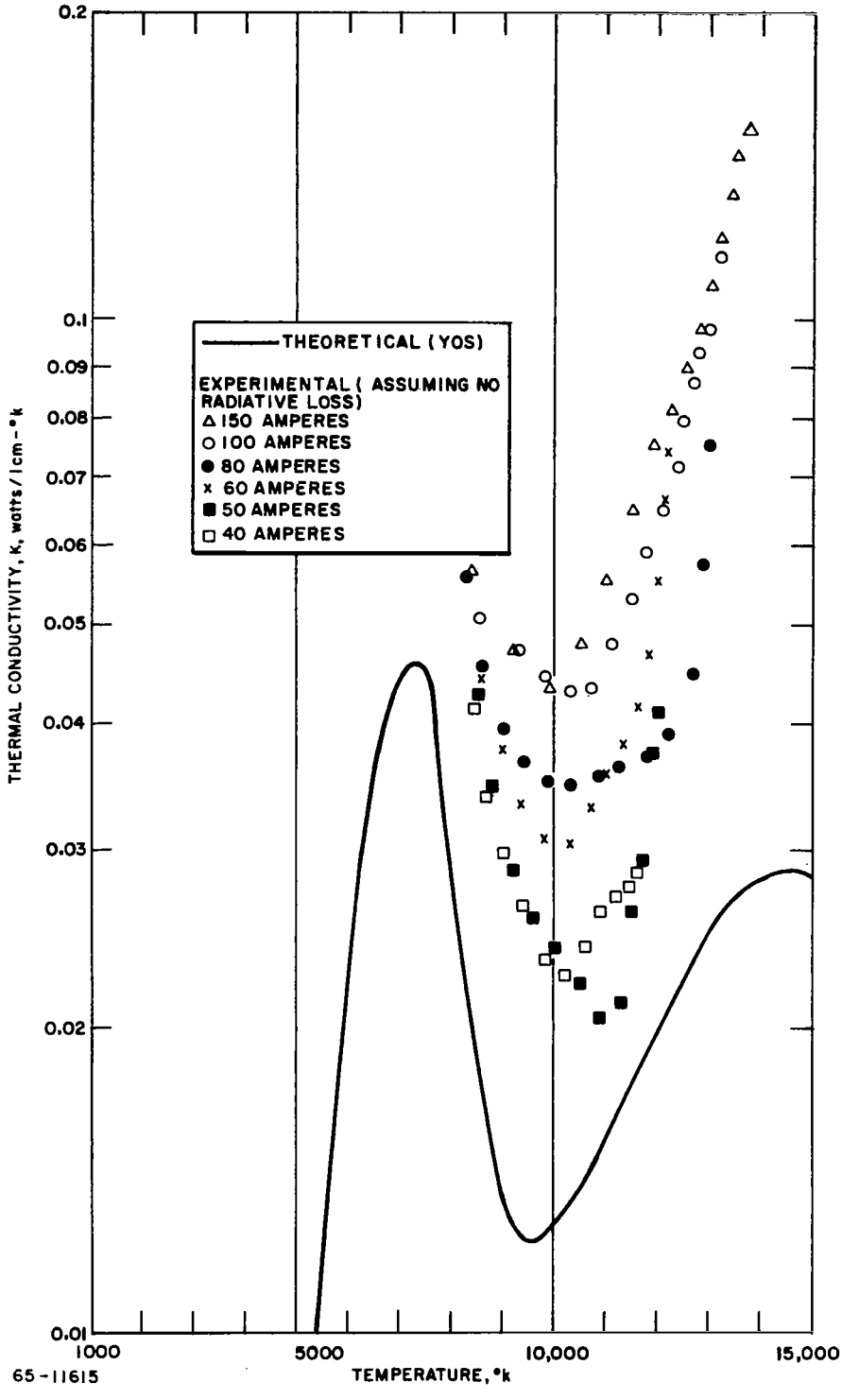

Figure 19 THERMAL CONDUCTIVITY OF NITROGEN AT 1 ATMOSPHERE FROM THE CALCULATED-CURRENT METHOD WITHOUT THE INCLUSION OF RADIATIVE LOSSES

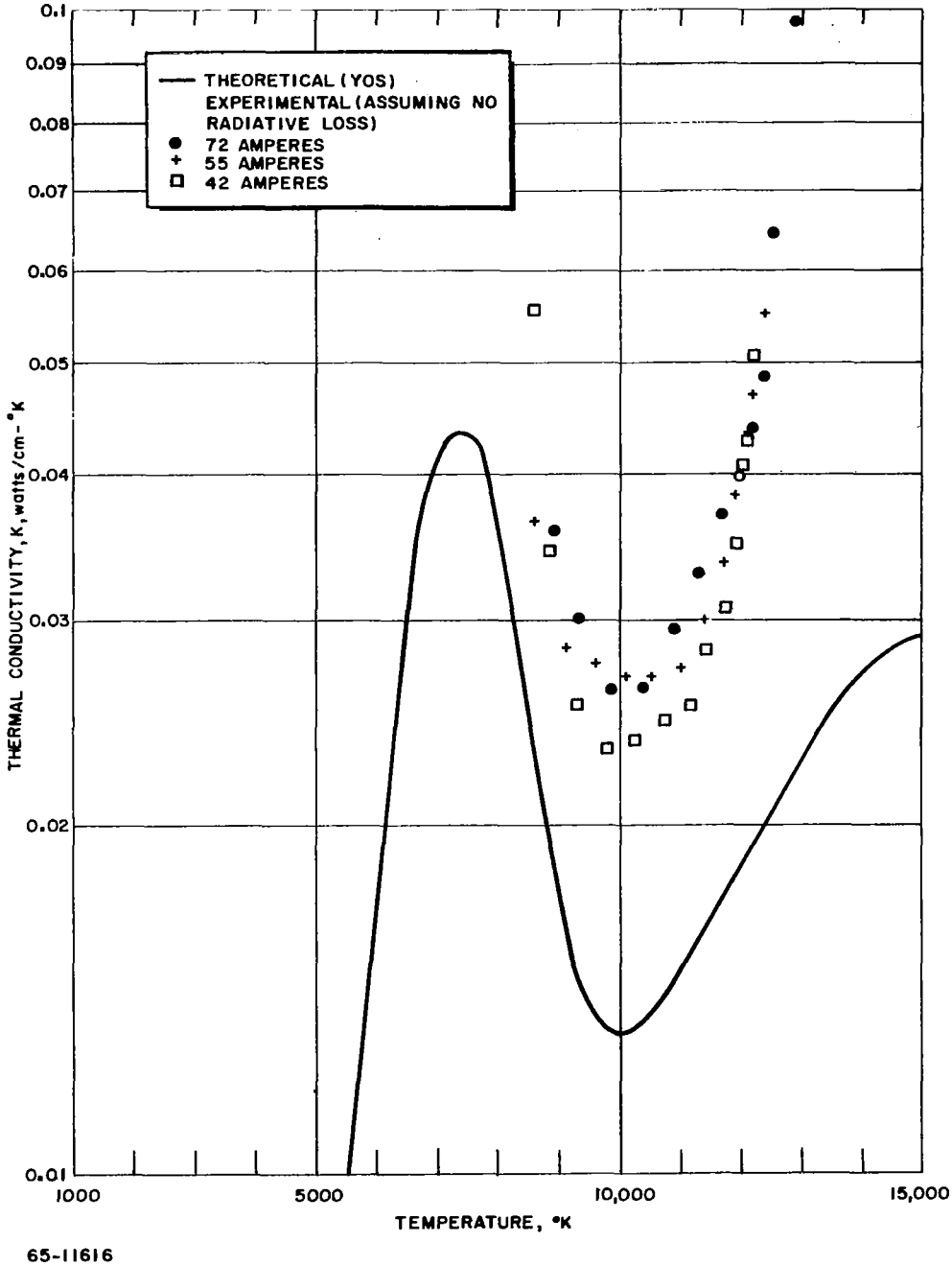

65-11616

Figure 20 THERMAL CONDUCTIVITY OF NITROGEN AT 2 ATMOSPHERES FROM THE CALCULATED-CURRENT METHOD WITHOUT THE INCLUSION OF RADIATIVE LOSSES

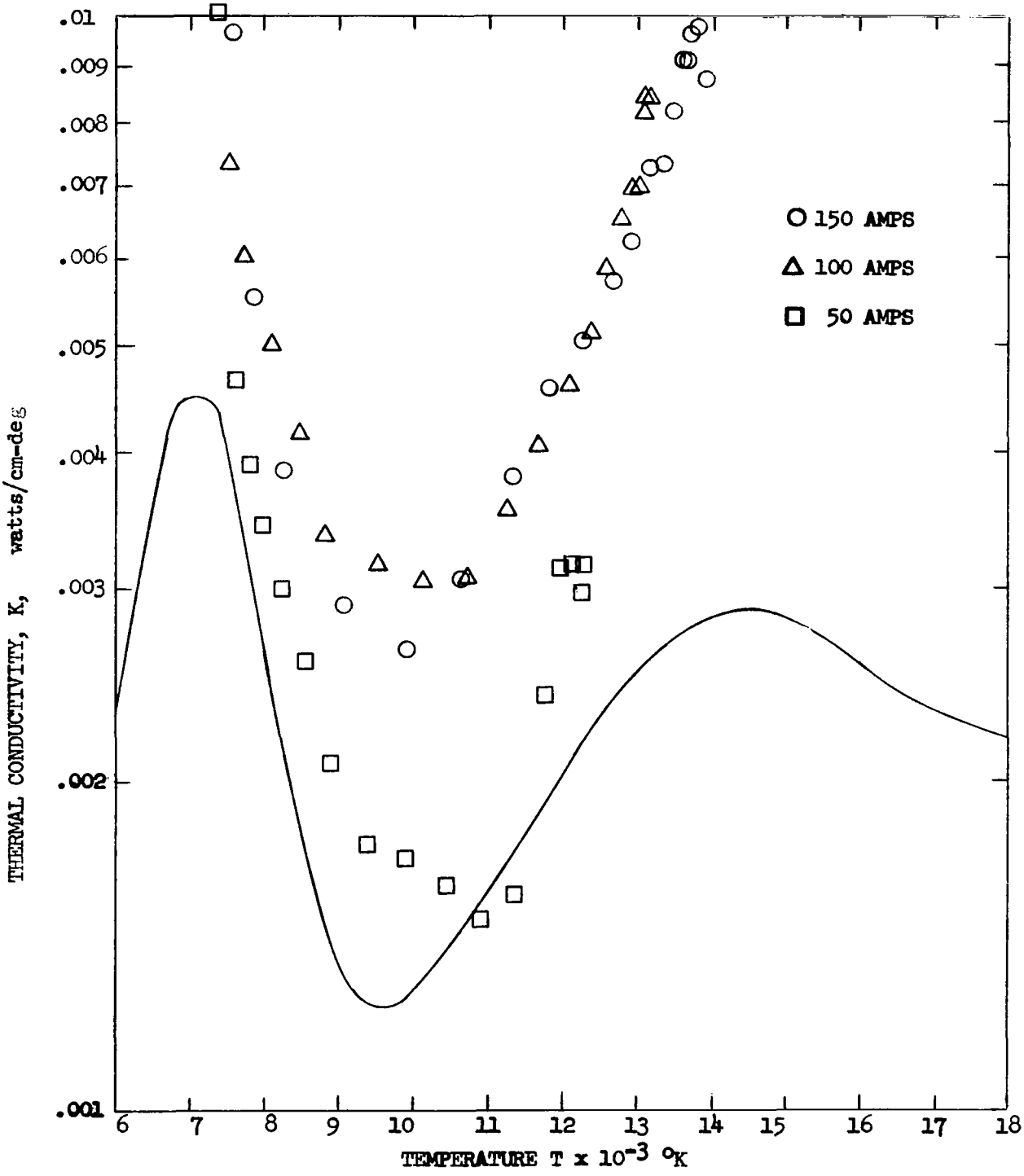

FIG. 21. THERMAL CONDUCTIVITY OF NITROGEN AT ONE ATMOSPHERE OBTAINED UTILIZING THE ARC COLUMN RADIATIVE TRANSFER CALCULATIONS FOR $\lambda > 0.0$ Å

TABLE I

ANALYSIS OF 50 AND 100 AMPERE ARC RUNS

A. 50 Ampere Run, Nitrogen, one atmosphere pressure

Temp °K	r, cm	P_{in}, watts/cm	P_{vis}, watts/cm	P_{vuv}, watts/cm	K_{exp} mw/cm-°K
12,300	0	--	--	--	--
12,270	0.0116	9.4	0.4	2.6	22.2
12,220	0.0232	37.4	1.6	9.6	24.1
12,100	0.0348	83.6	3.6	20.3	24.9
11,960	0.0464	147	6.1	33.1	25.5
11,740	0.0580	227	9.0	47.2	20.7
11,360	0.0696	321	12.1	60.5	14.1
10,820	0.0812	424	14.8	69.8	14.2
10,360	0.0928	530	16.6	73.6	16.4
9,846	0.1044	638	18.0	74.4	18.6
9,355	0.1160	741	18.8	73.1	20.6
8,862	0.1276	834	19.2	70.9	26.3
8,489	0.1392	915	19.5	68.5	34.1
8,197	0.1508	984	19.7	66.2	41.8
B. 100 Ampere Run, Nitrogen, one atmosphere pressure					
13,180	0	--	--	--	--
13,170	0.0126	12.6	0.8	5.7	44.6
13,140	0.0252	50.5	3.1	21.4	48.8
13,090	0.0378	113	6.9	45.6	49.3
13,010	0.0504	201	12.2	77.6	43.9
12,910	0.0630	312	18.6	115	44.9
12,760	0.0756	446	26.2	158	43.4
12,560	0.0882	601	34.5	202	40.3
12,360	0.1008	774	43.0	244	36.6
12,030	0.1134	964	51.5	282	34.0
11,650	0.1260	1165	59.2	310	31.4
11,210	0.1386	1374	65.7	327	28.9
10,670	0.1512	1582	70.6	332	26.6
10,090	0.1638	1783	73.7	327	28.0

Referring to Table 1, the first column lists the temperature and the second the radial location in the arc at which this temperature occurs. The third column gives the total power per unit length thermalized at radii smaller than or equal to r. That is,

$$P_{in}(r) = \int_0^r 2\pi r\sigma(r)E^2\, dr \tag{18}$$

The fourth column in Table 1, P_{vis}, is the power radiated per unit length by the cylindrical volume with radius $\leq r$, in the wavelength range 0.2 to 6μ. Because the arc is treated as non-absorbing in this wavelength range, all of this radiation passes out of the arc.

The vacuum ultraviolet continuum radiation is listed in the fifth column, P_{vuv}. The numbers given here are the net outward transfer of power in the wavelength range $\lambda < .2\mu$ at the listed radial stations. Radiation in this region is to some degree absorbed by the arc, and the net outward transfer is made up of the part of the radiation generated within the cylinder of radius r which escapes, less the amount generated at larger r values which is absorbed within the radius r.

Finally, column 6 lists the computed values of thermal conductivity, obtained from

$$k(r) = \frac{P_{in}(r) - P_{vis}(r) - P_{vuv}(r)}{2\pi r \frac{dT}{dr}} \tag{19}$$

In figures 22 through 25 the results of Table I have been graphed in a convenient form for assessing the relative importance of the different modes of energy transfer. As a function of radius we have plotted P_{in}, P_{vis}, P_{vuv}, and the quantity $2\pi rK \frac{dT}{dr}$, where for K we have used the best available theoretical value.[16]

Referring to figure 22, which is drawn for the 100 ampere arc run, it can be seen that there is, at each radial station, a positive quantity of power/unit length = D required to satisfy

$$P_{in} = P_{vis} + P_{vuv} + 2\pi r\, k\frac{dT}{dr} + D \qquad (20)$$

Further, for radii less than about 0.12 centimeters (or temperatures greater than 12,000°K) D is a fairly constant fraction of the input power, of the order of 25%. For $r > 0.12$ centimeters D grows, attaining the value 35% at $r = 0.16$ centimeters.

Figure 23 is a plot on an expanded scale of the inner region of the arc column for the 100 ampere run. In this region D is seen to be everywhere smaller than the power transferred by continuum radiation in the vacuum ultraviolet.

Figure 24 is similar to figure 22, but for the 50 ampere arc column. Here D is quite small for $r \leq 0.10$ cm, and is in fact negative for $0.06 \leq r \leq 0.085$ cm. However, it becomes large (~40%) at $r = 0.16$ cm. The region near the center of the arc column is replotted on an expanded scale in figure 25.

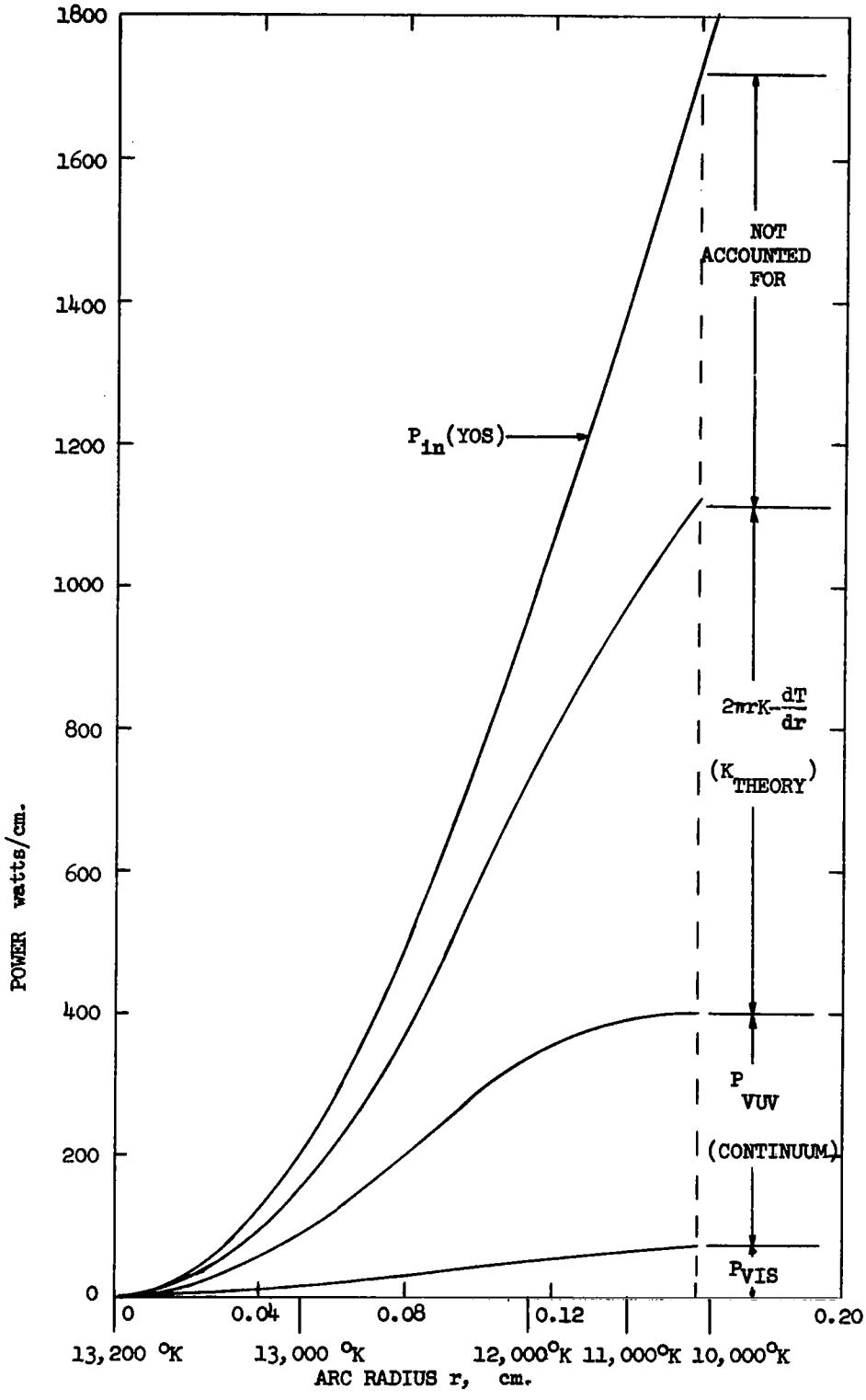

FIG. 22. POWER/UNIT LENGTH vs. r FOR THE VARIOUS POWER TRANSPORT MECHANISMS IN A 100-AMPERE NITROGEN ARC AT 1 ATMOSPHERE

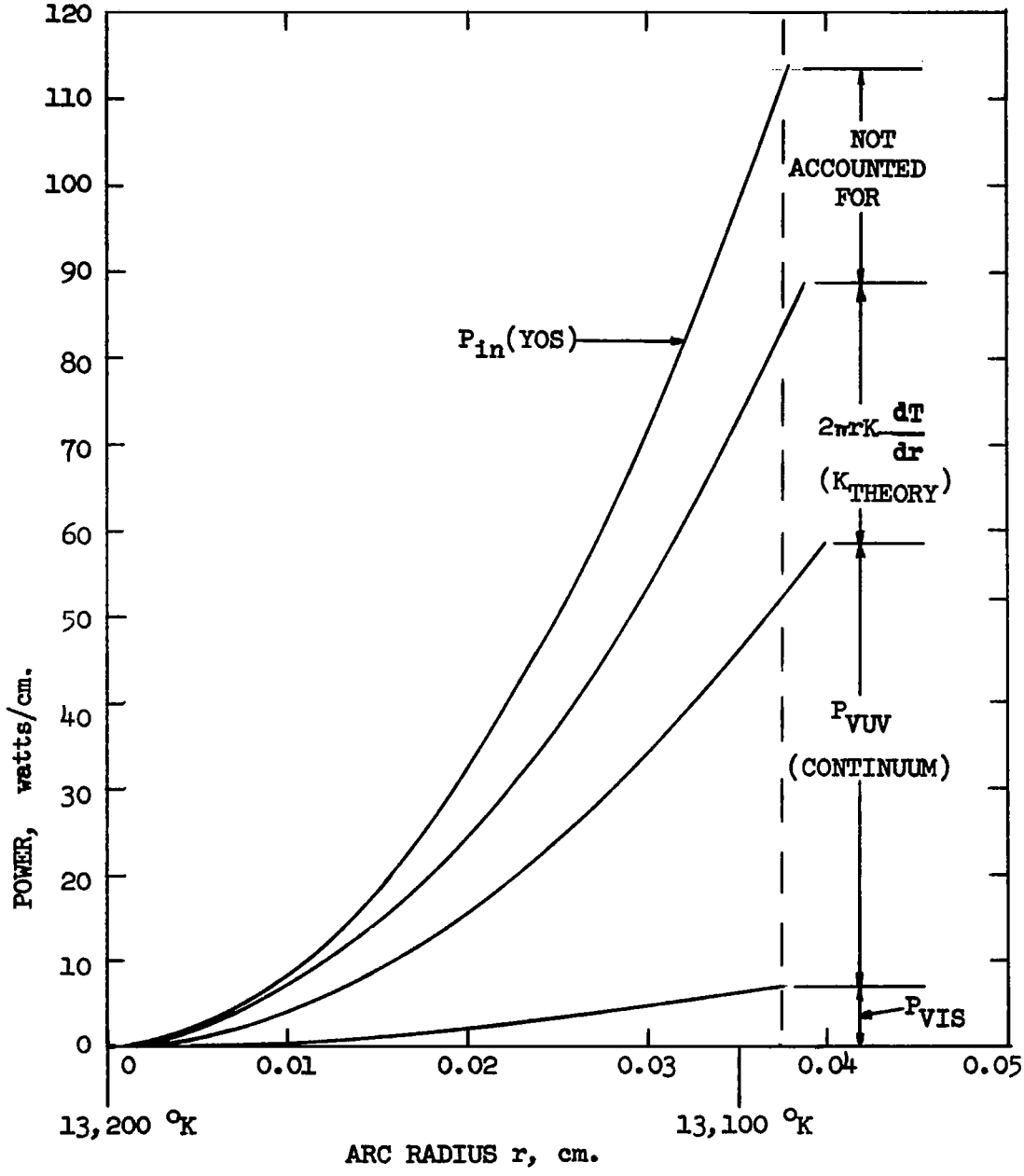

FIG. 23. POWER/UNIT LENGTH vs. r FOR THE VARIOUS POWER TRANSPORT MECHANISMS IN A 100-AMPERE NITROGEN ARC AT 1 ATMOSPHERE

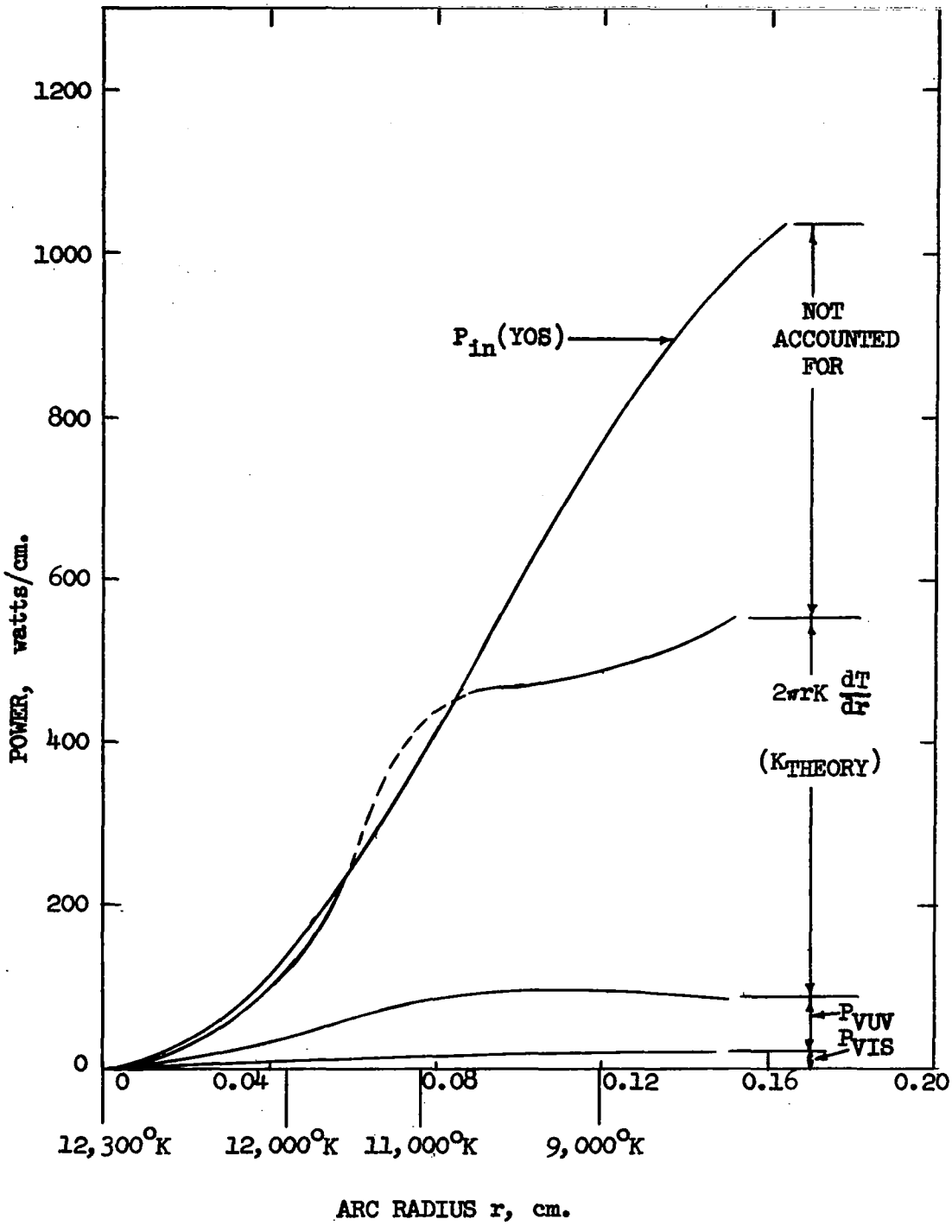

FIG. 24. POWER/UNIT LENGTH vs. r FOR THE VARIOUS POWER TRANSPORT MECHANISMS IN A 50-AMPERE NITROGEN ARC AT 1 ATMOSPHERE

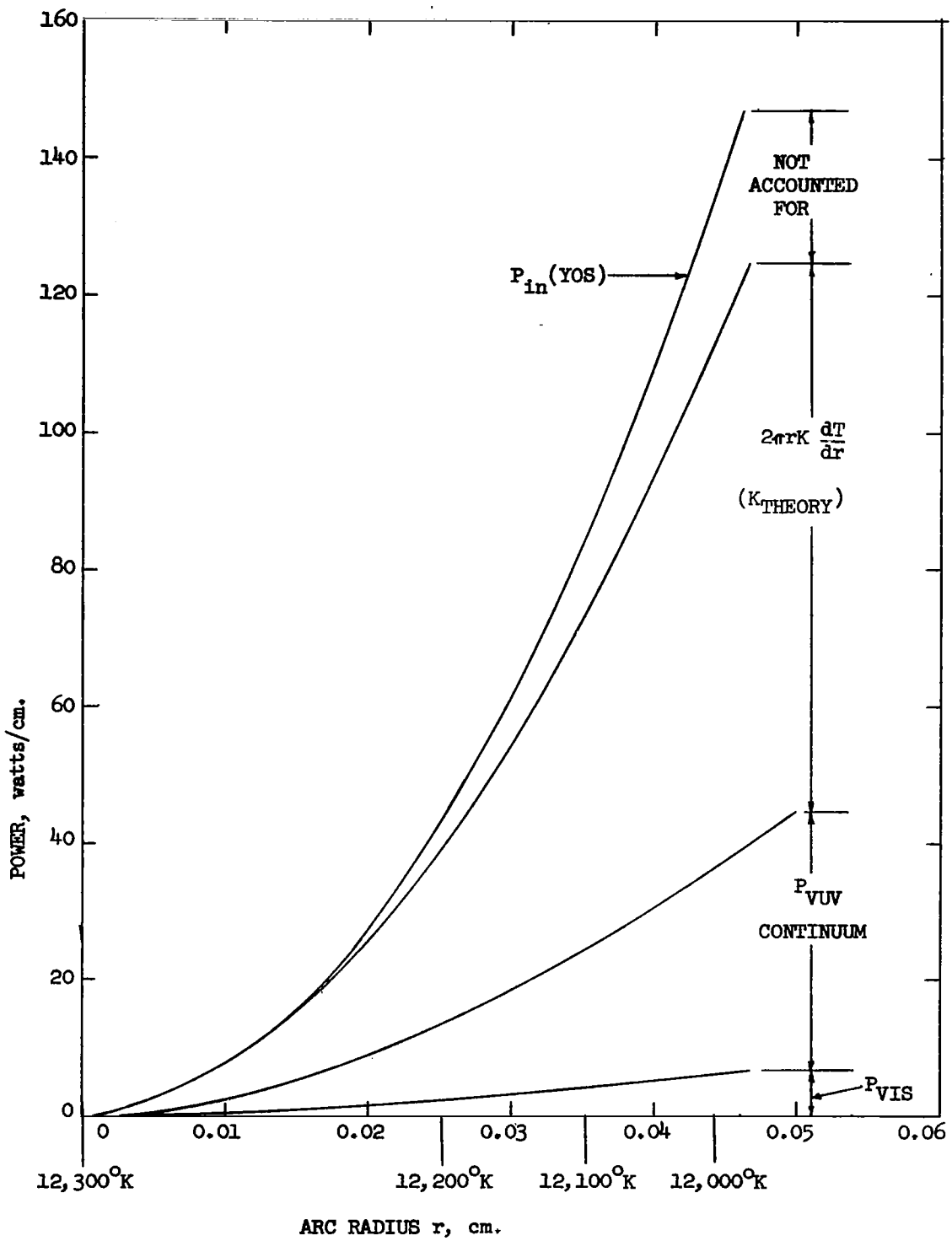

FIG. 25. POWER/UNIT LENGTH vs. r FOR THE VARIOUS POWER TRANSPORT MECHANISMS IN A 50-AMPERE NITROGEN ARC AT 1 ATMOSPHERE

The discrepancy between experimental and theoretical values of the thermal conductivity of nitrogen is of course symbolized by D. In our current experiments we are treating D as though it were zero, and including any power which D represents in the thermal conduction. Thus, since D appears for the most part to be greater than zero, the values of thermal conductivity deduced from our experiments are larger than the theoretical values. It should be noted that relatively small values of D can produce significant changes in the estimate of K. To illustrate this point, we have considered the effect of a variation of the measured input power, which has the effect of varying D. For the point at a radial location of 0.12 cm (T ~11,800°K) in the 100 ampere run we have plotted in figure 26 the value of thermal conductivity which would be deduced from our temperature profile as the input power (and thus D) is varied. From figure 26 it can be seen that a value of D of 25% of the input power (which is what we now find experimentally) causes the measured thermal conductivity to exceed the theoretical value by more than 60%. Reducing the input power by 12% would reduce D by about half and bring the measured value of K within about 30% of the theoretical value.

B. Sensitivity of the Analysis

In this section the sensitivity of the analysis to the various inputs is discussed.

1. Input power--The input power within r is arrived at from

$$P_{in} = 2\pi \int_{o}^{r} \sigma E^2 \, r dr \qquad (21)$$

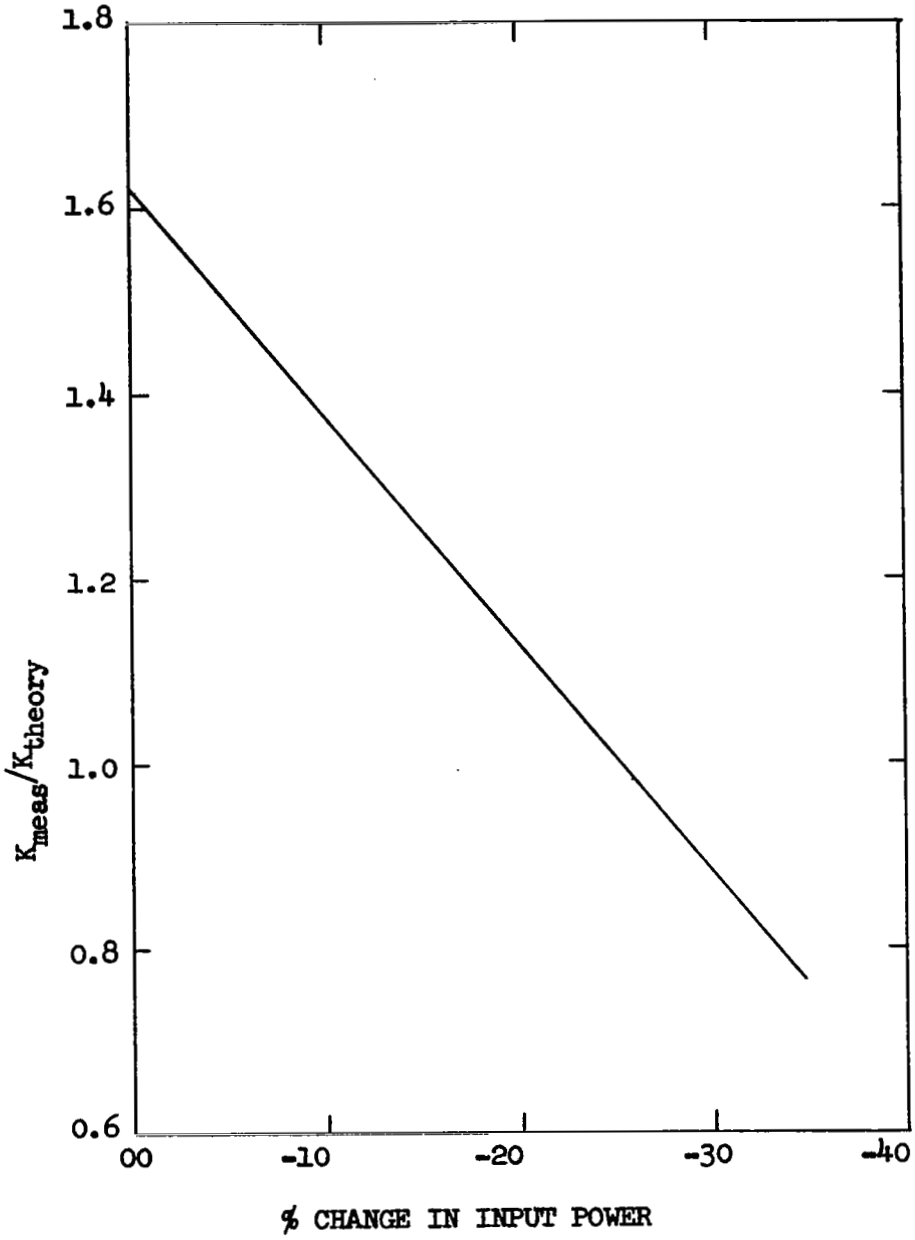

FIG. 26. EFFECT OF VARIATION OF INPUT POWER ON CALCULATED THERMAL CONDUCTIVITY

and is thus linearly dependent on σ and quadratically dependent upon E. For the calculations presented here we have used for σ the analytical values calculated by Yos[9], while E has been measured during the course of the experiment. The effect of an error in E would be to change the input power at each radial station by a constant fraction; this would be satisfactory in terms of reducing P_{in} in figure 22 (100 ampere) but would not improve the agreement in figure 24 (50 ampere). On the other hand, since σ has a temperature dependence, errors could conceivably exist in our tables of σ which would improve agreement for both arc runs, and for the others as well. There are two experimental checks available for the electrical conductivity. First, the relation

$$I = 2\pi \int_{o}^{r_{wall}} \sigma E \, r dr \qquad (22)$$

can be examined. Second, data from different arc runs can be used to measure the electrical conductivity[10]. With respect to the data presented here, the first check yields agreement within 10% for the 50 and 100 ampere runs, and closer agreement for runs at 80 and 150 amperes. A run at 40 amperes gives poorer agreement, the value of the integral being nearly 50 amperes. Because of uncertainties in the temperature profiles near the outer boundary of the arc column it is thought that agreement to this extent (~10%) is quite good.

The second check was presented in reference 10, and discussed under paragraph D from which figure 27 is reproduced. The measurements show no trend of disagreement with theory, but only some scatter.

Based on these two checks, it appears that the electrical conductivity we have used is not badly in error. However, referring to figure 26, small variations in input power could produce significant changes in K, so this possible source of error should still be investigated.

More recent calculations of electrical conductivity for nitrogen by Ahtye[11] have come to our attention; these calculations are based on the second Chapman-Enskog approximation to the Boltzmann equation and we have used these newer values in our analysis. Figure 27 shows a comparison between the electrical conductivity values of Yos[9] which we have been using, and those of Ahtye. Ahtye's values are larger at high temperatures and smaller at low temperatures, the crossover occurring at about 11,000°K.

Figure 28 shows the data for the 100 ampere run as presented earlier in figure 22, but with a new calculation of the input power using the electrical conductivity values of Ahtye. Figure 30 is drawn for the 50 ampere run, and contains the results given earlier in figure 24 along with the new calculation of input power using the electrical conductivity values of Ahtye.[11]

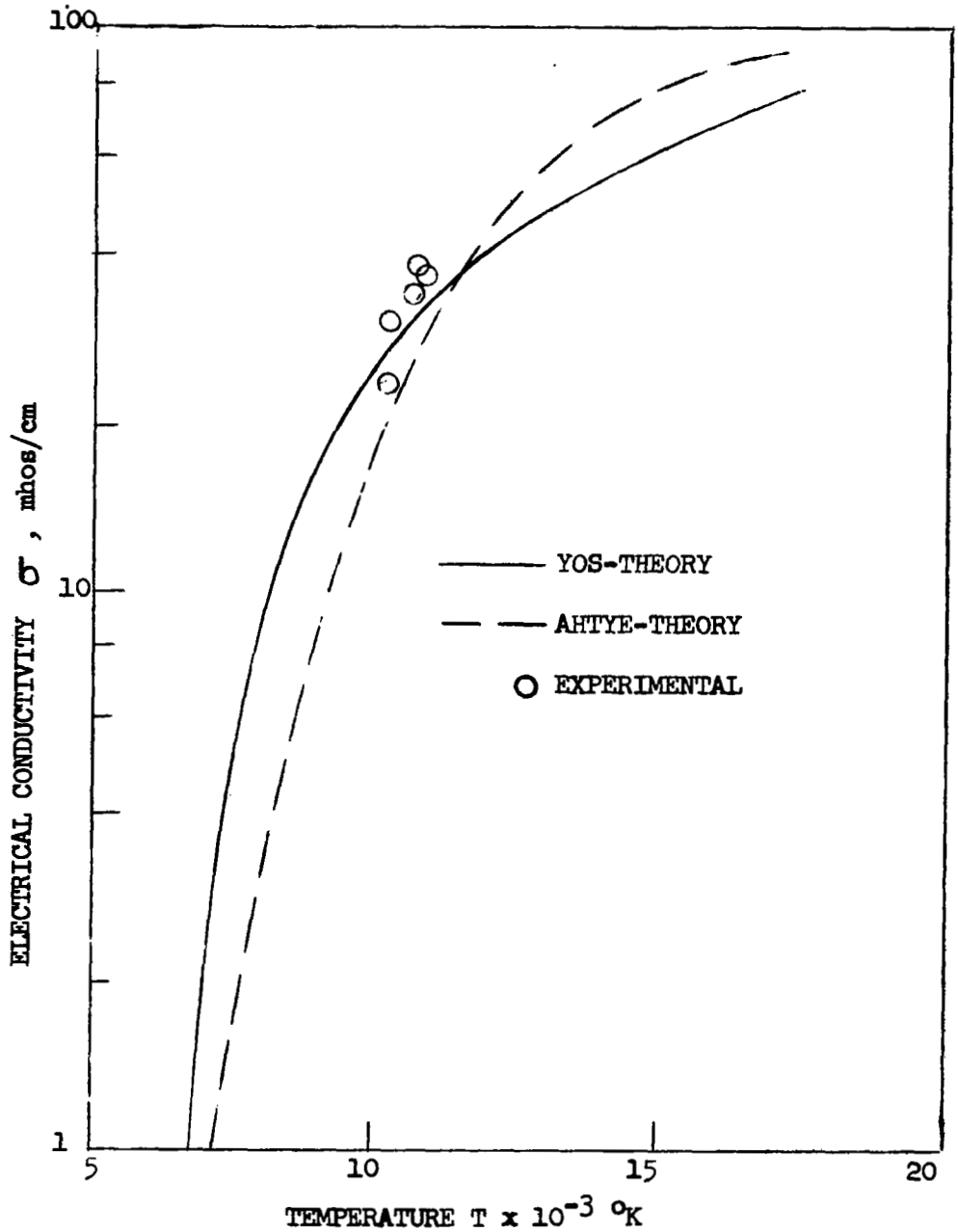

FIG. 27. ELECTRICAL CONDUCTIVITY DEDUCED FROM ARC COLUMN TEMPERATURE PROFILES OF NITROGEN AT ONE ATMOSPHERE

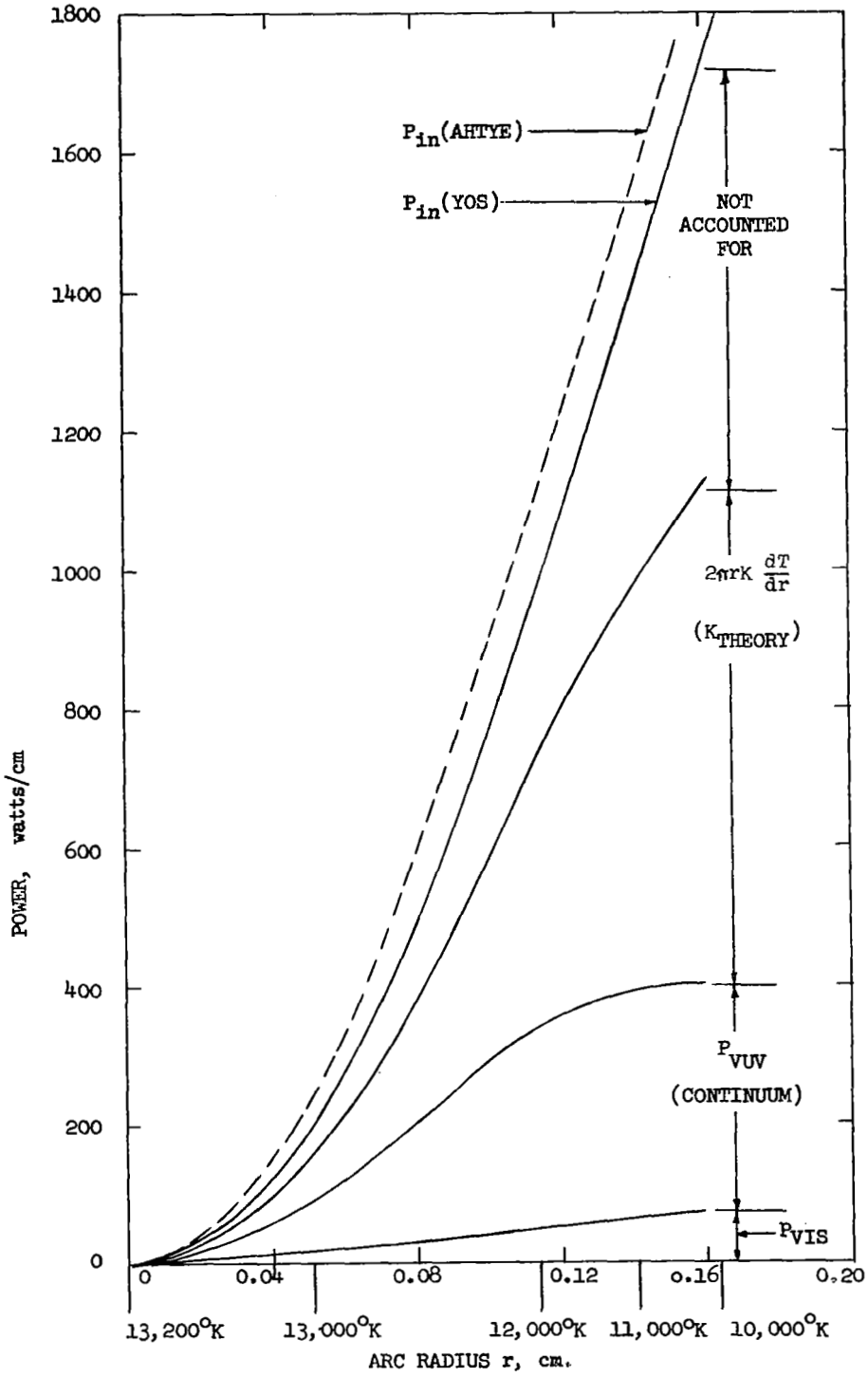

FIG. 28 POWER/UNIT LENGTH vs. r FOR THE VARIOUS POWER TRANSPORT MECHANISMS IN A 100-AMPERE NITROGEN ARC AT 1 ATMOSPHERE

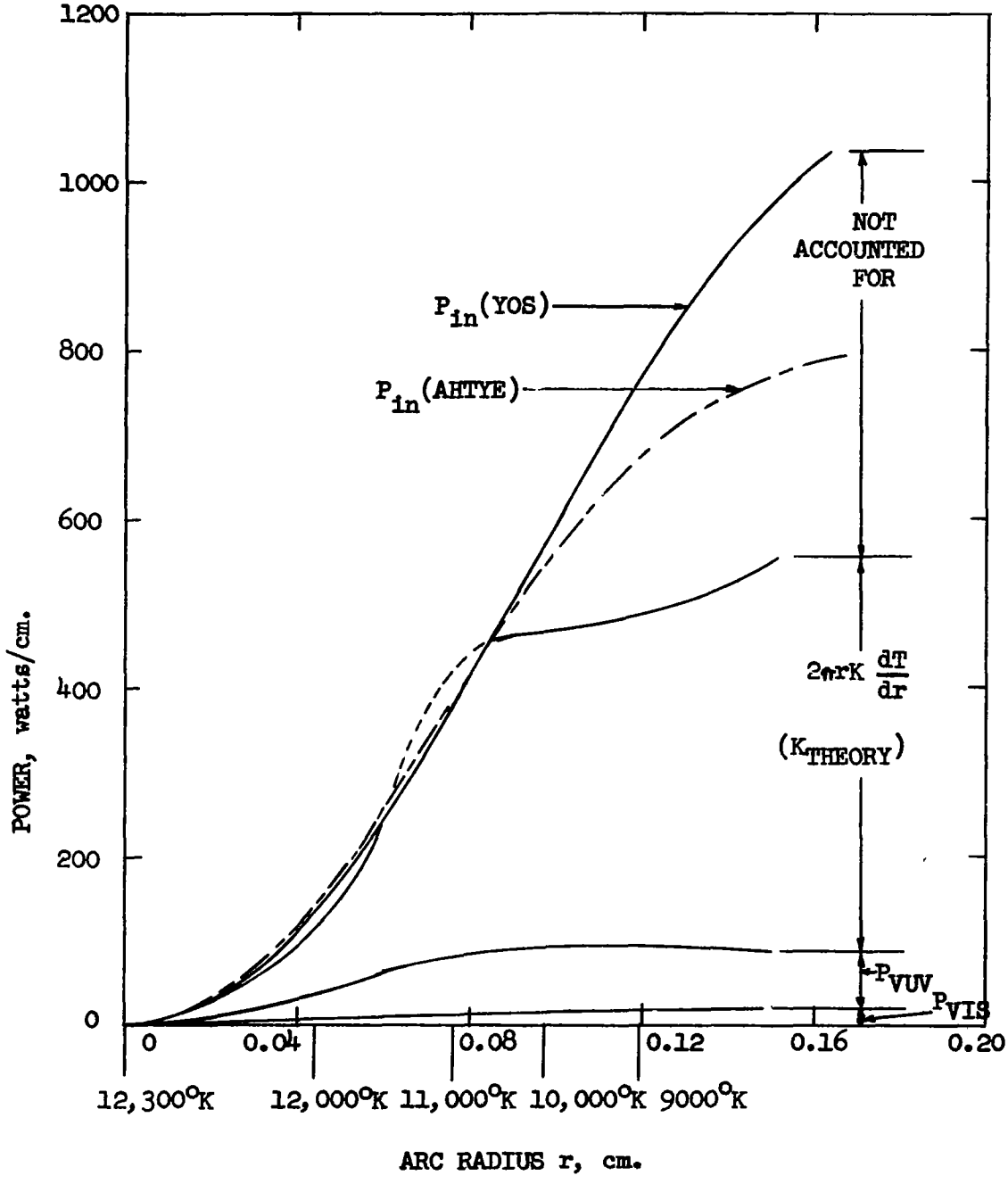

FIG. 29 POWER/UNIT LENGTH vs. r FOR THE VARIOUS POWER TRANSPORT MECHANISMS IN A 50-AMPERE NITROGEN ARC AT 1 ATMOSPHERE

Referring to figure 28, the effect of the new electrical conductivity values is to increase the disagreement between theory and experiment, that is, the sum of radial energy transfer at each radial station by visible radiation, vacuum ultraviolet continuum, and thermal conduction (using theoretical values for the conductivity) is a smaller fraction of the computer input power than before.

It should be noted, although we have not extended the curves to large radii, that the input powers based on the electrical conductivities of Yos and of Ahtye approach each other at large radii, crossing at 0.18 centimeters, with the Ahtye curve lower than the Yos curve at larger radii. The total calculated current found from the radial integral of σE is 111 amperes for the Yos electrical conductivities, and 99 amperes for the Ahtye electrical conductivities.

Referring to figure 29, there is in general better agreement between theory and experiment using the Ahtye electrical conductivities for the 50 ampere run. The difference between the two is small at small radii, where the agreement of each with theory is fairly good, and increases at large radii where the data agree very poorly with the input power calculated according to the Yos conductivities, and much better according to the Ahtye conductivities, although in neither case is the agreement good. In terms of computed current, with the Yos conductivities we find a current of 55 amperes, while the Ahtye conductivities yield 38 amperes.

It is difficult to draw general conclusions from this comparison. It does appear, however, that the discrepancies remain when either set of electrical conductivities is used, and are about of the same order. Thus, some other mechanism is probably operating to produce the discrepancy.

2. Errors in the Temperature Profile

An investigation was made into the error that would be caused in the K measurement from errors in the temperature profile. Temperatures as pointed out earlier were obtained from the continuum radiation. The temperature dependence of this continuum is understood reasonably well. However, if the absolute magnitude were in error then it would be reflected in the temperature profile. A test of the effect on K of this error was made by constructing a new temperature profiles using a different value for the absolute intensity of the continuum using the 50 amp hydrogen arc run, figure 30. This new profile was used to obtain new K values. A comparison of these conductivities with the values obtained from the originally calibrated continuum is shown in figure 31. The errors are seen to be relatively unimportant.

3. Visible Radiation

Inspection of figures 22 through 26 indicates that visible radiation accounts for very little power transfer compared

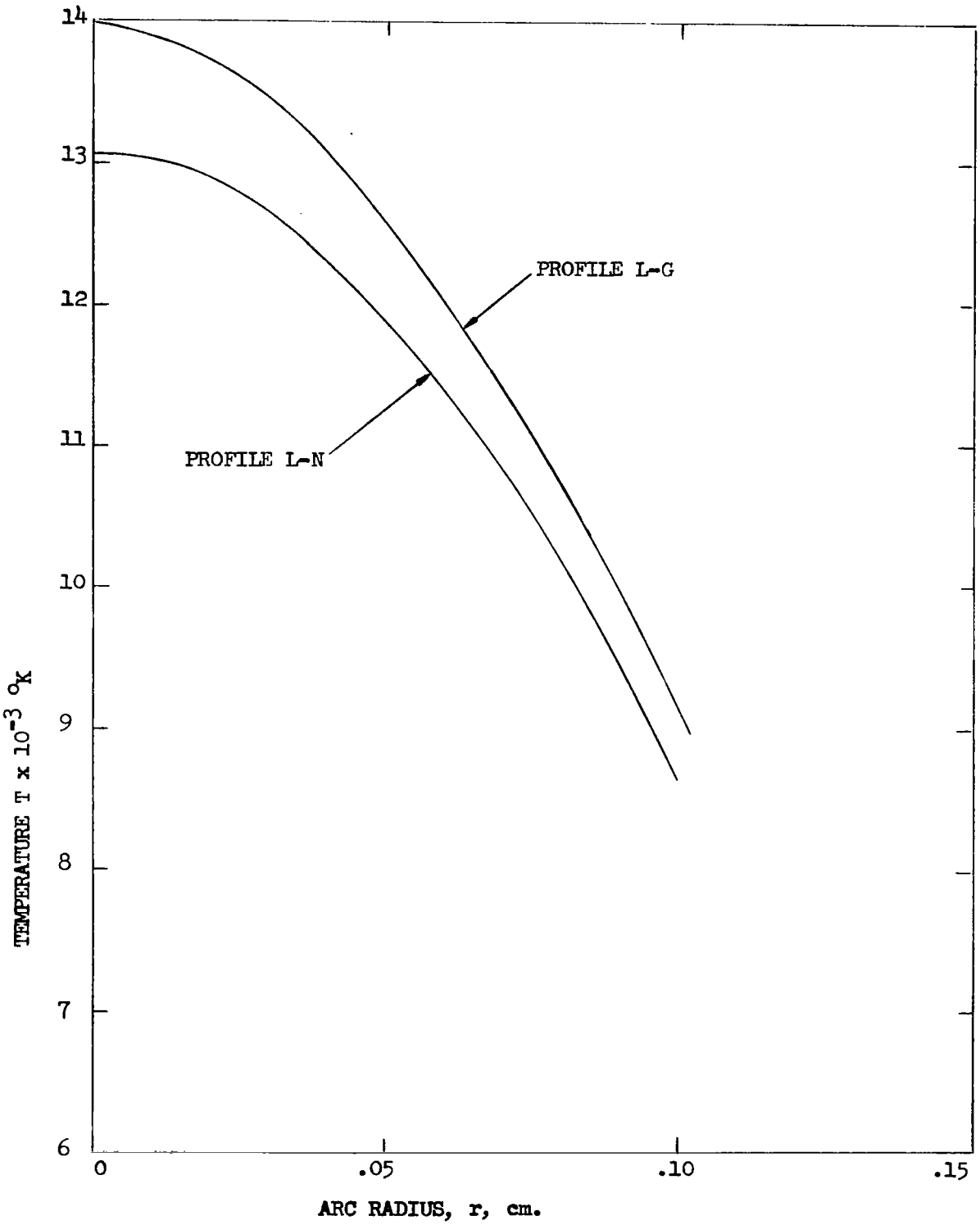

FIG. 30. RADIAL TEMPERATURE DISTRIBUTION OF 50-AMPERE HYDROGEN ARC AT ONE ATMOSPHERE USED IN DETERMINING THE EFFECT OF ERROR IN TEMPERATURE PROFILE ON CALCULATED THERMAL CONDUCTIVITY

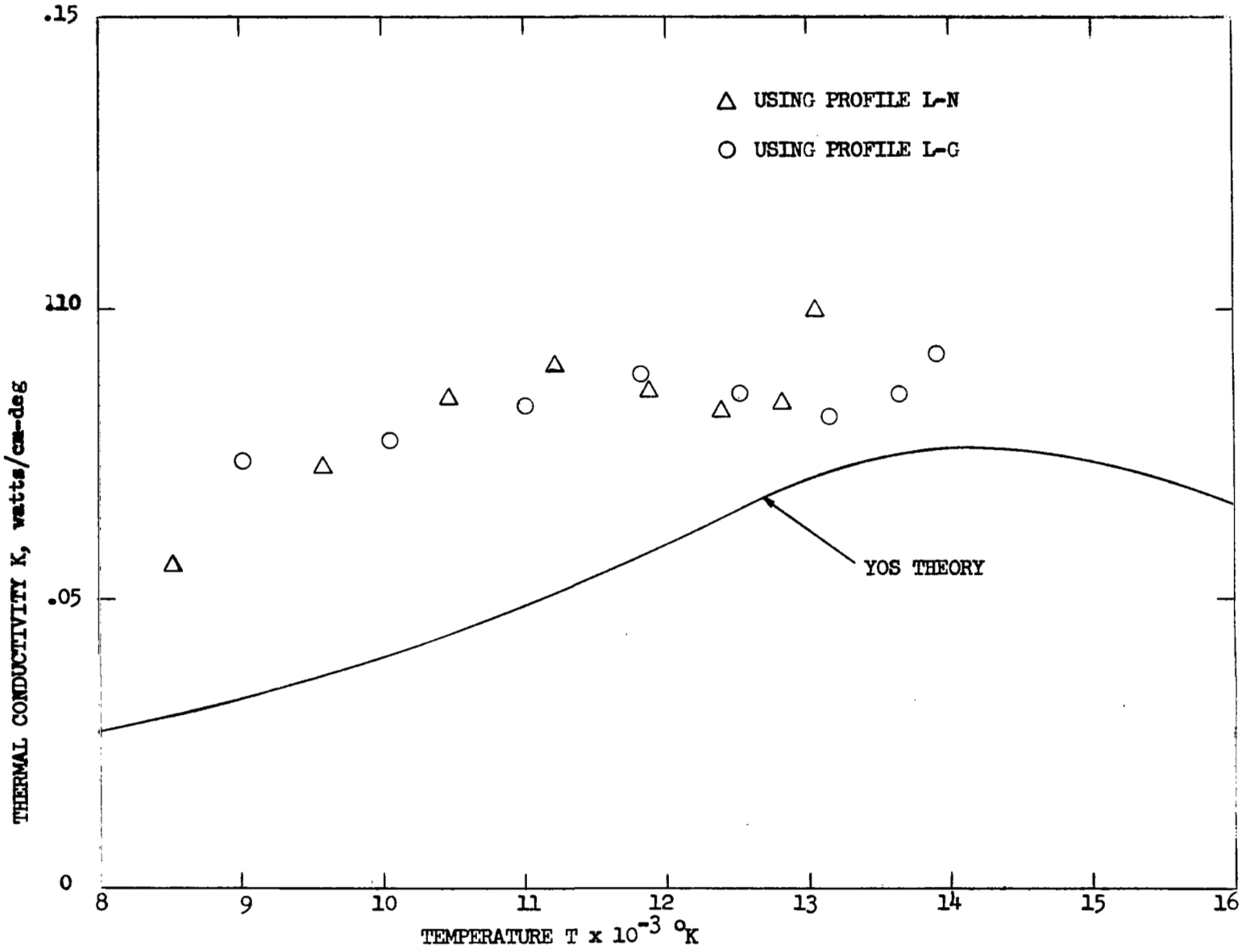

FIG. 31. ILLUSTRATION OF THE EFFECT OF USING DIFFERENT TEMPERATURE PROFILES ON THE CALCULATION OF THERMAL CONDUCTIVITY

with input power, thermal conduction, and vacuum uv continuum. It would be necessary for the visible radiation to increase by factors of the order of 5-10 to account for the power represented by D, and this seems highly unlikely. For the present, the uncertainties in visible radiation, which are thought to be less than about 30%, are ruled out as sources of the discrepancy in K.

4. VUV Continuum

Particularly at the higher temperatures the vuv continuum radiation represents an appreciable fraction of the total energy transfer within the arc column. At lower temperatures less radiation is emitted and absorption becomes important, so that the transfer of vuv continuum radiation is impeded.

The continuum radiation absorption and emission coefficients we have employed are based on the cross section calculations of Burgess and Seaton[3]. In a parallel research effort[12] conducted under contract AF33(615)-2976 we are measuring the continuum absorption coefficients in an end-on arc operated in argon with a small mixture of nitrogen. Preliminary data have been obtained which agree fairly well with the Burgess and Seaton calculations and which differ on the side of yielding less radiation than Burgess and Seaton. Figure 32, reproduced from

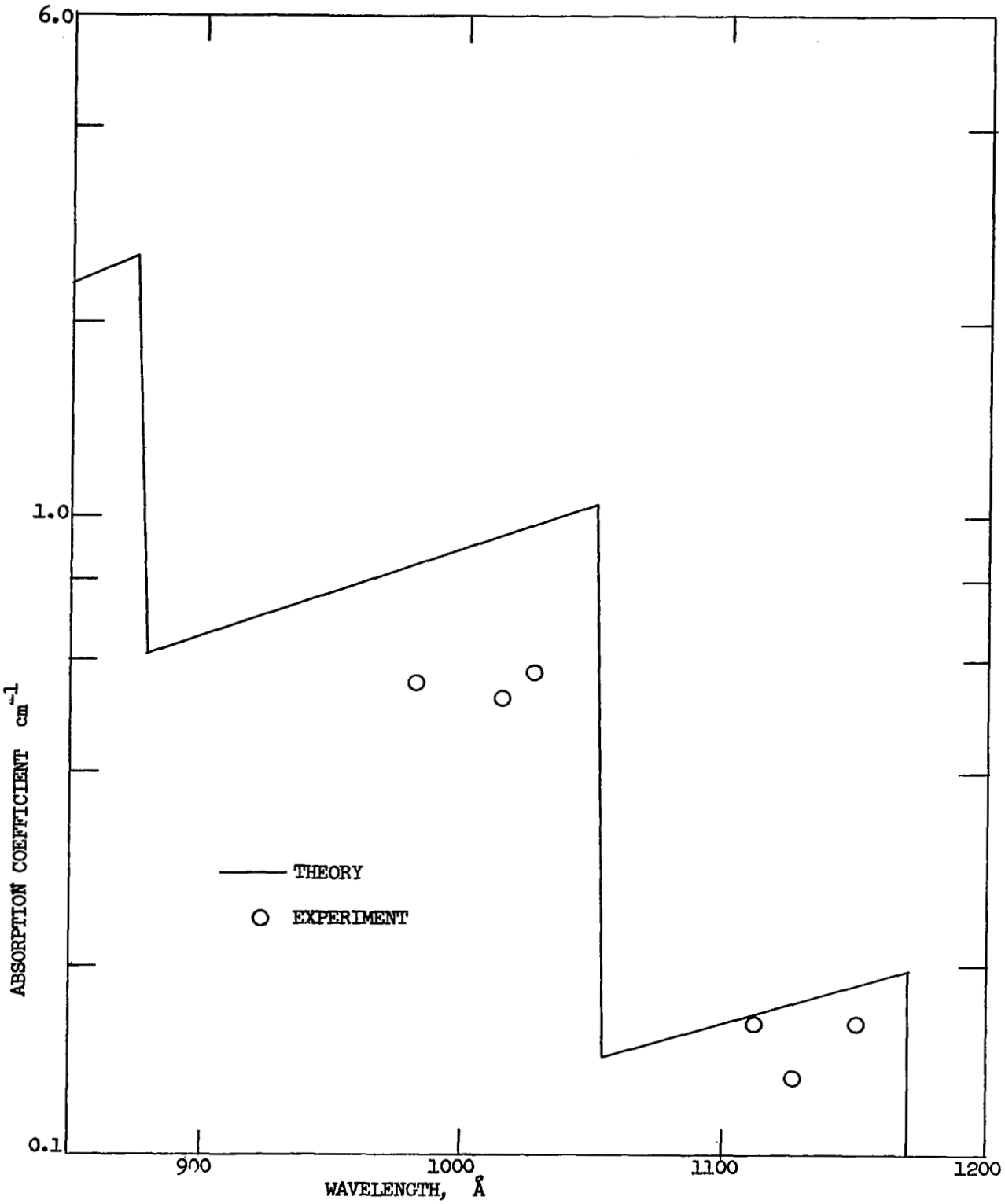

FIG. 32 VACUUM ULTRAVIOLET CONTINUUM COMPARED WITH BURGESS AND SEATON AT 12,000°K, 1 ATMOSPHERE

reference 11, compares our experimental measurements with calculations based on the Burgess and Seaton cross-sections.

Based on these experimental data, we believe that we are not underestimating the vuv continuum radiation as a source of energy transfer.

5. VUV Lines--To date we have not included any contribution to energy transfer by line radiation in the vacuum ultraviolet. The computer program will accept line shape information, but even beyond this the input data describing line shapes and oscillator strengths are poorly known. The available experimental data disagrees significantly with the latest theoretical work.

Still, it is possible to make certain approximate statements about the effects which could be produced by line radiation, in order to determine if the order of magnitude is such as to warrant more detailed investigation. To do this we note, based on elementary considerations of blackbodies and averaging over the wavelength range 0.1 to 0.2μ, that at best a blackbody at 12,000°K can emit 16 watts/cm^2-Å in the spectral range of interest. (This actually varies between about 4 watts/cm^2-Å at 0.1μ to about 28 watts/cm^2-Å at 0.2μ). If we now consider a black cylindrical radiator of radius r, we can calculate the radiative loss per unit length and per unit bandwidth as a function of r. This is done in figure 33. It is of interest to compare this quantity with D.

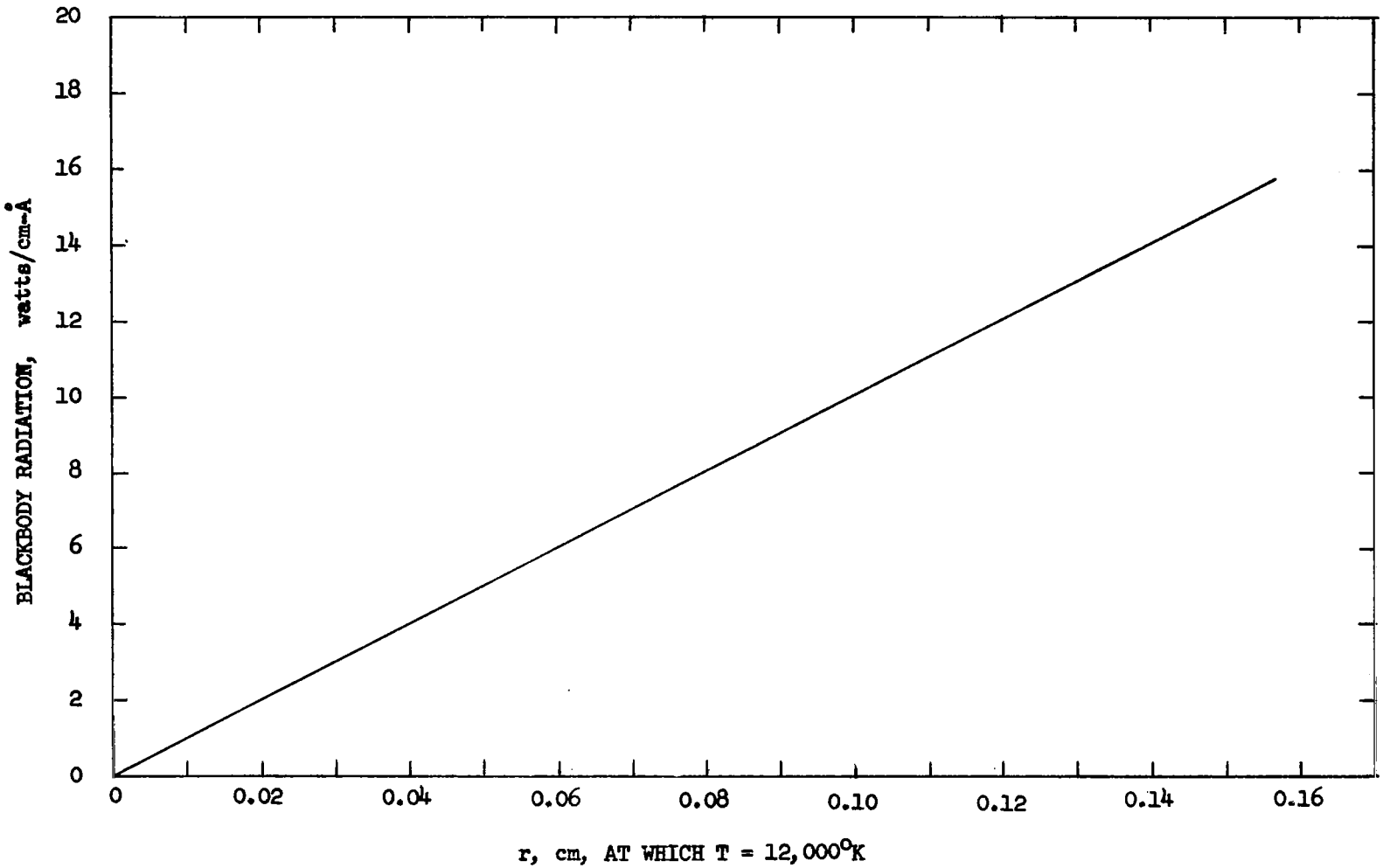

FIG. 33. RADIATIVE LOSS AVERAGED OVER THE SPECTRAL RANGE 0.1 TO 0.2μ AT 12,000°K WITH $\epsilon = 1.0$

It is difficult in view of the existing uncertainties and disagreements between theory and experiment to estimate the sum of all the line widths, but there appear to be of the order of 15 to 30 lines of some magnitude in the nitrogen spectrum (between 0.1 and 0.2μ) at temperatures of the order of 12,000°K; if we assign arbitrarily for this discussion a width in the range 0.1 to 1 angstrom for each line, the total half width will be of the order of 10Å; further, since there can be significant energy transfer at wavelengths several half widths from the line center, one may assume that a bandpass of the order of 20 to 30Å is available for energy transfer. Referring now to figure 33 if the temperature 12,000°K occurs at a radius of 0.12 cm, and if we can sum up all the line radiation processes within this radius by giving an emissivity of unity to a band of 20 to 30Å, then the amount of energy radiated would be of the order of 240 to 360 watts/cm. There would be also, of course, absorption of radiation from outer regions of the arc, and it is beyond the accuracy of this approximation to try to obtain a value for the net transfer, but it could clearly be of the order of 100 watts/cm, which is the same order as D in the appropriate arc column (see figure 22 r = 0.12 cm). If this temperature (12,000°K) occurred at a smaller value of r, say r = 0.04 cm, then the total radiation would be (referring to figure 34) of the order of 80 to 120 watts/cm, while the net transfer would probably be of the order of 20 to 50

watts/cm, not inconsistant with D for the 50 ampere arc column (see figure 25, r = 0.04 cm).

We stress that the numerical implications of this discussion of lines should not be weighted too heavily, for the discussion is crude at best. However, it does serve to indicate that, if the line widths are sufficiently great, an amount of power large enough to affect the results significantly could be transferred; thus it motivates a closer examination of the role of line radiation.

We also point out that the importance of radiation should decrease at lower temperatures, while D seems to grow at lower temperatures (figure 22 and 25), so that line radiation does not appear by itself to be the entire answer.

6. Local Thermal Equilibrium

It appears probable at this time that the addition of line radiation and perhaps a modification of electrical conductivity will result in fairly close agreement between measured and theoretical values of the thermal conductivity of nitrogen at temperatures in the range 10,000 to 15,000^{o}K. However, referring to figure 24, this does not appear to be the case at lower temperatures. It is entirely possible that the constricted arc technique for measurement of thermal conductivity is not applicable at these temperatures, owing to a breakdown in one or more of the assumptions. For example, referring to figure 24, the temperature gradient at a radial station of 0.12 cm is of the order of 50,000^{o}K/cm. It is possible that gradients of this order are sufficient to introduce non-equilibrium populations at

these regions in the arc.

Two measurable parameters which affect the degree of thermal equilibrium which in turn effect the temperature measured in the arc column are the voltage and thermal gradients. The following discussion gives the criteria commonly used to test for equilibrium based upon these two quantities.

a. Influence of the Column Voltage on LTE

The electrons in an arc column are continuously gaining energy from the electric field between collision and thus are always at a higher temperature than the heavy particles in the plasma. This temperature difference can be roughly estimated by the following equation.

$$\frac{\Delta T}{T_e} \approx \frac{T_e - T_g}{T_e} = \frac{(\lambda e E)^2}{(3/2K\ T_e)^2} \quad \frac{M}{4m} \tag{23}$$

where T_e and T_g are the temperatures of the electrons and gas respectively, λ is the mean free path of the electrons, e is the charge of the electron and m its mass. E is the electric field strength, K is Boltzmann's constant and M the mass of the gas atom. Figures 14 and 15 are plots of electric field strength versus current for 1 atmosphere hydrogen and nitrogen arcs.

Figure 34 gives $\Delta T/T_e$ for both nitrogen and hydrogen as a function of total arc current. The absolute accuracy of these data is questionable since the values calculated do not take into account any radial dependency of the plasma operating conditions

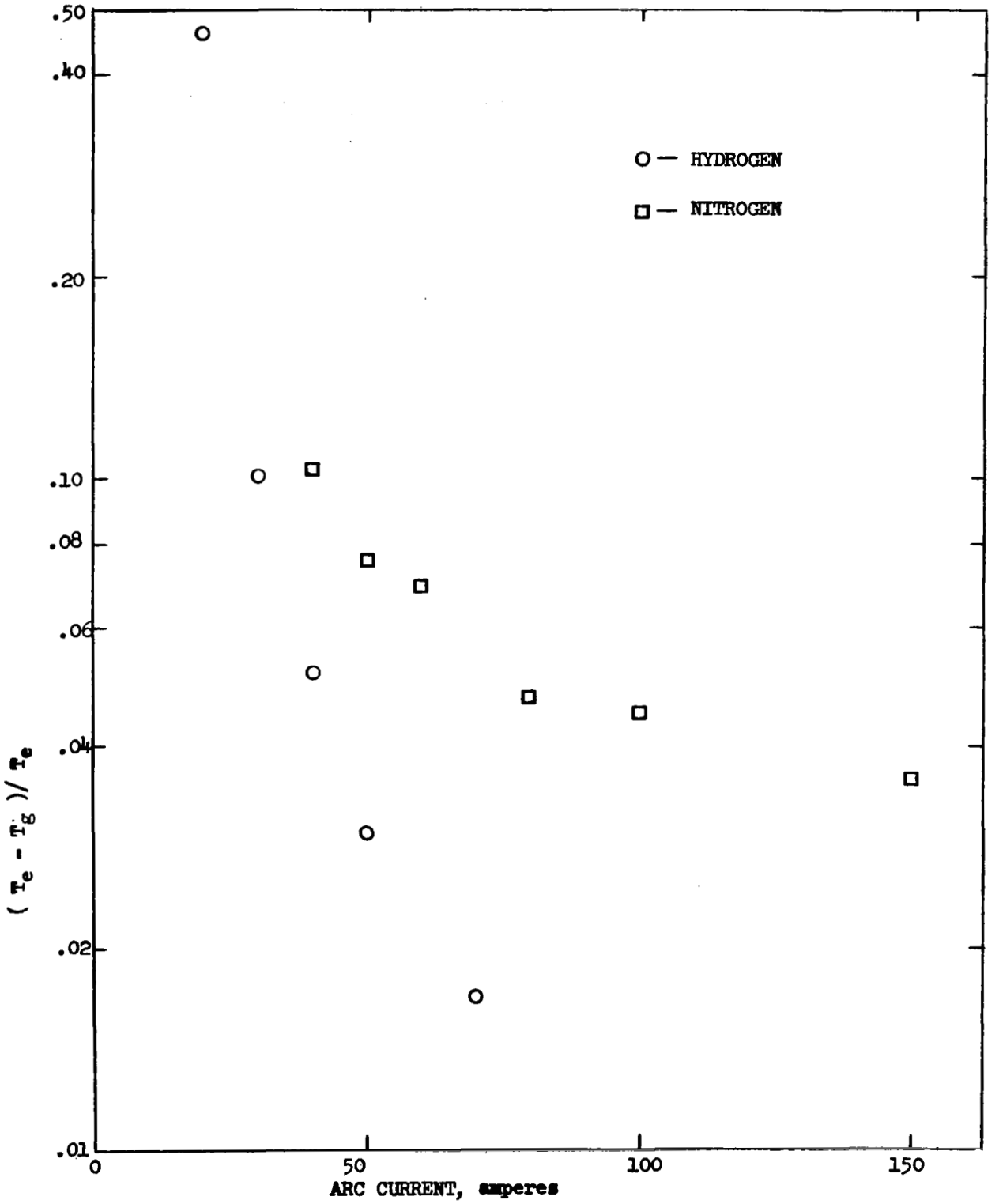

FIG. 34 DEGREE OF INEQUILIBRIUM OF HYDROGEN AND NITROGEN ARCS AT VARIOUS CURRENTS AND ONE ATMOSPHERE PRESSURE AS DETERMINED USING THE ARC COLUMN VOLTAGE GRADIENT

such as temperature or density. Nor does it account for other energy inputs or losses to the heavier particles, such as excitation or de-excitation through radiation. However, the general trend indicates that there will be greater departures in LTE for decreasing currents.

b. The Influence of Radial Temperature Gradients

The condition of LTE of a plasma in an arc column is also a function of radius and the radial temperature graidents. If the electron number densities and atom excitations are to be in LTE with the ground state number density, the following condition must be met

$$\frac{T(o) - T(d)}{T(o)} = \varepsilon << 1 \tag{24}$$

where d is the average equilibrating distance given by

$$d \propto \left[\frac{\frac{E_2^{0,a} T}{f_{21}} \exp\left(\frac{E_2^{0,a}}{KT}\right) \frac{1}{M_a^{1/2}}}{(N_a + N'_a)\ (N_a + 10N'_a)} \right]^{1/2} \tag{25}$$

where $E_2^{0,a}$ is the ionization potential of the first atomic excited level having an allowed transition to the ground state whose absorption oscillator strength is f_{21}.

M_a is the atomic mass,

N_a is the total density of atoms and ions,

and N_a^1 is the density of singly ionized atoms of chemical species "a".

Figure 35 gives calculations of d versus temperature for nitrogen and hydrogen for a pressure of one atmosphere. The criterion of equation (25) has been applied to both nitrogen and hydrogen not only for the column axis, figure 36, but for a radius where the temperature is 10^{4}°K, Figure 37.

For the latter calculation, d was relaxed by a factor of ten because of the additional excitation and ionization gained by the radiation input at these radii coming from inner regions of the column. In addition, there is also an input from the diffusion of ions and excited atoms to these radii. To a first approximation the temperature as measured by lines or continuum is lower by a factor of $(1+\varepsilon)^{-1}$ than the actual electron temperatures if LTE existed.

Both of these tests show that departures from LTE are greater at low currents. The actual magnitude of the departures however probably can not be established better than a factor of ten because of the approximations which have been made to develop equation (23) and (25). The results of these calculations would suggest that the difference observed between theoretical and experimental values of thermal conductivity at the high temperature

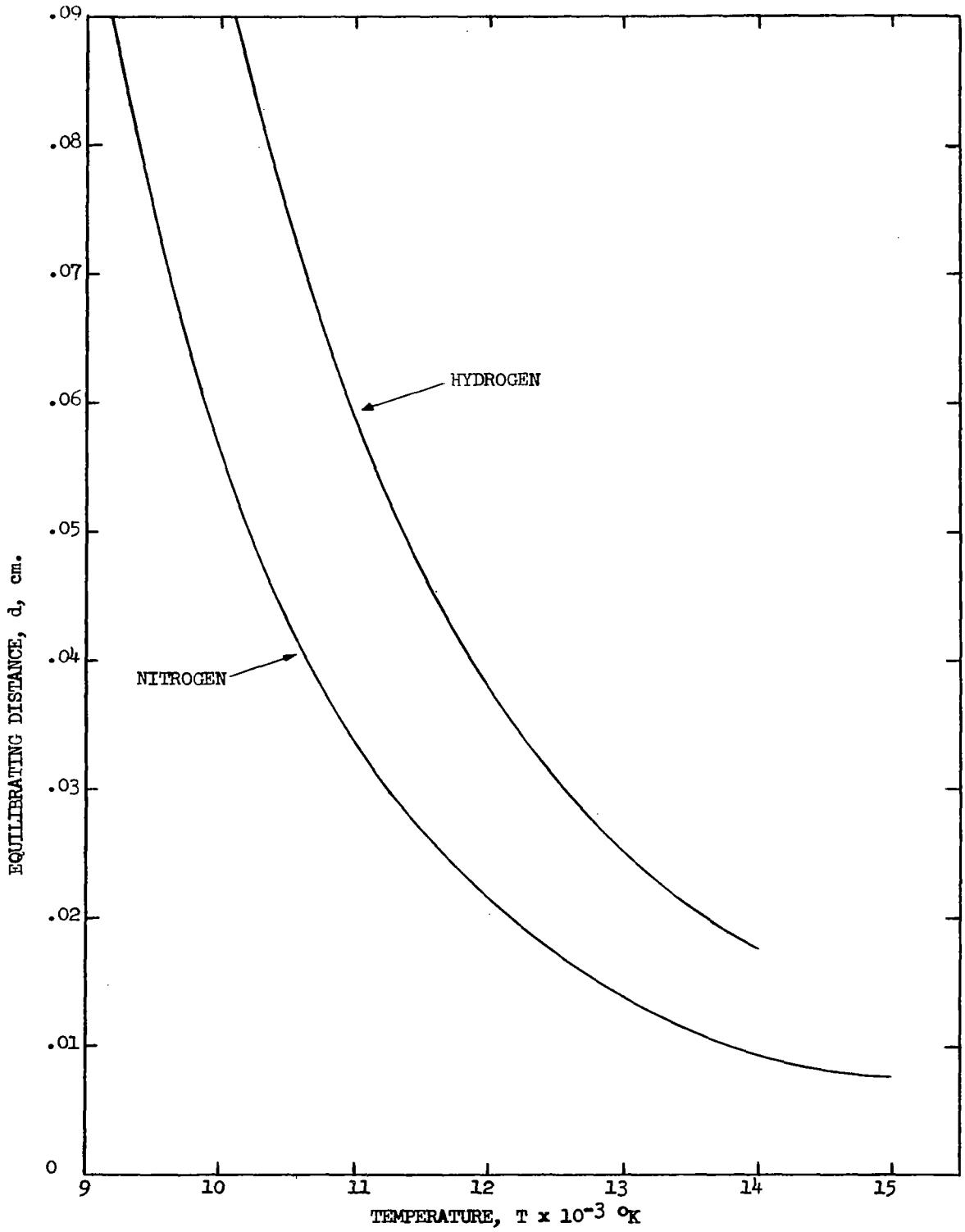

FIG. 35. CALCULATED EQUILIBRATING DISTANCES IN ONE ATMOSPHERE NITROGEN AND HYDROGEN ARCS AS A FUNCTION OF ARC CENTRAL CORE TEMPERATURES.

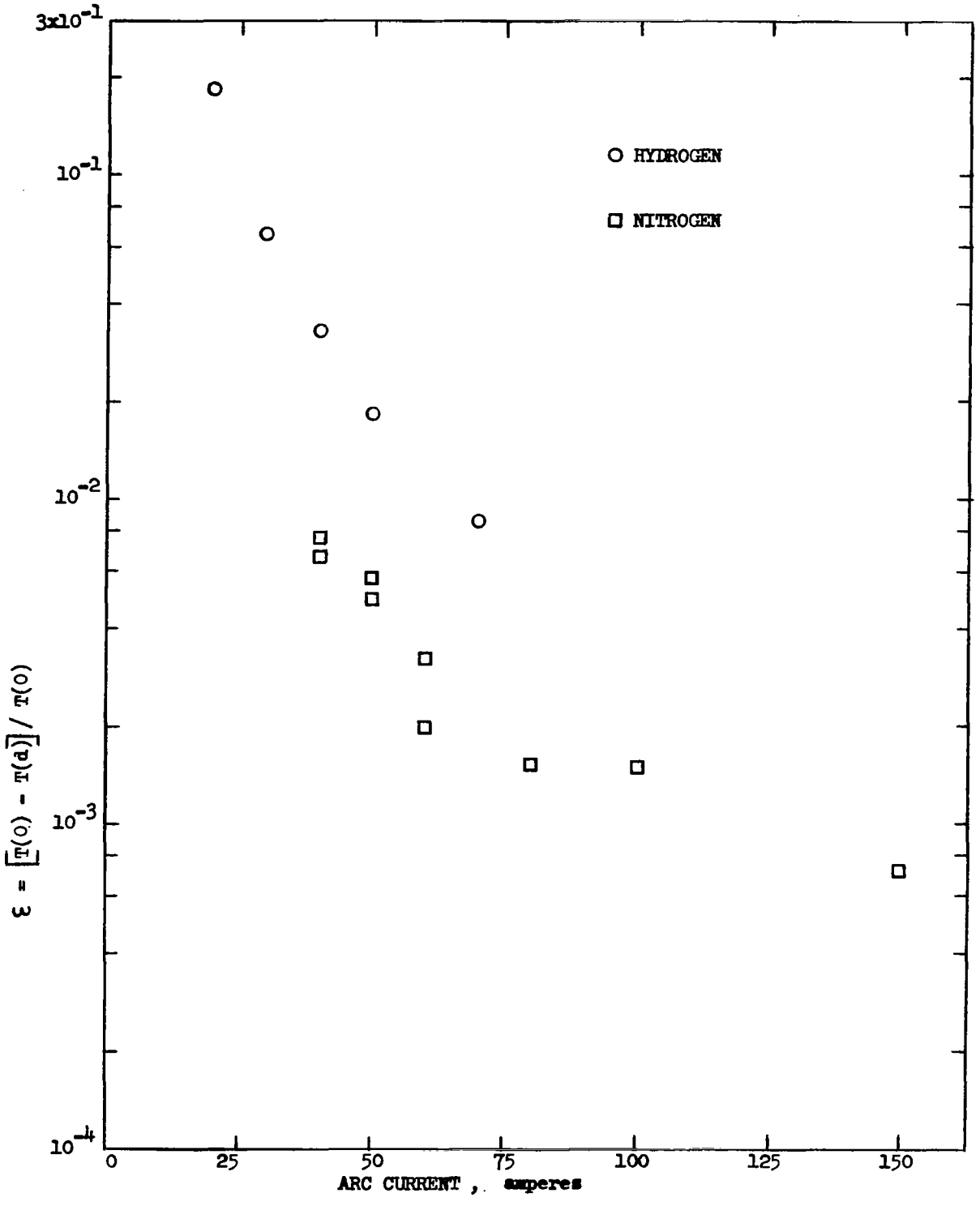

FIG. 36. DEGREE OF INEQUILIBRIUM OF HYDROGEN AND NITROGEN ARCS AT VARIOUS CURRENTS AND ONE ATMOSPHERE PRESSURE AS DETERMINED USING THE AVERAGE EQUILIBRATING DISTANCE

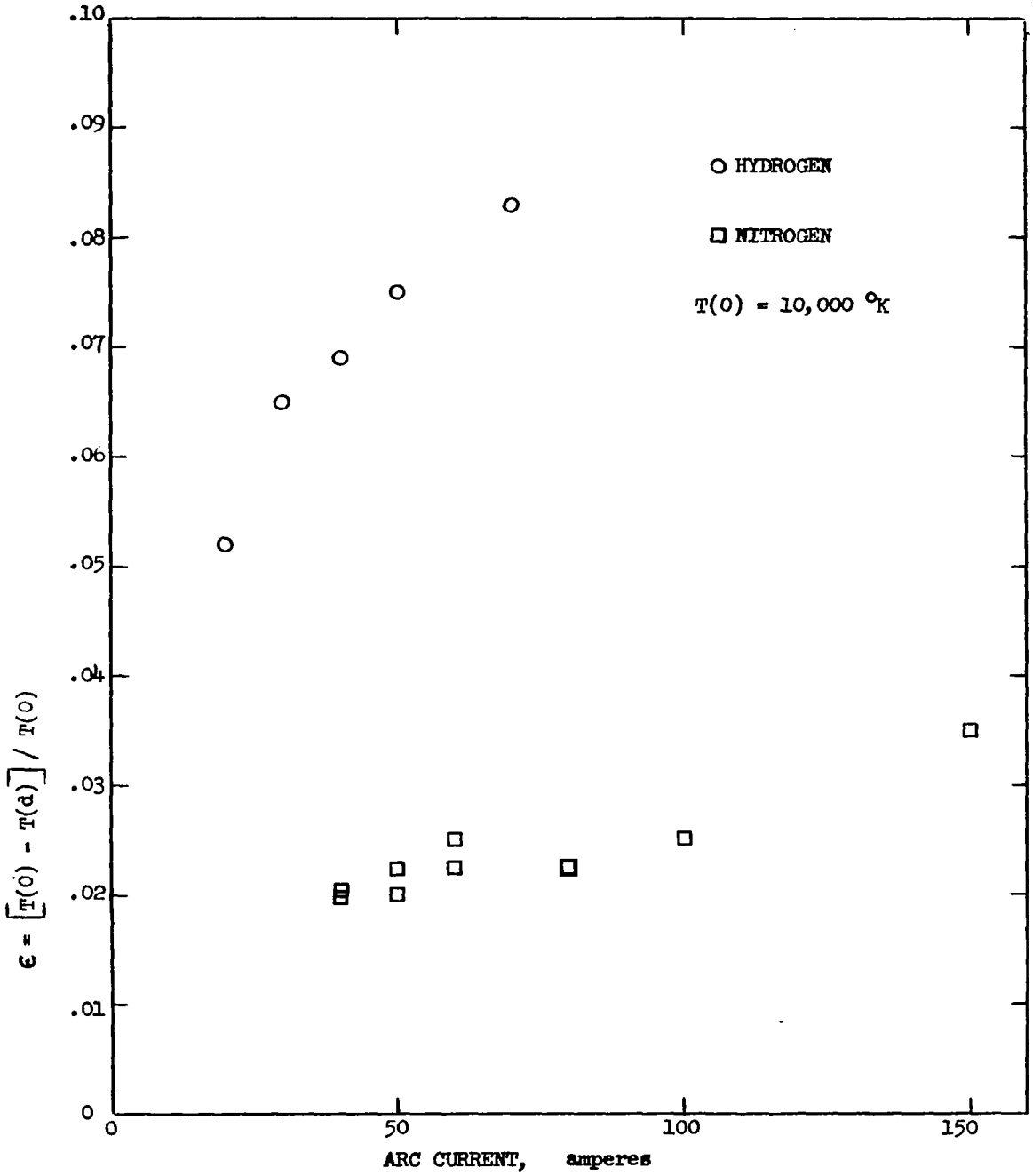

FIG. 37. DEGREE OF INEQUILIBRIUM OF HYDROGEN AND NITROGEN ARCS AT VARIOUS CURRENTS AND ONE ATMOSPHERE PRESSURE AS DETERMINED BY THE AVERAGE EQUILIBRATING DISTANCE RELAXED BY A FACTOR OF TEN

would not be a result of a departure from LTE, however there is certainly a significant non LTE trend near the outer radius or at low current $I < 30$ amp where wall voltage or temperature gradients are large. This possibly could give rise to an anomaly in the measured values of K.

C. Hydrogen

The hydrogen data were analyzed by the same procedure as was used above for nitrogen. The total power losses by various mechanisms are plotted in figures 38 and 39 for the 50 and 70 amp runs in hydrogen. The power inputs and thermal conductivity losses shown in these figures were calculated from the measured temperature distributions and electric field strengths using the theoretical electrical and thermal conductivity values shown in figures 16 and 40 (ref. 9, 16). The radiative losses were included in the calculations shown in figures 38 and 39; however, rough calculations indicate that this type of radiation is not important in the case of hydrogen.

Figures 38 and 39 indicate that the discrepancies between the calculated input and output powers in hydrogen are similar to or perhaps somewhat larger than those found above in nitrogen. In order to attempt to account for these discrepancies, we consider in turn the possible errors in each of the components of the arc energy balance.

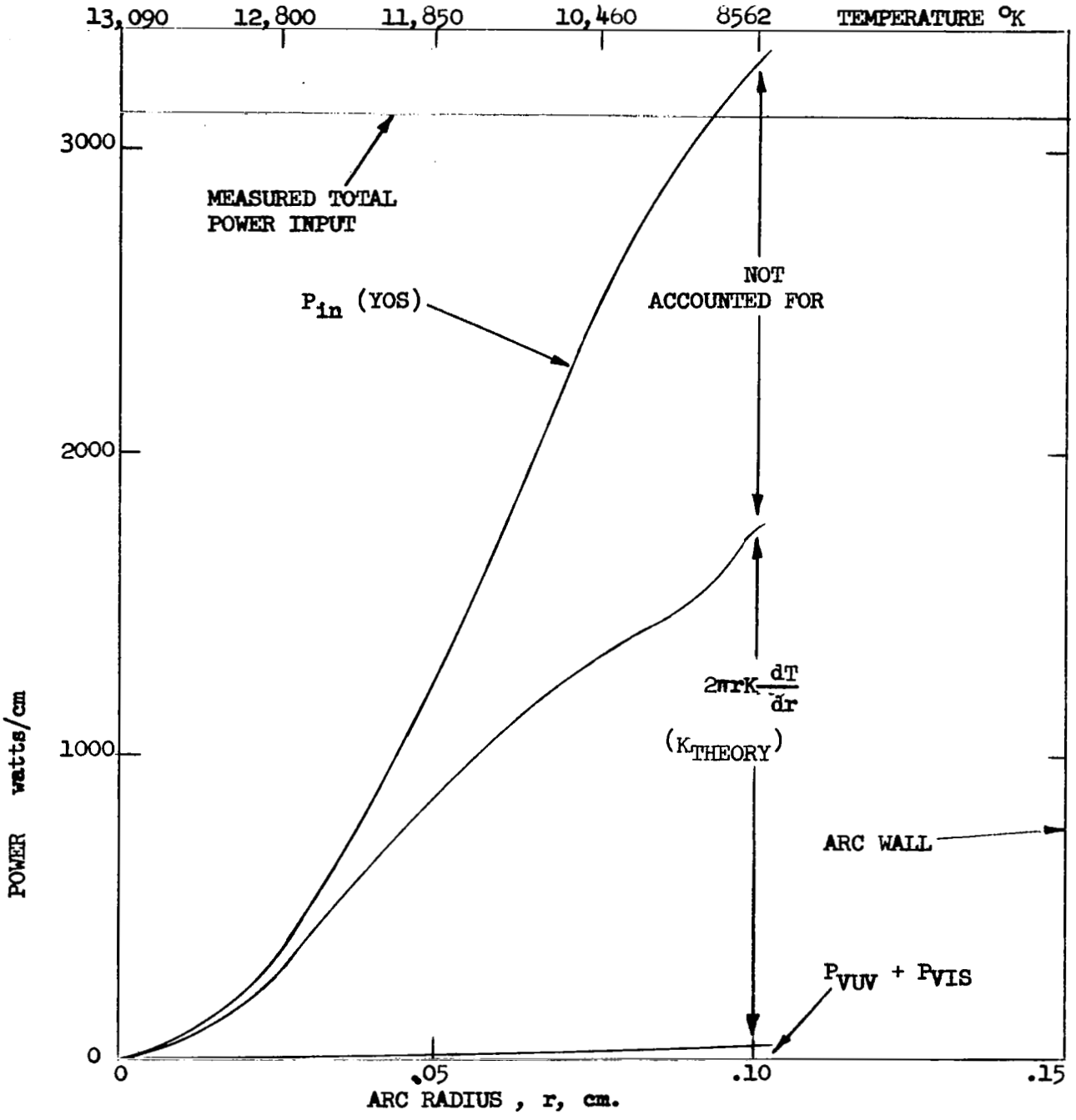

FIG. 38 . POWER/UNIT LENGTH vs. r FOR VARIOUS POWER TRANSPORT MECHANISMS IN A 50-AMPERE HYDROGEN ARC AT ONE ATMOSPHERE

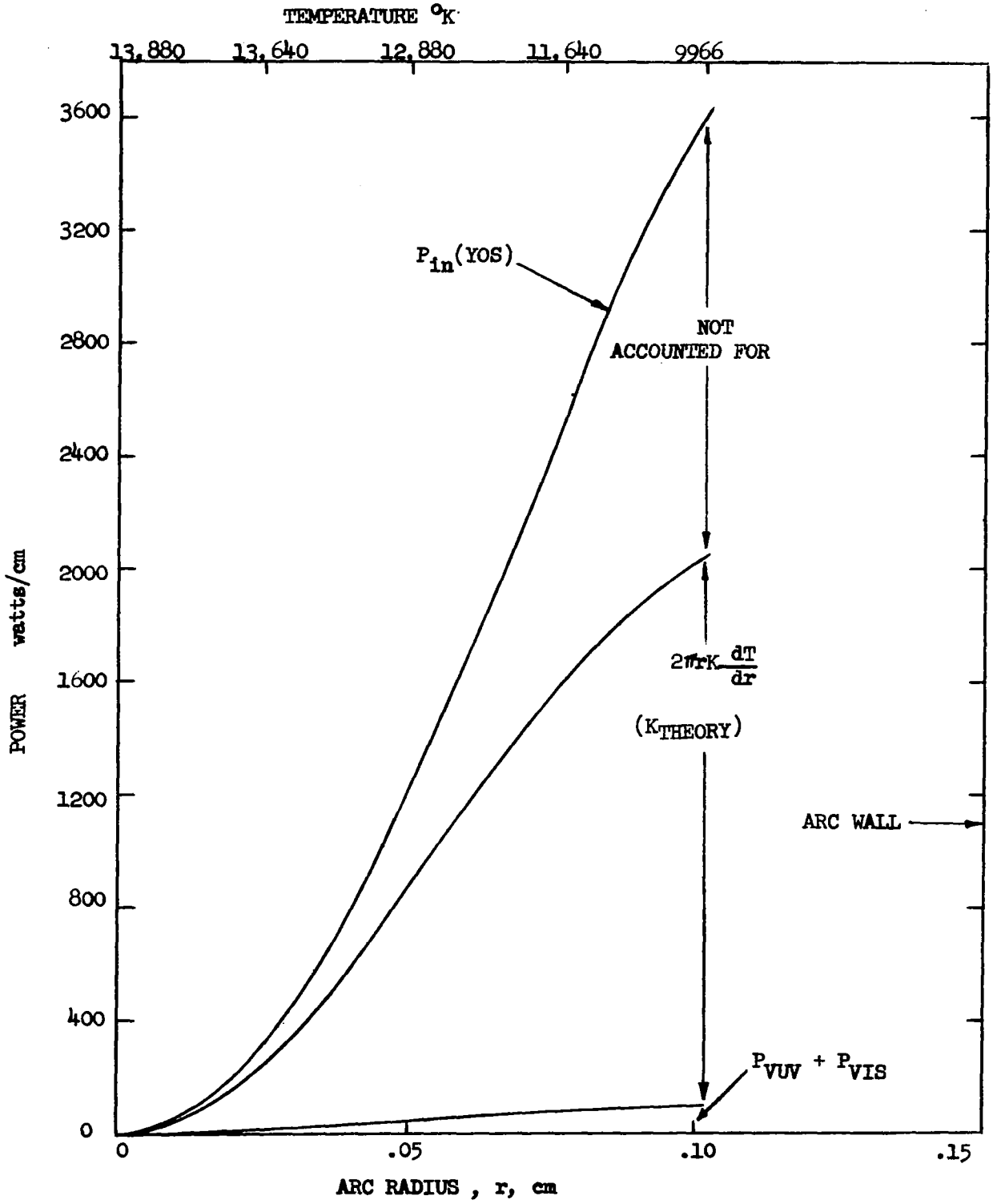

FIG. 39 . POWER/UNIT LENGTH vs. r FOR VARIOUS POWER TRANSPORT MECHANISMS IN A 70-AMPERE HYDROGEN ARC AT ONE ATMOSPHERE

The total power input to the arc calculated from the product of the experimental field strength and arc current is indicated by the solid horizontal lines in figures 38 and 39; this value is seen to be in reasonably good agreement with the total power input calculated from the theoretical electrical conductivity values. The same fact is indicated in another way in figure 16, where the theoretical electrical conductivity is compared with values calculated from the experimental data s as described in Section III, D.

It thus appears from this comparison that the power input to the arc used in our analysis can not be greatly in error. Consideration of possible errors in the experimental values used for the electrical field strengths and temperature distributions and in the theoretical electrical conductivity values leads to a similar conclusion. Altogether, it appears reasonable to assign a maximum possible error of perhaps 20 to 30% in our final values for the power input to the arc.

According to the calculations shown in figures 38 and 39, radiation is only a minor component of the arc energy balance in hydrogen for the operating conditions of our work. Since, moreover, the radiative properties of hydrogen are fairly well known, it appears that radiation could not be responsible for

any major part of the discrepancy between the input and output powers indicated in figures 38 and 39. Including the effects of ultraviolet line radiation and of possible errors in our treatment of the radiative transport problem, it appears that the maximum error in the calculated radiative power loss could not be greater than perhaps about 5 to 10% of the total arc input power.

The only remaining power loss mechanism indicated in figures 38 and 39 is thermal conduction. If the difference between the power input and the radiative power loss is attributed entirely to this mechanism, then one obtains the experimental thermal conductivity values shown in figure 40. These values agree within the errors believed to be in the theoretical calculations at the highest temperatures studies, but the agreement becomes progressively poorer at lower temperature until at around 10,000^{o}K the experimental values are about a factor of 2 higher than the theoretical ones.

In view of this inconsistency between the results for the different arc currents, as well as for other reasons which shall be outlined below, we do not regard the discrepancy between the theoretical and experimental values of the thermal conductivity shown in figure 40 as significant.

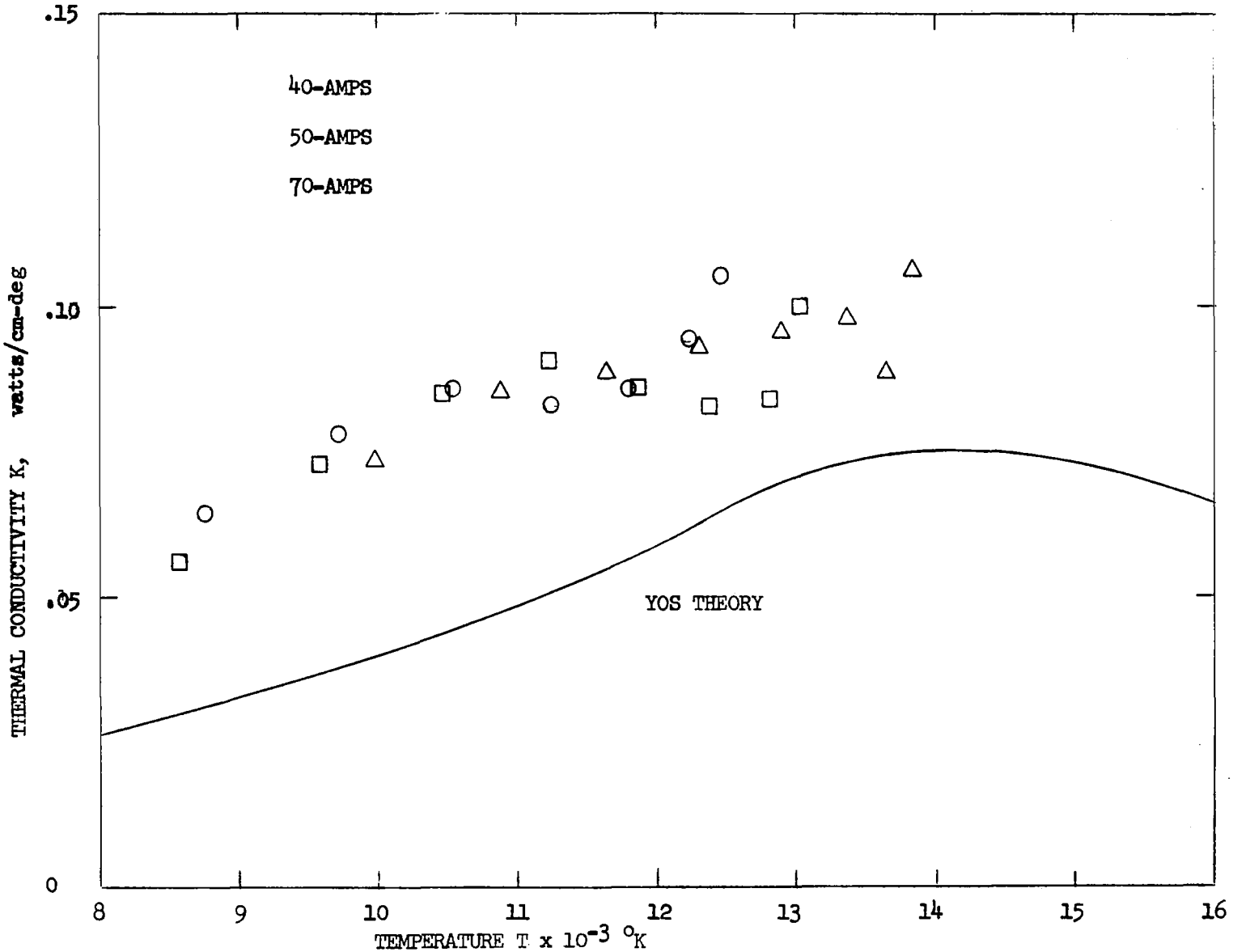

FIG. 40. EXPERIMENTAL THERMAL CONDUCTIVITY OF HYDROGEN AS CALCULATED USING THE DATA OF ONE ATMOSPHERE HYDROGEN ARC RUNS OF 40-, 50-, AND 70-AMPERES

If it is assumed that the arc column is described correctly by the generalized Heller-Ellenbass equation (eq.4), then the possible error in the experimental thermal conductivity values can be estimated from the maximum errors in the power input and the radiative power loss given above.

If it is assumed that the experimental thermal conductivities are actually in error by this maximum amount and the values shown in figure 40 are reduced accordingly, then one finds that the experimental values are only about 20 to 40% above the theoretical values at the lower temperatures. Since this is within the estimated error of the theoretical calculations, it appears conceivable that the discrepancy between the input and output powers noted in figures 38 and 39 may be due entirely to errors in the theoretical values of the calculations and the experimental data. However, it is also reasonable to suspect that the discrepancy may also be partially due to convection and non LTE at the outer region of the hydrogen column. It should be noted here that both convection effects and the failure of LTE, the latter being noted in figures 34 thru 37, appear to be considerably more important in the case of hydrogen than they are for nitrogen.

REFERENCES

1. RAD, Evaluation of High-Temperature Gas Transport Properties, First Quarterly Report Avco RAD-SR-65-190, Contract NASw-1188 (August 1965).

2. Maecker, H. "The Properties of Nitrogen up to 15,000°K" AGARD Report No. 324 (September 1959).

3. Burgess, A. and M. J. Seaton, Rev. Mod. Phys., 30, 992 (1958).

4. Stewart, J. C. and K. D. Pyatt, Jr., "Theoretical Study of Optical Properties" AFSWC TR 61-71, Vol. III, September 1961, p. 356.

5. RAD, Theoretical and Experimental Studies of High-Temperature Gas Transport Properties, Final Report, Avco RAD-TR-65-7, Contract NASw-916, (May 1965).

6. RAD, Research on Radiation from Arc Heated Plasma, Final Report, Avco RAD-TR-65-17, Contract AF33(616)-8390, Project 7063, Task 7063-3 (July 1965).

7. Drellishak, K. S., et al, Tables of Thermodynamic Properties of Argon, Nitrogen, and Oxygen Plasmas. Technical Documentary Report No. AEDC-TDR-64-12, Arnold Engineering Development Center, Air Force Systems Command, USAF.

8. Burhorn and Wienecke Z. f Phys. Chemie, 215 269, 285 (1960).

9. "Transport Properties of Nitrogen, Oxygen and Air to 30,000°K, "Avco RAD TM-63-7, March 1963.

10. "Evaluation of High Temperature Gas Transport Properties" Second Quarterly Progress Report, Avco RAD SR-65-302.

11. Private Communication from Warren Ahtye, NASA/Ames Research Center, February 1966.

12. "Research on Radiation from Arc Heated Plasma," Avco RAD Second Quarterly Progress Report on Contract AF33(615)-2976, December 1965.

13. Lochte-Holtgreven--"Production and Measurement of High Temperatures" Reports on Progress in Physics Vol. XXI The Physical Society 1958.

REFERENCES (Cont'd)

14. "Research on Radiation from Arc Heated Plasma Contract AF33(615)-2976.

15. Barr, W. L., JOSA 52, 885 (1962).

16. Yos, J. Avco RAD Unpublished Calculation, 1966.

APPENDIX I

TREATMENT OF RADIATIVE TRANSPORT IN THE ARC COLUMN

A. General Expression for the Radiative Flux

As pointed out under Part II, in the absence of convection, the energy balance for a long cylindrically symmetric arc column may be written in the form

$$\int_0^r \sigma E^2 \, 2\pi r \, dr = 2\pi r \, (q_k + q_{rad}) \qquad \text{(I-1)}$$

where $\int_0^r \sigma E^2 \, 2\pi r \, dr$ is the electrical energy input per unit length to the gas inside a cylinder of radius r, and

$$q_K = -K\frac{dT}{dr} \qquad \text{(I-2)}$$

and q_{rad} are the energy fluxes per unit area across the boundary of the cylinder due to conduction and radiation, respectively. If the arc column is optically thin to the emitted radiation, the radiated flux q_{rad} may be written simply as an integral over the radiated power per unit volume inside the cylinder,

$$2\pi r \, q_{rad} = \int_0^r P_{rad} \, 2\pi r dr \qquad \text{(I-3)}$$

and one obtains the ordinary, "optically thin" Elenbaas-Heller equation

$$\sigma E^2 = -\frac{1}{r}\frac{d}{dr}\left(rK\frac{dT}{dr}\right) + P_{rad} \qquad \text{(I-4)}$$

which we have used in our previous analyses of the arc column. As we have indicated previously however[1], the approximation of optical thinness is not adequate for the treatment of the high-temperature nitrogen arc, since for this (and many other) gases there is a sizeable contribution to the total energy balance due to far ultraviolet radiation, for which the absorption length is comparable to or smaller than the arc dimensions. We have therefore undertaken to modify our previous analysis of the arc data to take account of the effects of the absorption of radiation within the arc volume itself.

For the general case, where there is absorption of radiation, the total radiative flux in the outward direction q_{rad}, which occurs in the energy balance equation (I-1), may conveniently be written as an integral over all frequencies ν of the outward radiative flux q_ν at each individual frequency,

$$q_{rad} = \int_0^\infty q_\nu \, d\nu \qquad \text{(I-5)}$$

q_ν, in turn, may be expressed as an integral over all directions $\vec{\Omega}$ of the radiative intensity I_ν,

$$q_\nu = \int I_\nu \cos\theta \, d\Omega \qquad \text{(I-6)}$$

In this expression the unit vector $\vec{\Omega}$ represents the direction in which the radiation is traveling, θ is the angle between this direction and the outward radial direction, and the radiative intensity I_ν in any direction $\vec{\Omega}$ is defined by the condition that the power dP carried across a plane normal to the direction of propagation by radiation traveling in the element of solid angle $d\Omega$ and in the frequency interval $d\nu$ should be given by

$$dP \equiv I_\nu \, d\Omega \, dA \, d\nu \qquad \text{(I-7)}$$

where dA is the element of area in the plane. Now it can readily be shown that a general expression for the radiative intensity I_ν in a medium in which the absorption coefficient α_ν and the temperature T are arbitrary functions of position is given by[2]

$$I_\nu = \int_0^{\tau_\nu} I_B(\tau_\nu') \, e^{-(\tau_\nu - \tau'_\nu)} \, d\tau'_\nu \qquad \text{(I-8)}$$

where the integral is evaluated along the direction of propagation of the ray considered,

$$\tau_\nu \equiv \int_{-\infty}^{s} \alpha_\nu(s') \, ds' \qquad \text{(I-9)}$$

is the optical depth to point s along the ray trajectory and

$$I_B = \left(\frac{2\ h\nu^3}{c^2}\right) \Big/ \left(\frac{h\nu}{e^{kT}-1}\right) \qquad \text{(I-10)}$$

is the blackbody intensity for the indicated temperature and frequency. For the case of an infinitely long circular cylinder of radius R in which all gas properties depend only on the radial coordinate r, equations (I-6) and (I-8) may be combined to yield the following general expression for the outward radiative flux q_ν:

$$q_\nu = \frac{2}{r} \int_0^r dr_0 \int_0^\pi \sin\psi\ d\psi \int_{r_0}^R \frac{\alpha_\nu(r')\ I_B\ (r')}{(r'^2 - r^2_0)^{\frac{1}{2}}} \qquad \text{(I-11a)}$$

$$\times\ g(r, r', r_0, \sin\psi)\, r' dr'$$

with

$$g(r, r', r_0, \sin\psi) \equiv \exp\left[-\frac{1}{\sin\psi}\ (t(r_0, r') + t(r_0, r))\right] \qquad \text{(I-11b)}$$

$$+ \frac{r - r'}{|r - r'|} \exp\left[-\frac{1}{\sin\psi}\ |t(r_0, r') - t(r_0, r)|\right]$$

$$t(r_0, r) \equiv \int_{r_0}^r \frac{\alpha_\nu(r')\, r'\ dr'}{(r'^2 - r_0^2)^{\frac{1}{2}}} \qquad \text{(I-12)}$$

In this equation, ψ and r_0 are variables describing the direction of propagation $\vec{\Omega}$ of the radiation, ψ being the angle between the direction of propagation and the cylinder axis and r_0 the minimum distance between the ray trajectory and the axis.

An alternative expression for q_ν which is sometimes more convenient may be obtained from equation (I-11a) by integrating by parts over r', yielding the result

$$q_\nu = -\frac{2}{r}\int_0^r dr_o \int_0^\pi \sin^2\psi \, d\psi \int_{r_o}^R \frac{dI_B}{dr'} h(r,r',r_o,\sin\psi)\, dr' \quad \text{(I-13a)}$$

with

$$h(r,r',r_o,\sin\psi) = \exp\left[-\frac{1}{\sin\psi}\left| t(r_o,r') - t(r_o,r)\right|\right] - \exp\left[-\frac{1}{\sin\psi}\left(t(r_o,r') + t(r_o,r)\right)\right] \quad \text{(I-13b)}$$

Equations (I-5), (I-12), and (I-11) or (I-13) thus provide the desired generalization of equation (I-3) for the case when the arc column is not optically thin.

B. <u>Simplification of the Formula for an Arbitrary Absorption Coefficient</u>

In order to determine the thermal conductivity of a gas from electric arc data using equations (I-1) and (I-2), it is first necessary to evaluate the radiation flux q_{rad} for each value of the radial coordinate r for which calculations are being carried out. Assuming that the absorption coefficient α_ν is known, this could be done in principal by straightforward numerical integration of the general equations for q_{rad} developed in the preceding section. One sees, however, that this would involve a three-dimensional spatial

integration and an integral over frequencies for each value of the radial coordinate r, the evaluation of q_{rad} for any given arc run would be essentially equivalent to a five-dimensional integration. This would be rather lengthy, even for a high speed digital computer, so that it is desirable to simplify the general formulas as much as possible before proceeding to numerical computations. Fortunately, this proves to be possible in the present case without significant loss in accuracy, as we shall now show.

Let us use the form (I-11) for q_ν and consider first the integral over ψ. This integral can be written in terms of the single function

$$Y(x) \equiv \int_0^\pi \sin\psi \; e^{-\frac{x}{\sin\psi}} \, d\psi, \qquad \text{(I-14)}$$

where, from (I-11), the argument x may be either $|t(r_0,r') - t(r_0,r)|$ or $(t(r_0,r') + t(r_0,r))$. Equation (I-14) can be integrated in terms of hyperbolic Bessel functions to yield the result

$$Y(x) = 2xK_1(x) - 2x \int_x^\infty K_0(x)\, dx \qquad \text{(I-15)}$$

where K_0, K_L, and $\int K_0\, dx$ are tabulated functions.[3] Values of Y(x) calculated from equation (I-15) are plotted in Figure I-1 for x in the range $0 \leq x \leq 10$. For larger values of x, Y(x) decreases asymptotically as $\sqrt{2\pi/x}\; e^{-x}$.

For numerical calculations, it is convenient to have a simple analytical approximation for Y(x). From the form of the function Y(x), as indicated by equation (I-14) and Figure I-1, it appeared that a suitable form for this approximation might be a sum of exponentials,

$$Y(x) \approx \sum_{i=1}^{n} a_i \, e^{-b_i x} \qquad \text{(I-16a)}$$

with the coefficients a_i and b_i determined by curvefitting the exact result (I-15). Using the form (I-16a), we obtained the simple two term curvefit

$$Y(x) \approx 1.385 \, e^{-1.0762x} + 0.600 \, e^{-2.100x} \qquad \text{(I-16b)}$$

which agrees with the exact result (I-15) within 0.8% for $0 \leq x \leq 6$ and within ~10% for $x \leq 10$. The percentage error increases gradually for larger values of x, but since Y(x) itself decreases exponentially with x, errors in Y(x) for large x will have a negligible effect on the integrated radiative flux q_ν given by equation (I-11). Thus the simple approximation (I-16b) for Y(x) should be adequate for practical calculations of the radiative flux in practically all cases. For those cases in which better than 1% accuracy is required one can simply use a few additional terms in the curvefit (I-16a) until the desired accuracy is attained.

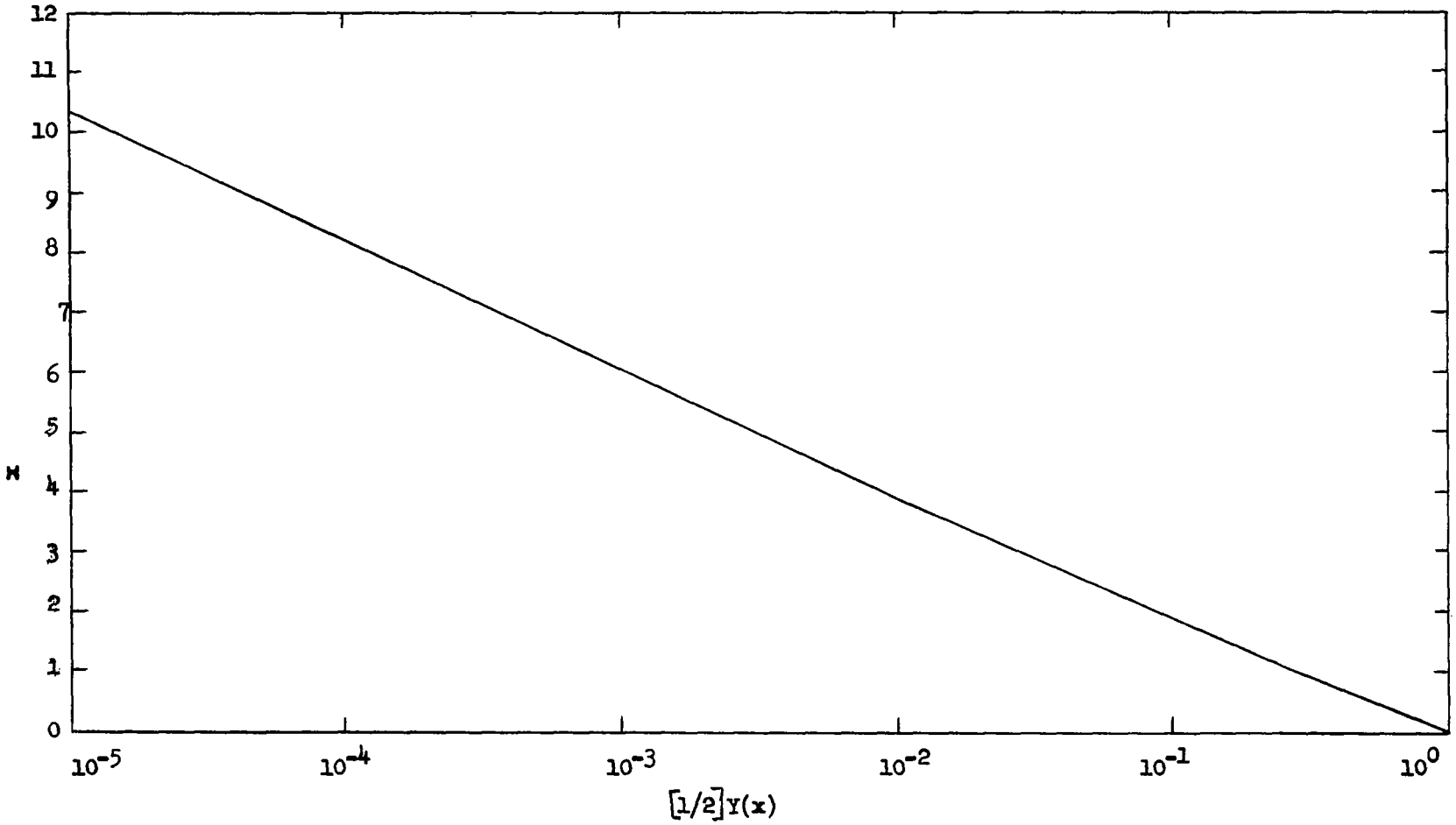

FIG. I-1. KERNEL FOR THE RADIATIVE TRANSPORT CALCULATION

With the approximation (I-16) for Y(x), equation (I-11) for q_ν becomes

$$q_\nu = \frac{2}{r} \sum_{i=1}^{n} a_i \int_0^r dr_0 \int_0^{t(r_0, R)} I_B(t') \left[e^{-b_i(t+t')} + \left|\frac{t - t'}{t - t'}\right| e^{-b_i|t-t'|} \right] dt' \tag{I-17}$$

where

$$t \equiv t\ (r_0, r)$$

and

$$t' \equiv t\ (r_0, r') \tag{I-18}$$

are given by equation (I-12), and the sum over i from i = 1 to 2 has now replaced the integral over ψ. A further important simplification can now be made by noting that the radial coordinate r occurs in equation (I-17) only through the factor $e^{\pm b_i t}$. The r- dependence can thus be factored completely out of the integral over t', yielding the result

$$q_\nu = \frac{2}{r} \sum_{i=1}^{n} a_i \int_0^r \{ e^{-b_i t} \int_0^t I_B(t')\ e^{b_i t'} dt' - e^{b_i t} \int_t^{t(r_0, R)} I_B(t')\ e^{-b_i t'} dt' + e^{-b_i t} \int_0^{t(r_0, R)} I_B(t')\ e^{-b_i t'} dt' \}\ dr_0 \tag{I-19}$$

With this factorization, it is no longer necessary to re-evaluate the integrals over t' in equation (I-19) for each value of the radial coordinate r considered, so that the dimensionality of the problem is effectively reduced by one. Thus, by the use of equations (I-5), (I-12), (I-18), and (I-19) the calculation of $q_{rad}(r)$ is reduced from the original five-dimensional problem to an effectively three-dimensional problem, i.e., to two spatial dimensions and the frequency.

C. Numerical Computation Procedure

The equations discussed in the preceeding sections have been programmed for digital computation of the radiative flux q_{rad} (r) and the thermal conductivity K(T) from given arc data. For given values of the arc temperature distribution T(r) and the absorption coefficient $\alpha(\nu,T)$, the program first calculates $q_{rad}(r)$ in the arc column from equations (I-5), (I-12), (I-18), and (I-19); the corresponding values of K(T) are then calculated from the energy balance (equations (I-1) and (I-2)), using the previously calculated values of $q_{rad}(r)$ and given values of $\sigma(T)$ and E.

The main features of the computational procedure used in obtaining $q_{rad}(r)$ are briefly as follows: First, the temperature distribution in the arc is specified in tabular form by giving values of the arc temperature T and the corresponding radial coordinate r at a number of division points across the arc column profile. The values of the gas properties σ and α_ν at these division points are then obtained by linear interpolation in tables of the property values versus temperature. The radial

integrals in equations (I-1), (I-12), and (I-19) are evaluated analytically between division points in r, assuming an interpolation of the gas properties which is linear in r^2. (This interpolation scheme was chosen because it is known to give a rather good representation of the experimental data in many cases, especially for small values of r (see Figure I-2)). The integration over t' in equation (I-19) is done similarly, using a linear interpolation in t'^2 for I_B. Although this integration can be done in closed form for all values of the parameters, cancellation of terms in the resulting formula leads to serious numerical errors when the difference Δt between the values of t at the two ends of the integration interval is small. Hence, the program uses the closed form formula for the integral only when $\Delta t > 0.2$ and uses a power series expansion in Δt for values of $\Delta t \leq 0.2$.

Values of $q_\nu(r)$ are calculated from equation (I-19) for a series of specified frequencies ν_j, and the integration over frequencies (equation (I-5)) is then performed using the formula

$$q'_{rad}(r) = \sum_j A_j \, q_{\nu_j}(r), \qquad \text{(I-20a)}$$

where the integration frequencies ν_j and the weighting coefficients A_j are specified in the input data. In addition an option is provided to treat part of the radiation according to the optically thin approximation (equation (I-3)) if desired, so that the total radiative flux becomes

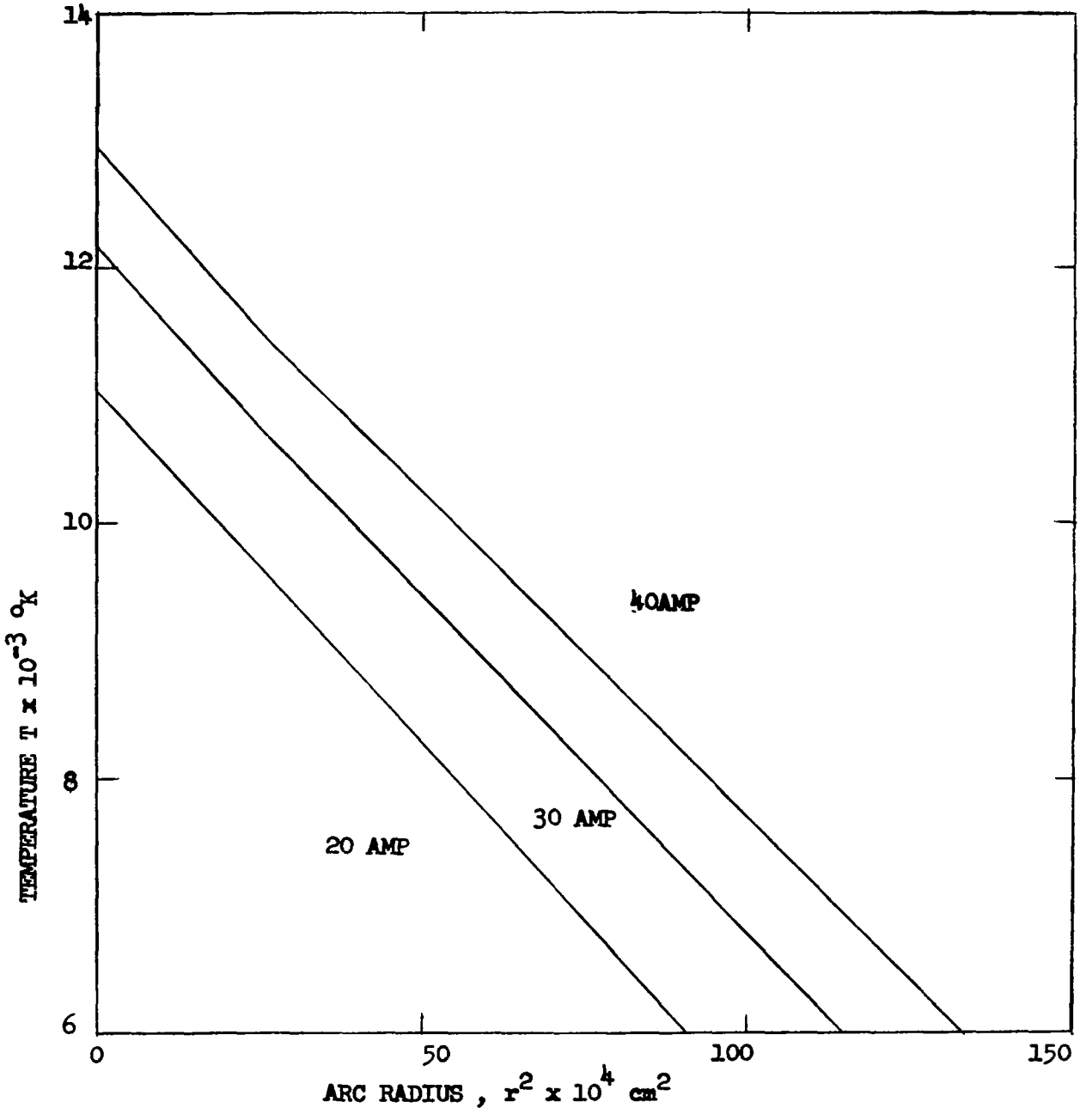

FIG. I-2. ILLUSTRATION OF STRAIGHT LINE DEPENDENCE OF TEMPERATURE VERSUS r^2 USING AS AN EXAMPLE THE 20-, 30-, AND 40-AMPERE HYDROGEN ARC RUNS AT ONE ATMOSPHERE

$$q_{rad}(r) = q'_{rad}(r) + \frac{1}{r}\int_0^r P_{rad}(T)\ r\ dr \qquad \text{(I-20b)}$$

where $P_{rad}(T)$ is the radiated power per unit volume for the optically thin part of the radiation. The values of $q_{rad}(r)$ from equation (I-20) are then inserted into equations (I-1) and (I-2) to obtain the thermal conductivity K as a function of radius r and hence of arc temperature T.

Estimated accuracy for the calculations of $q_\nu(r)$ is ~1% or better for values of the optical depth parameter t ranging from 0 to 1000 or more, assuming that the input data is known to this accuracy. For a typical case with about 25 radial division points, the present version of the program requires ~5 to ~10 seconds on the IBM 7094 to calculate $q_\nu(r)$ for a single frequency and all values of r; no attempt was made to minimize this running time, however, and it might well be possible to reduce it considerably in future versions of the program.

The total running time of the program for a given arc run of course depends on the number of frequencies ν_j which it is necessary to use in the frequency integration (I-20). Because of the complicated way in which the absorption coefficient α depends on frequency and temperature, the number of integration frequencies ν_j required to specify the radiation adequately may in general become very large. The following section discusses ways in which this number may be reduced in the important special case in which the absorption coefficient α is a separable function of frequency and temperature. This analysis is then applied to determine appropriate values for the coefficients ν_j and A_j in equation (I-20) for two types of radiation of interest for the present work, namely

continuum radiation and line radiation with a constant half-width. A third important type of radiation, namely line radiation with a strongly temperature-dependent half-width is non-separable; the analysis for this case appears to be much more difficult and is not considered here.

D. Optimization of the Frequency Integration for a Separable Absorption Coefficient

The present section describes a procedure for determining the numerical integration constants A_j and ν_j in equation (I-20) to obtain a specified accuracy in the total radiative flux $q_{rad}(r)$, independent of the temperature distribution in the arc. In this method it is assumed that the absorption coefficient α is a separable function of ν and T, i.e.,

$$\alpha_\nu (T) = \alpha_{\nu_0}(T) \; f(\nu) \qquad \text{(I-21)}$$

where α_{ν_0} (T) is the absorption coefficient at a fixed frequency $\nu = \nu_0$ and $f(\nu)$ is assumed to be normalized such that $f(\nu_0) = 1$. In this case the expressions given above for the spectral radiative flux q_ν can be considerably simplified by taking the factor $f(\nu)$ outside of the spatial integrations. Thus equation (I-12) for the optical depth parameter t becomes

$$t(r_o, r) = f(\nu)\ t_o(r_o, r) \qquad \text{(I-22a)}$$

where

$$t_o(r_o, r) \equiv \int_{r_o}^{r} \frac{\alpha_{\nu_o}(r')r'\ dr'}{(r'^2 - r_o^2)^{\frac{1}{2}}} \qquad \text{(I-22b)}$$

represents the value of t at the frequency $\nu = \nu_o$ and is, of course, independent of frequency. Substituting equation (I-22) into (I-19) and carrying out the integral over frequencies then yields an expression for the total radiative flux in the form

$$\int q_\nu\ d\nu = \frac{2}{r} \sum_{i=1}^{n} a_i \int_0^r \Big\{ \int_0^{t_o} F\left[b_i(t_o - t_o'),\ T'\right] dt_o'$$

$$- \int_t^{t_o(r_o,R)} F\left[b_i(t_o' - t_o),\ T'\right] dt_o' \qquad \text{(I-23)}$$

$$+ \int_0^{t_o(r_o,R)} F\left[b_i(t_o + t_o'),\ T'\right] dt_o' \Big\}\ dr_o$$

where we have defined the function

$$F(\xi, T') \equiv \int_0^\infty I_B\ (\nu, T')\ e^{-\xi f(\nu)}\ f(\nu)\ d\nu \qquad \text{(I-24)}$$

If, on the other hand, $\int q_\nu\ d\nu$ is evaluated from the approximate formula (I-20), one obtains an expression of exactly the same form as equation (I-23) except that the function $F(\xi, T')$ in equation (I-23) is replaced by the new function

$$G(\xi, T') \equiv \sum_j A_j\ I_B\ (\nu_j, T')\ e^{-\xi f(\nu_j)}\ f(\nu_j) \qquad \text{(I-25)}$$

Thus it follows that equation (I-20) will give a good approximation

to $\int q_\nu \, d_\nu$ if we choose the constants ν_j and A_j in (I-20) such that $G(\xi,T')$ is approximately equal to $F(\xi,T')$ for all values of ξ and T' occurring in the problem i.e.,

$$G(\xi,T') \approx F(\xi,T') \tag{I-26}$$

1. Line Radiation with a Temperature-Independent Profile

For a single spectral line, equation (I-26) may be further simplified by neglecting the variation of the black-body intensity I_B across the line profile. Hence I_B may be factored out of (I-26) to obtain the condition

$$\sum_j A_j \; f(\nu_j) \; e^{-\xi f(\nu_j)} \approx \int_0^\infty f(\nu) \; e^{-\xi f(\nu)} \, d\nu \tag{I-27}$$

Thus in the case of an isolated spectral line with a temperature-independent profile, the problem of choosing suitable values for the constants A_j and ν_j in equation (I-20) reduces to that of curvefitting a single function of one variable, as defined in equation (I-27).

Explicit values of the coefficients A_j and ν_j have been obtained from equation (I-27) for two line shapes of general interest; namely, the Lorentz and Doppler profiles. For the Lorentz profile, one has

$$f(\nu) = \frac{1}{1 + \left(\frac{\nu-\nu_0}{b}\right)^2} \tag{I-28a}$$

where b is the half-width parameter and ν_0 is the frequency of the line center. Hence for this case one has

$$I_L(\xi) \equiv \int_0^\infty f(\nu)\ e^{-\xi f(\nu)} d\nu$$
$$\approx 2b \int_0^\infty \frac{1}{(1+x^2)}\ e^{-\xi/(1+x^2)}\ dx \qquad \text{(I-28b)}$$

The integral (I-28b) is readily evaluated in terms of the Bessel function of imaginary argument and is plotted in Figure I-3 for values of ξ between 0 and 10. The simple two-term curvefit

$$I_L(\xi) \approx \pi\ b \left(.6527\ e^{-.6839\xi} + .3397\ e^{-.0627\xi}\right) \qquad \text{(I-28c)}$$

fits the calculated data within 0.8% over this range of ξ. Comparing this result with equations (I-23) and (I-27), we conclude that using the values

$$\nu_1 = \nu_0 + .6799b \qquad A_1 = 2.998b$$
$$\nu_2 = \nu_0 + 3.866b \qquad A_2 = 17.02b \qquad \text{(I-29)}$$

in equation (I-20) will give an accuracy ~1% in the calculated radiative flux $q_{rad}(r)$ for a Lorentz broadened line with constant half-width provided that the optical depth at the line center is everywhere $\lesssim 10$.

A similar calculation has also been carried through for the Doppler profile,

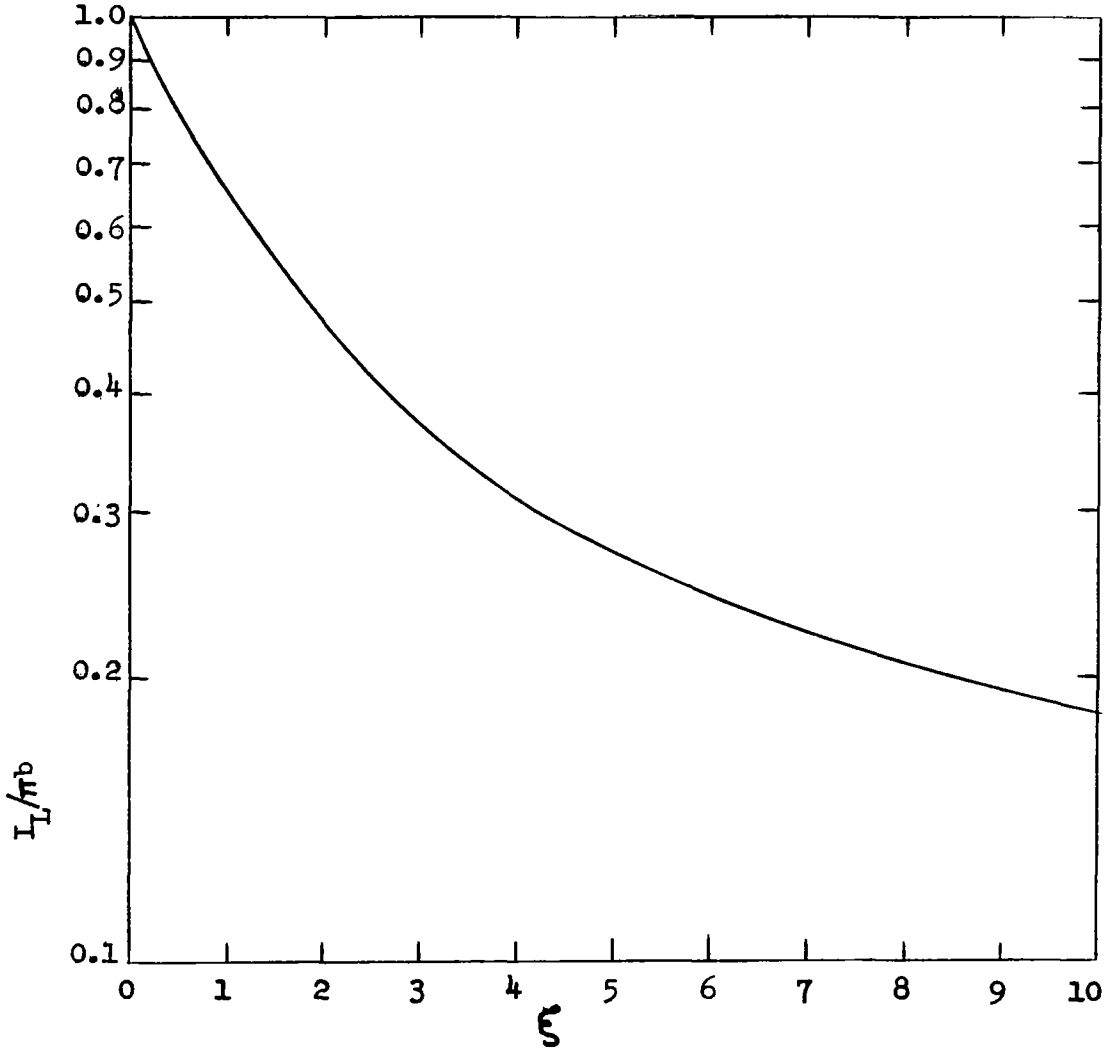

FIG. I-3. EVALUATION OF THE LORENTZIAN PROFILE INTEGRAL AS A FUNCTION OF THE OPTICAL DEPTH PARAMETER

$$f(\nu) = \exp\left[-(\nu-\nu_0)^2/b^2\right] \qquad \text{(I-30a)}$$

where the parameters ν_0 and b have the same significance as in equation (I-28) above. For this case one has

$$I_D(\xi) \equiv \int_0^\infty f(\nu)\, e^{-\xi f(\nu)}\, d\nu \qquad \text{(I-30b)}$$

$$\approx 2b \int_0^\infty \exp(-x^2-\xi\, e^{-x^2})\, dx$$

This function has been evaluated by numerical integration and is plotted in Figure I-4 for values of ξ in the range $0 \leq \xi \leq 3000$. Fitting the calculated values to the form (I-27) gives the coefficients

$$\begin{aligned} \nu_1 &= \nu_0 + .691b & A_1 &= 2.42b \\ \nu_2 &= \nu_0 + 1.57b & A_2 &= 1.32b \\ \nu_3 &= \nu_0 + 2.15b & A_3 &= 1.00b \\ \nu_4 &= \nu_0 + 2.64b & A_4 &= 1.10b \end{aligned} \qquad \text{(I-30c)}$$

with an error of $\leq$ 10% for values of ξ in the range $0 \leq \xi \leq 2000$. The coefficients (I-30c) are thus suitable for moderately accurate calculations of the total radiative flux from Doppler broadened lines for all cases in which the total optical depth at the line centers does not exceed ~1000.

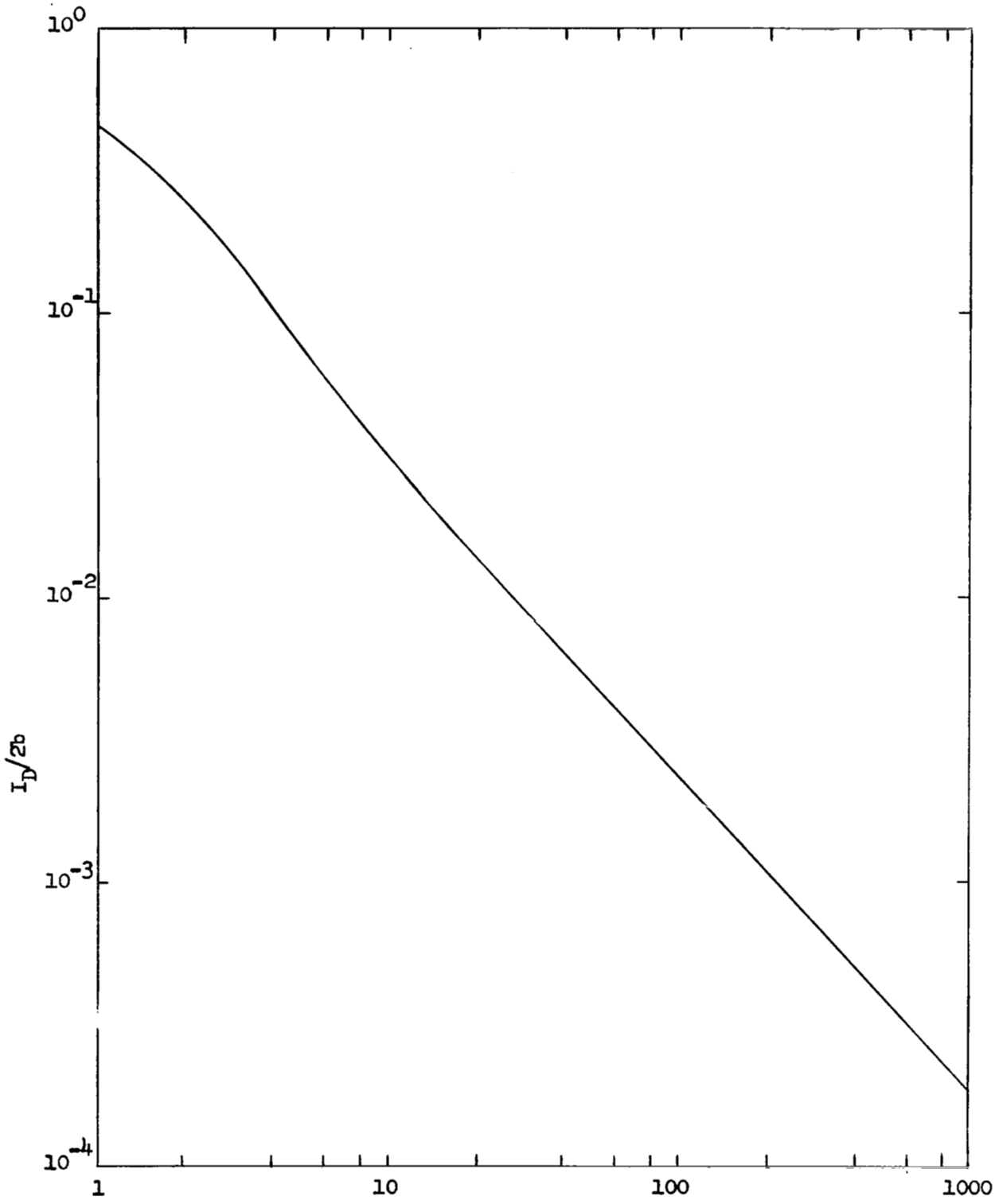

FIG. I-4. EVALUATION OF THE DOPPLER INTEGRAL AS A FUNCTION OF THE OPTICAL DEPTH PARAMETER

2. Continuum Radiation

Values of the integration constants ν_j and A_j may also be found from equation (I-26) for the case of continuum radiation. For this type of radiation, the absorption coefficient between two adjacent absorption edges $\nu_i^{(e)}$ and $\nu_{i+1}^{(e)}$ is ordinarily represented rather well by a formula of the form

$$f(\nu) = (\nu_i^{(e)}/\nu)^n \qquad \nu_i^{(e)} \leq \nu \leq \nu_{i+1}^{(e)} \qquad \text{(I-31)}$$

where n is a constant which is typically ~3, though values ranging from ~0 to ~6 occur in a few cases. With the form (I-31) for $f(\nu)$ equation (I-24) becomes

$$F(\xi,T') = \frac{2h(\nu_i^{(e)})^4}{c^2} \int_1^{1/\gamma} x^{3-n}\, e^{-\xi x^{-n}}/(e^{\beta x}-1)\, dx \qquad \text{(I-32a)}$$

where

$$\begin{aligned} \gamma &= \nu_i^{(e)}/\nu_{i+1}^{(e)} \\ \beta &= h\,\nu_i^{(e)}/kT' \\ x &= \nu/\nu_i^{(e)} \end{aligned} \qquad \text{(I-32b)}$$

and the explicit form (I-10) has been used for I_B. Integrating equation (I-32) by a Gaussian quadrature[4] using the variable of integration

$$y = 1/x^3 = (\nu_i^{(e)}/\nu)^3 \qquad \text{(I-33)}$$

then yields an approximation for $F(\xi,T)$ of the desired form (I-26) with the integration constants A_j and ν_j given by the formulas

$$\nu_j = \left[\gamma^3 + (1-\gamma^3)\ y_j\right]^{-1/3} \nu_i^{(e)}$$

$$A_j = 1/3 \left[(\nu_i^{(e)})^{-3} - (\nu_{i+1}^{(e)})^{-3}\right] \nu_j^4\ w_j \qquad \text{(I-34)}$$

where the constants y_j and w_j are the nodes and weights for a Gaussian quadrature on the interval 0 to 1, as given, for example, in table 25.8 of reference 4.

The approximation (I-34) for $F(\xi,T)$ has been tested by numerical calculations for values of the parameters in the range

$$\begin{aligned} -1 &\leq n \leq 10 \\ 7 &\leq \beta \leq 25 \\ 0 &\leq \xi \leq 10 \\ 0 &\leq \gamma \leq 1 \end{aligned} \qquad \text{(I-35)}$$

which covers most cases of interest for the treatment of ultraviolet continuum radiation in the arc, and it has been found that, for almost all cases in this range, two to four terms in the Gauusian quadrature are sufficient to hold the error in the frequency integration within a few percent. Typical results of these calculations are shown in Figures I-5 through I-10 where we have plotted the relative error in the approximation (I-34) versus the parameter values for various numbers of terms N in the Gaussian quadrature. For n = 0, the error is independent of the optical depth parameter ξ, and one sees from Figures I-5 and I-6 that three terms in the Gaussian quadrature are sufficient to give an error of $\leq$ 1% for

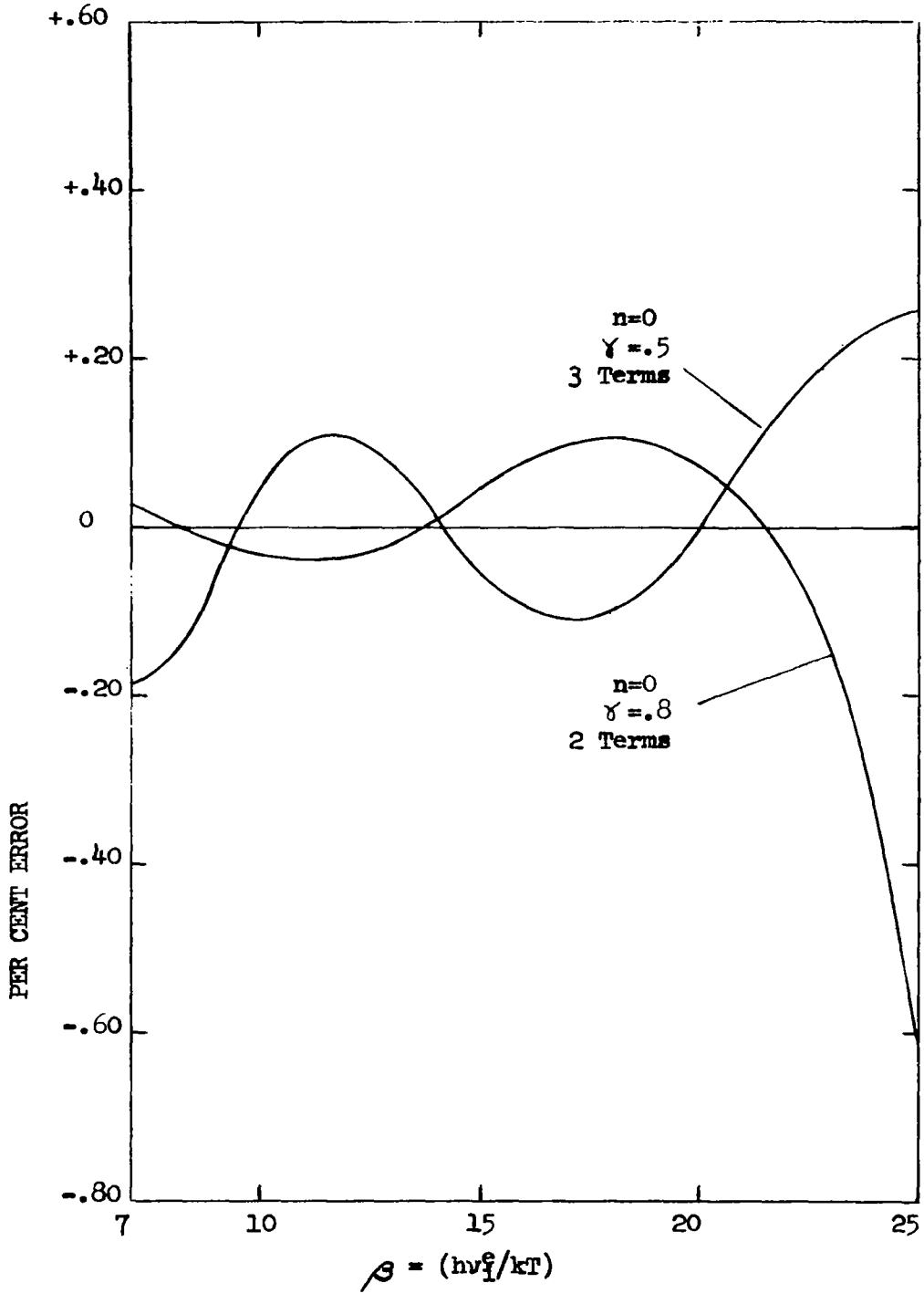

FIG. I-5. ERROR IN FREQUENCY INTEGRATION VERSUS PARAMETER VALUES FOR CONTINUUM RADIATION (n=0, γ =.8, two terms inGaussian Quadrature; n=0, γ =.5, three terms in Gaussian Quadrature)

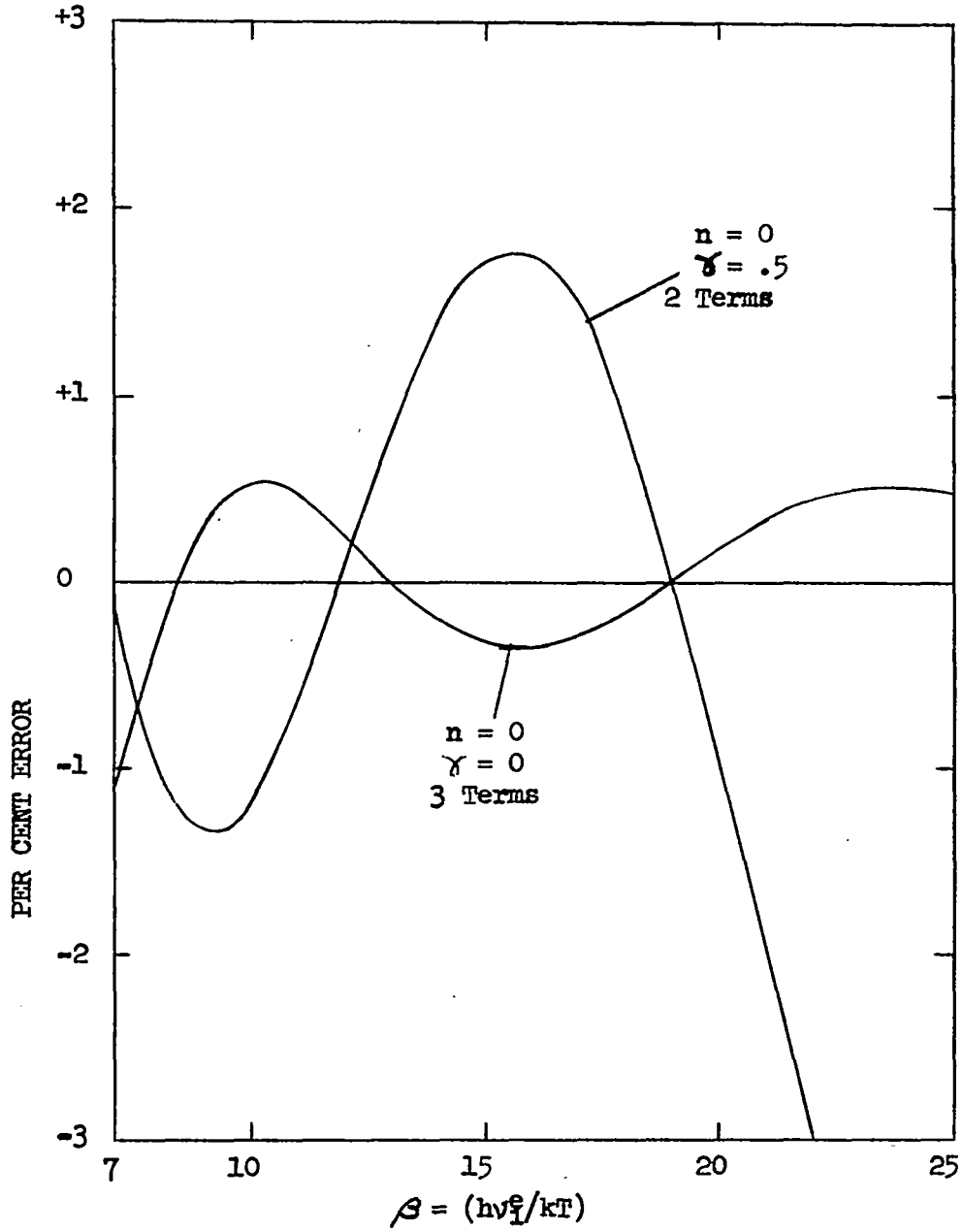

FIG. I-6. ERROR IN FREQUENCY INTEGRATION VERSUS PARAMETER VALUES FOR CONTINUUM RADIATION(n=0, γ =.5, two terms in Gaussian Quadrature; n=0, γ =0, three terms in Gaussian Quadrature)

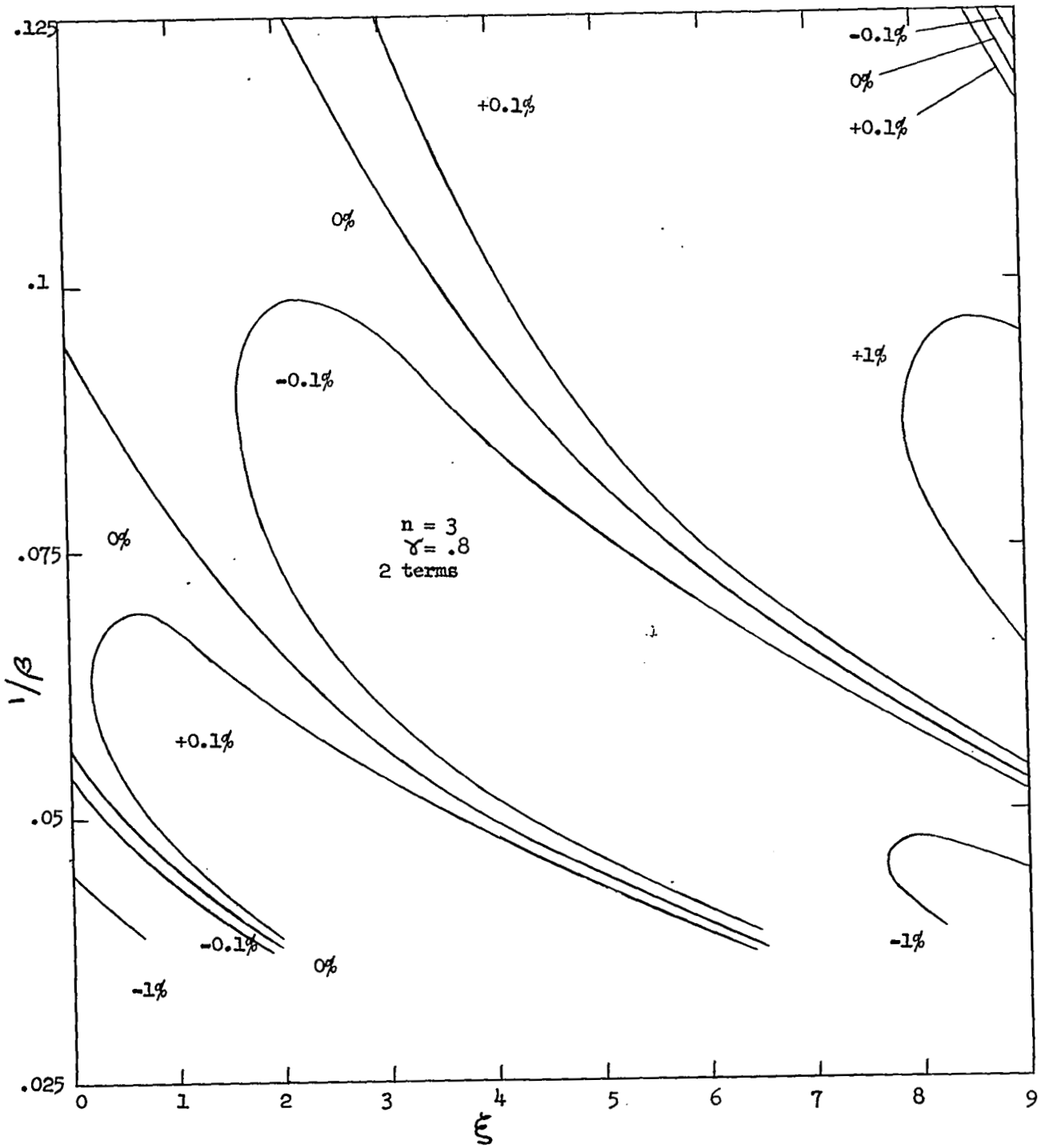

FIG. I-7. ERROR IN FREQUENCY INTEGRATION VERSUS PARAMETER VALUES FOR CONTINUUM RADIATION (n=3, γ =.8, two terms in Gaussian Quadrature)

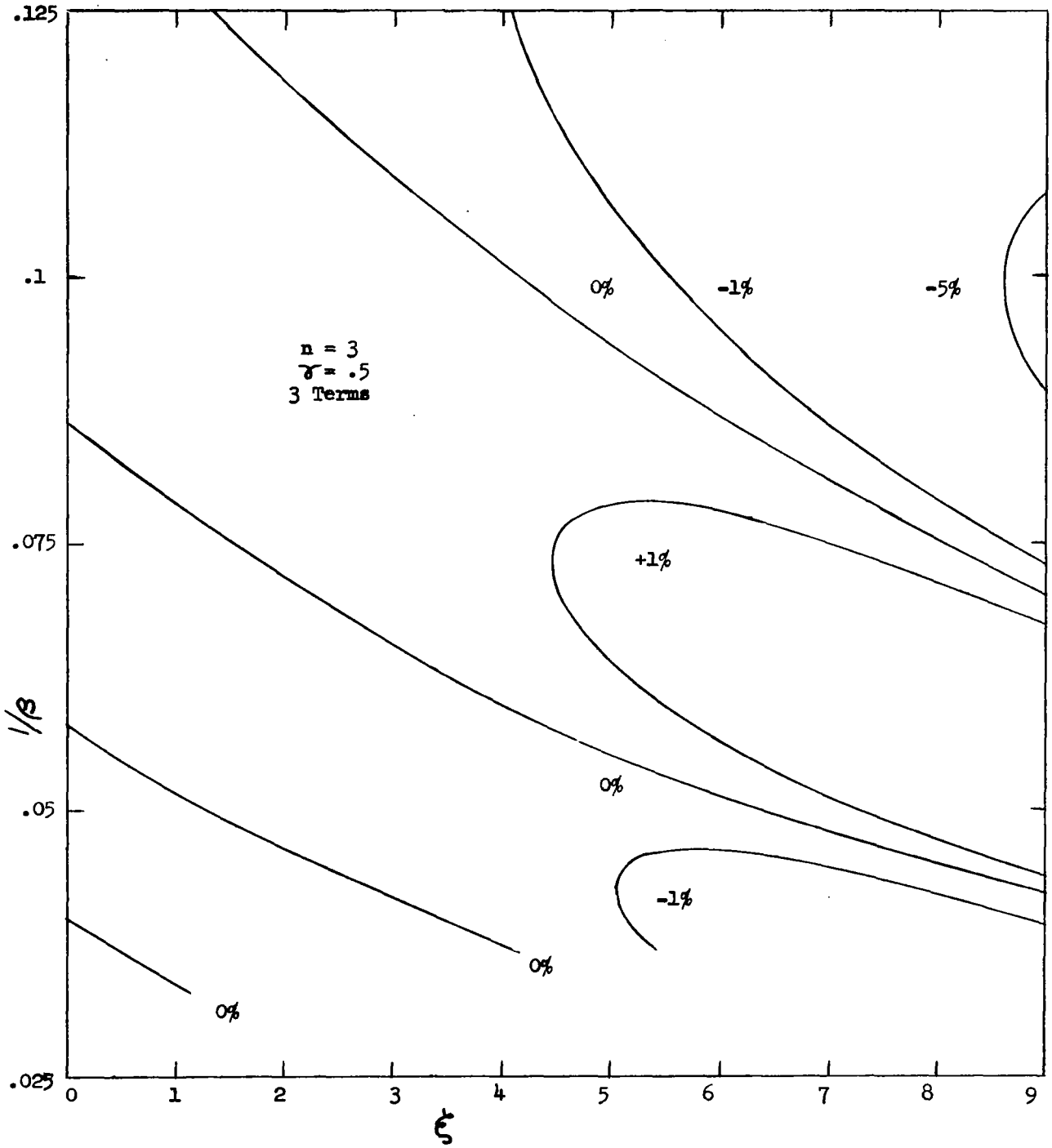

FIG. I-8. ERROR IN FREQUENCY INTEGRATION VERSUS PARAMETER VALUES FOR CONTINUUM RADIATION(n=3, γ=.5, three terms in Gaussian Quadrature)

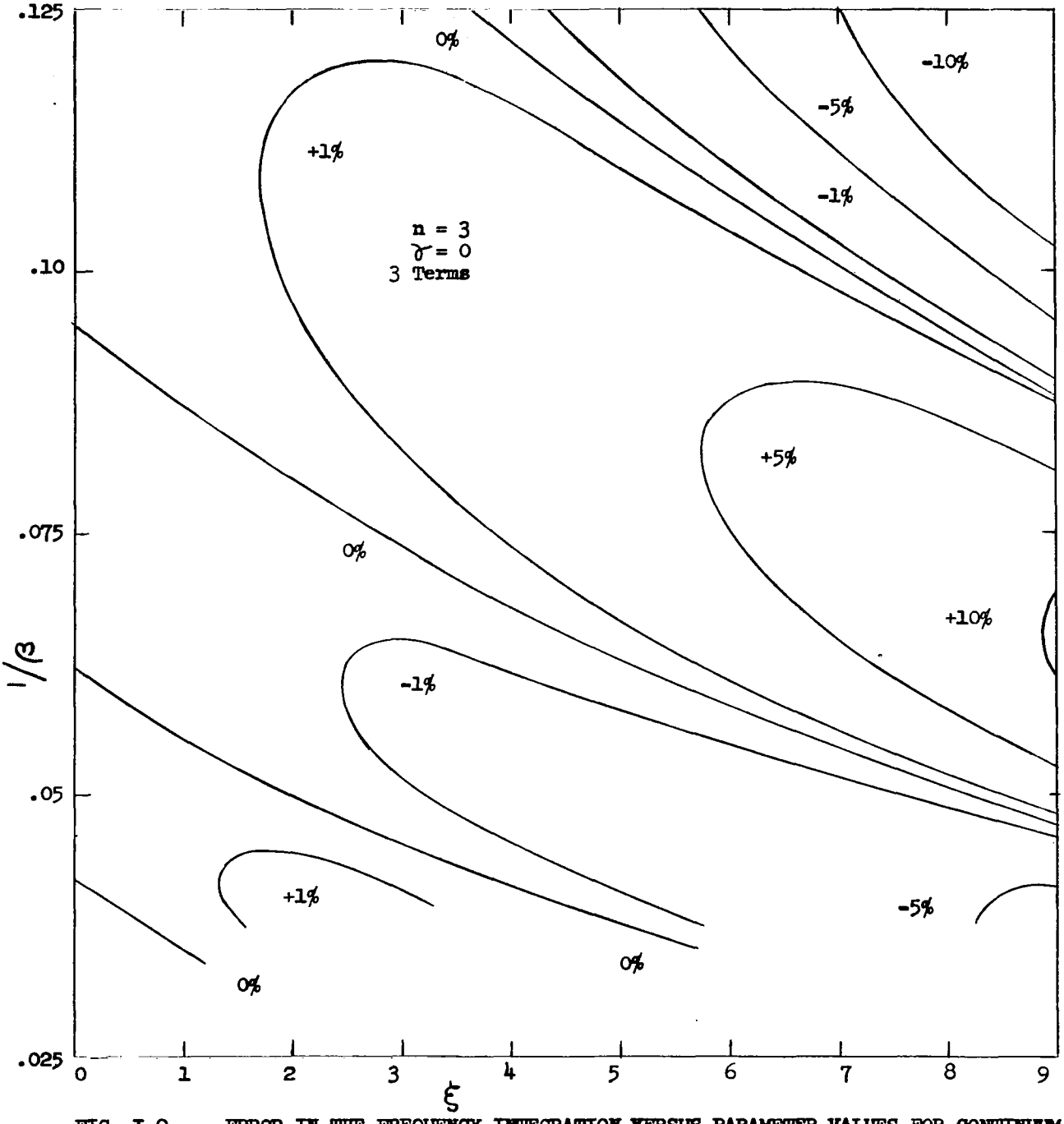

FIG. I-9. ERROR IN THE FREQUENCY INTEGRATION VERSUS PARAMETER VALUES FOR CONTINUUM RADIATION(n=3, γ=0, three terms in Gaussian Quadrature)

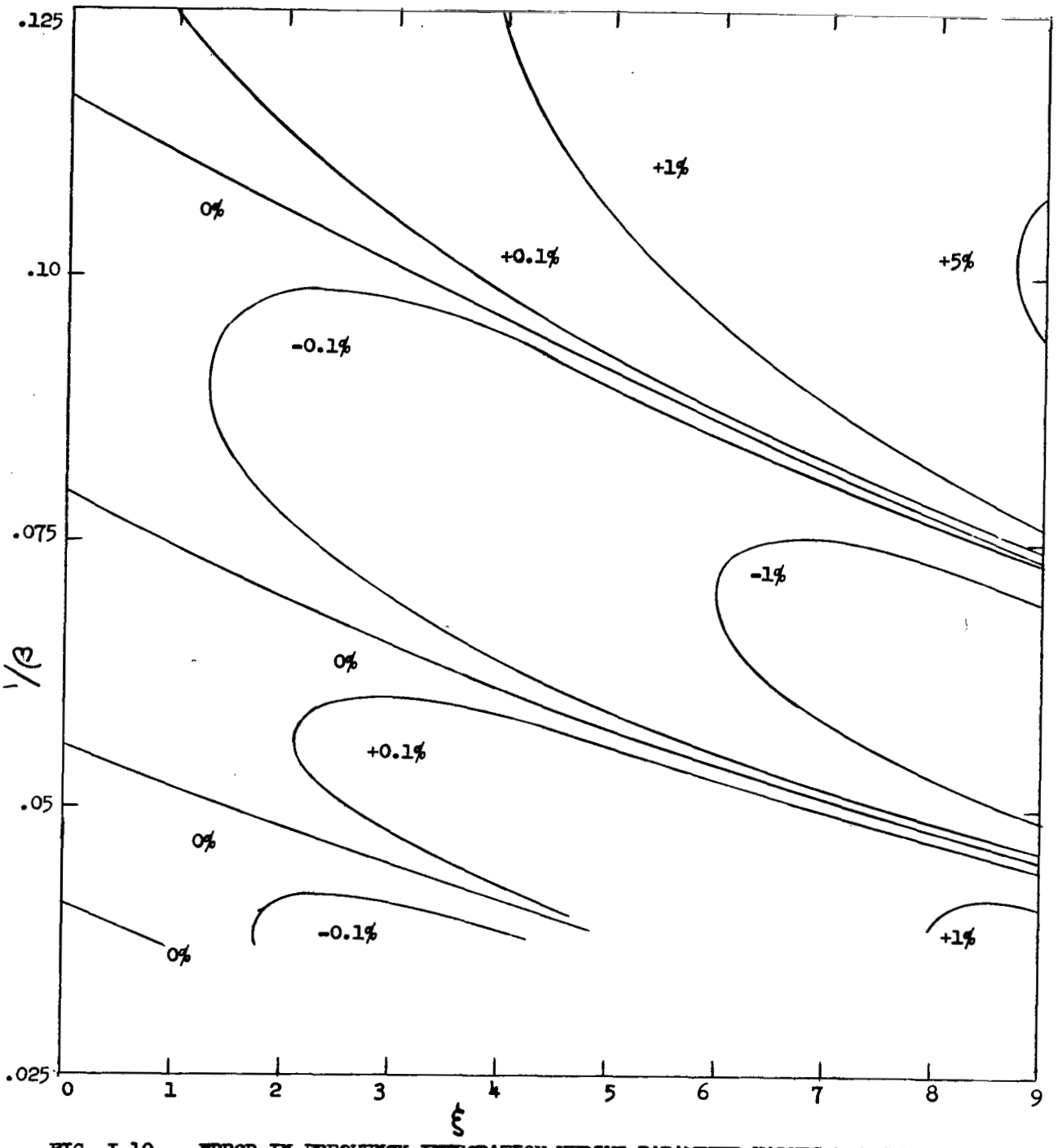

FIG. I-10. ERROR IN FREQUENCY INTEGRATION VERSUS PARAMETER VALUES FOR CONTINUUM RADIATION ($n=3, \gamma=0$, four terms in Gaussian Quadrature)

all cases in the range (I-35). The error is somewhat greater for $n = 3$ (Figures I-7-I-11), but nevertheless one sees that four terms in the quadrature formula are sufficient to hold the error within $\pm$ 5%, except for values of $\xi \sim 10$ or more. For typical cases in the subsequent arc data analysis, ξ is ~ 1 or 2, so that the corresponding error is of course much smaller than this.

Besides the error shown in Figures I-5 through I-10 which results from the use of the approximation (I-34) in place of equation (I-32) for $F(\xi,T)$, there is of course an additional error in the present analysis due to the use of an approximate form (equations (I-21) and (I-31)) for the continuum absorption coefficient $\alpha(\nu,T)$. The magnitude of this latter error has not been evaluated in detail; however it appears that in general it should be smaller than the error resulting from uncertainties in the experimental absorption coefficient data used in the analysis.

APPENDIX I REFERENCES

1. RAD, Theoretical and Experimental Studies of High-Temperature Gas Transport Properties, Final Report, Avco RAD-TR-65-7 Contract NASw-916 (May 1965).
2. See, for example, S. Chandrasekhar, Radiative Transfer.
3. Handbook of Mathematical Functions, M. Abramowitz and I. A. Stegun, Eds., National Bureau of Standards, Applied Mathematics Series, No. 55 (U.S. Dept. of Commerce, Washington, 1964) Chapter 9 and 11.
4. IBID, Chapter 25.

APPENDIX II

RADIATION CALCULATIONS

It was necessary for the purpose of calculating the thermal conductivities using the experimental arc column data of voltage gradients and temperature profiles, to estimate the net outward radiant power transfer at all arc column radii. This problem was divided into two parts. 1) The plasma was treated as being optically thin for all radiant emission of the visible and near IR spectra. 2) The plasma was treated as thick for all radiant emission of the vacuum UV spectrum. Referring to case #1 the radiant power loss per unit arc column length was calculated as:

$$P_{vis}(r) = 2\pi \int_0^r \epsilon(r')\, r'\, dr \qquad \text{(II-1)}$$

where r is the arc column radius and ϵ (r) is the total emission coefficient of the gas at temperature T(r). Referring to case #2 the radiant power loss per unit arc column length was calculated using the arc column radiative transfer computer program described in detail in Appendix I of this report. The net outward radiant power transfer at a given arc column radius was then determined as:

$$P_{net}(r) = P_{vis}(r) + P_{vuv}(r) \qquad \text{(II-2)}$$

and was applied to equation (19) along with the other necessary arc column parameters for determination of the thermal conductivity K(r). The following discussion briefly discusses the methods used to

determine the emission coefficients of equation (II-1) and the radiative values submitted in the above mentioned energy transfer computer programs.

1. Total emission coefficient--Visible and IR Spectrums

The total emission coefficients for an infinitesimal volume of radiating gas can be described quite briefly as

$$\epsilon\ (T) = \int \epsilon\ (T,\nu)\ d\nu \qquad \text{(II-3)}$$

where the spectral emission coefficient, $\epsilon\ (T,\nu)$, represents the sum of all radiative processes contributing appreciable amounts of radiant energy at frequency ν for gas temperature T. For our plasma temperatures, the radiative processes of interest where those of the free-free, free-bound, and bound-bound mechanisms which in part included effects due to electrons in the presence of neutral atoms and in fields of singly ionized atoms.

The bremsstrahlung, i.e., free-free transition, spectral emission coefficient was obtained using the expression

$$\epsilon_{ff}\ (T,\ ) = \frac{16\ (\alpha\ a_0)^3}{3\ \sqrt{3}\ \pi} \left(\frac{E_H}{KT}\right)^{\frac{1}{2}} g_f\ (T,\nu)\ N_e N_i\ \exp\ (-\ \frac{h\nu}{KT}) \qquad \text{(II-4)}$$

where α, a_0, k, E_H and h are the usual constants; and N_e is the electron number density, N_i is the number density of the reacting particle field, and $g_f\ (T,\nu)$ is the associated gaunt factor a function of both temperature T and frequency ν. For our purposes, when N_i represented the number density of singly ionized atoms, we used the tables of Karzas and Latter[1] to determine the free-free gaunt factors.

The recombination, i.e., free-bound transition, spectral emission coefficient was obtained using the expression

$$\epsilon_{fb}(T,\nu) = \sum_{n,\ell} B_\nu \, \sigma'_{n\ell}(\nu) \, N_{n\ell} \qquad \text{(II-5)}$$

where the sum is made over principal and orbital quantum numbers n, and ℓ respectively; and B_ν is the Planck function in frequency units, $\sigma'_{n\ell}$ is the net absorption cross section in that it takes into account effects due to induced emission, and $N_{n\ell}$ is number density of the given n,ℓ state. For a more detailed discussion on how equation (II-4) and (II-5) were utilized the reader is referred to reference 2 . For the present it suffices to state that these equations along with those to follow have been programmed for solution on our IBM 7094 computer, the input of which will be briefly discussed here.

The true aborption (photo ionization) cross section is defined as

$$\sigma_{n\ell} \equiv \sigma'_{n\ell} \left[1 - \exp\left(-\frac{h\nu}{KT}\right)\right]^{-1} \qquad \text{(II-6)}$$

and was calculated for the gases in question for all possible processes of $N^o + h\nu = N^+ + e^-$, which occur in the UV as well as in the visible and IR spectra, using the generalized quantum defect method proposed by Burgess and Seaton[2], the values of which have been calculated by, for example, Griem[3] and Hahne[4], and substantiated experimentally by Morris et al.[5] For large principal quantum numbers, n, we have employed the hydrogenic formula, namely,

$$\sigma_n = \frac{64}{3\sqrt{3}} \alpha \pi a_o^2 \left(\frac{E_H}{h\nu}\right)^3 \frac{1}{n^5} g_{fb} \qquad \text{(II-7)}$$

where g_{fb} is the free-bound gaunt factor of which we used Peach's[6] expression.

The visible and near IR line, i.e., bound-bound transition, spectral emission coefficient was obtained and integrated independently of the free-free and free-bound transitions. The total line emission coefficient is given for one line as

$$\epsilon_{bb}(T) = \frac{h\nu}{4\pi} A_{mm'} N_{m'} \qquad \text{(II-8)}$$

where ν is the unperturbed frequency of the line, $A_{mm'}$ is the transition probability for spontaneous emission for transitions from an initial state m' to a final state m and $N_{m'}$ is the number density of the initial state. In terms of absorption oscillator strength $f_{m'm}$,

$$\epsilon_{bb}(T) = \frac{2r_o \pi h\nu^3}{c} \frac{g_m}{g_{m'}} f_{mm'} N_{m'} \qquad \text{(II-9)}$$

where r_0, h and c are the usual constants; and the g terms are the statistical weights of the initial and final states. In the form of equation (II-9) a sum of the total bound-bound emission coefficients was made using the absorption oscillator strengths calculated by Bates and Damgaard (Griem[3]), and Allen[7].

This sum was then added to the above integrated results of free-free and free-bound estimates due to electrons in fields of singly ionized atoms and also due to electrons reacting with neutral atoms. For the latter case ($N^o + e$) the radiative cross sections used were, dependent upon the gas in question, those calculated and /or listed by Bates[8] and Griem[3] and those found experimentally by Morris et al.[5]

Figures II-1 and II-2 show the total visible and near IR emission coefficients used for our nitrogen and hydrogen calculations of thermal conductivities.

2. Radiative Continuum Input to Arc Column Radiative Transfer Computer Program, UV Spectrum

As mentioned previously the net radiant energy transferred at various stages of the arc column due to UV free-bound continuum processes was calculated by utilizing the arc column radiative transfer computer program (Appendix I). The input of this program requires knowledge of the photo-ionization cross sections as a function of frequency for all possible $N^o + h\nu = N^+ + e^-$ processes. For nitrogen we used the six absorption edges calculated by Hahne[4] which in part have been substantiated magnitude wise by experiments carried out in this laboratory (See Sec. IV). For hydrogen the photo-ionization cross sections used were those calculated by Griem[3] using the Burgess and Seaton[2] approach. These cross sections agreed well with those obtainable from the works of Karatz and Latter[1] and also Bethe and Salpeter[9].

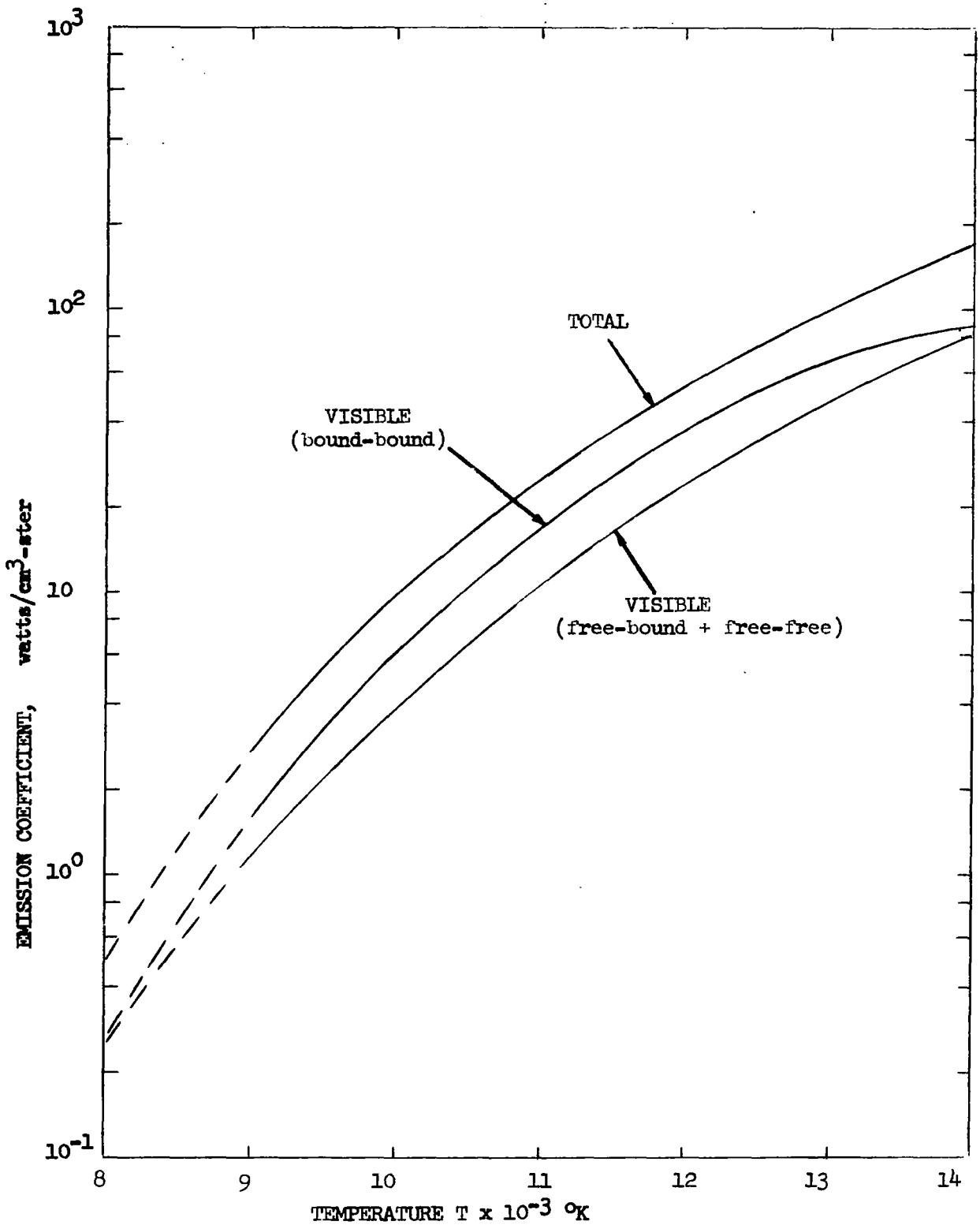

FIG. II-1 . EMISSION COEFFICIENT OF ONE ATMOSPHERE NITROGEN FOR $\lambda > 2000$ Å USED IN THE CALCULATION OF THERMAL CONDUCTIVITY

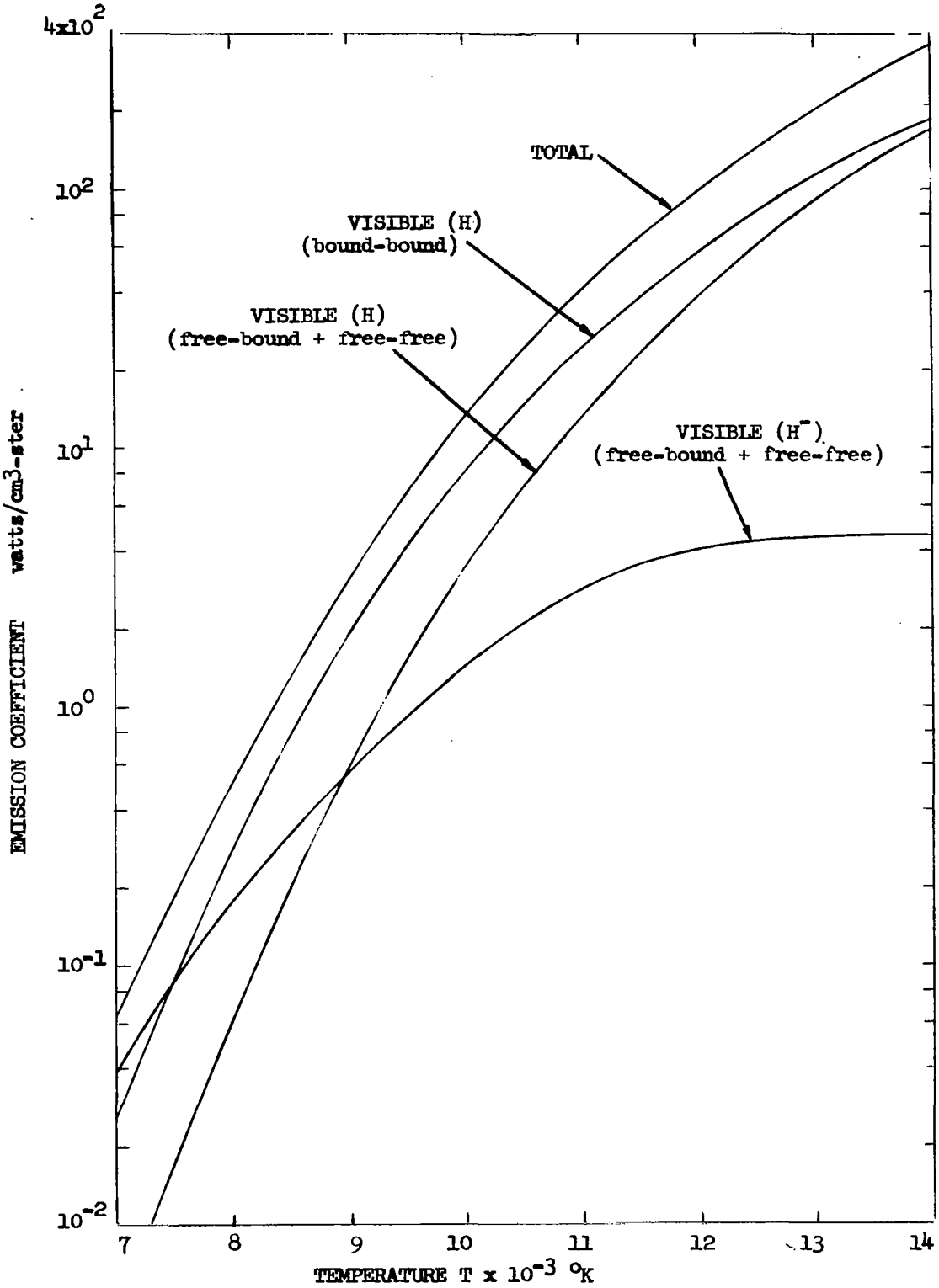

FIG. II-2. EMISSION COEFFICIENT OF ONE ATMOSPHERE HYDROGEN FOR $\lambda > 2000$ Å USED IN THE CALCULATION OF THERMAL CONDUCTIVITY

REFERENCES

1. Karzas, W. J., and R. Latter, 1961. Astrophys. J. Suppl. No. 55, Vol. VI, 167.

2. Burgess, A. and M. F. Seaton, A General Formula For the Calculation of Atomic Photo-Ionization Cross Section. Monthly Notices Roy. Astron. Soc., 120, pp. 121-151 (1960).

3. Griem, Hans R., Plasma Spectroscopy, McGraw-Hill Book Co., 1964.

4. Hahne, G. E., "The Vacuum Ultraviolet Radiation from N^+ and O^+ Electron Recombination in High Temperature Air", NASA Report TN-D2794 NASA/Ames Research Center.

5. RAD, Research on Radiation from Arc Heated Plasma, Final Report, AVCO RAD-TR-65-17, Contract AF33(616)-8390 Project 7067, TASK 7063-03 (July 1965).

6. Peach, G., Continuous Absorption Coefficients for Non-Hydrogenic Atoms Monthly Notices Roy. Astron. Soc., 124, pp 372-381, 1962.

7. Aller, L. G., Astrophysics, New York, The Ronald Press Company, 1953.

8. Bates, D. R., "Collisions Between Atomic Systems", Atomic and Molecular Processes (D. R. Oates, Ed.) Academic Press, New York, 1962, p 549.

9. Bethe, H. A., and E. E. Salpeter, Quantum Mechanics of One-and-Two Electron Atoms, Academic Press, 1957.

NASA-Langley, 1966 CR-575

"The aeronautical and space activities of the United States shall be conducted so as to contribute . . . to the expansion of human knowledge of phenomena in the atmosphere and space. The Administration shall provide for the widest practicable and appropriate dissemination of information concerning its activities and the results thereof."

—NATIONAL AERONAUTICS AND SPACE ACT OF 1958

NASA SCIENTIFIC AND TECHNICAL PUBLICATIONS

TECHNICAL REPORTS: Scientific and technical information considered important, complete, and a lasting contribution to existing knowledge.

TECHNICAL NOTES: Information less broad in scope but nevertheless of importance as a contribution to existing knowledge.

TECHNICAL MEMORANDUMS: Information receiving limited distribution because of preliminary data, security classification, or other reasons.

CONTRACTOR REPORTS: Technical information generated in connection with a NASA contract or grant and released under NASA auspices.

TECHNICAL TRANSLATIONS: Information published in a foreign language considered to merit NASA distribution in English.

SPECIAL PUBLICATIONS: Information derived from or of value to NASA activities. Publications include conference proceedings, monographs, data compilations, handbooks, sourcebooks, and special bibliographies.

TECHNOLOGY UTILIZATION PUBLICATIONS: Information on technology used by NASA that may be of particular interest in commercial and other nonaerospace applications. Publications include Tech Briefs; Technology Utilization Reports and Notes; and Technology Surveys.

Details on the availability of these publications may be obtained from:

SCIENTIFIC AND TECHNICAL INFORMATION DIVISION

NATIONAL AERONAUTICS AND SPACE ADMINISTRATION

Washington, D.C. 20546